THE EFFECTS OF FRICTIONAL HEATING ON THE THERMAL, HYDROLOGIC, AND MECHANICAL RESPONSE OF A FAULT

by

Charles William Mase

B.Sc. San Diego State University, 1974

M.Sc. The University of Utah, 1979

A THESIS SUBMITTED IN PARTIAL FULFILLMENT OF

THE REQUIREMENT FOR THE DEGREE OF

DOCTOR OF PHILOSOPHY

in

THE FACULTY OF GRADUATE STUDIES

(Department of Geological Sciences)

We accept this thesis as conforming

to the required standard

THE UNIVERSITY OF BRITISH COLUMBIA

September 1986

In presenting this thesis in partial fulfilment of the requirements for an advanced degree at the University of British Columbia, I agree that the Library shall make it freely available for reference and study. I further agree that permission for extensive copying of this thesis for scholarly purposes may be granted by the head of my department or by his or her representatives. It is understood that copying or publication of this thesis for financial gain shall not be allowed without my written permission.

Department of Geological Sciences

The University of British Columbia
1956 Main Mall
Vancouver, Canada
V6T 1Y3

Date 1986 October 03

ABSTRACT

The mechanical response of a fault zone during an earthquake may be controlled by the diffusion of excess heat and fluid pressures generated by frictional heating. In this study a numerical model is formulated which incorporates the effects of frictional heating on the thermal, hydrologic, and mechanical response of a small patch of the failure surface. This model is used to examine the parameters that control the fault response, and to determine their critical range of values where thermal pressurization is significant. The problem has two time scales; a characteristic slip duration and a characteristic time for thermal pressurization. The slip duration is set by the fault geometry. The characteristic time for thermal pressurization is set by the slip rate, friction coefficient, and the thermal and hydraulic characteristics of the medium. Results suggest that the fault width, and hydraulic characteristics of the fault zone and adjacent medium are the primary parameters controlling the mechanical response. For narrow zones with a low porous medium compressibility ($<10^{-9}$ Pa^{-1}) and permeability ($<10^{-18}$ m^2), frictional heating can cause fluid pressures to approach lithostatic values and the temperature rise to stabilize at a maximum value dependent on the pore-dilatational and transport properties of the porous medium. Moderate slip events where shear strains exceed two cause substantial strain-weakening of the fault and, consequently, large stress drops, accelerations, and displacements. Both the dynamic stress drop

and total displacement decrease for zones with larger compressibility, permeability or width. The diffusion of excess pore pressures during the latter stages of slip causes strain hardening and a decline in slip velocity. Whether the patch experiences substantial strain-weakening or acts as a barrier depends on the shear strain across the fault. Thus it is possible for the patch to act as a barrier for small earthquakes but not for large ones. If the compressibility or permeability exceed 10^{-8} Pa^{-1} or 10^{-14} m^2, or the shear strain is less than one, then the effects of frictional heating may be negligible and the fault will exhibit no strain-weakening characteristics. Consequently, the patch acts as barrier that halts or resists further fault motion regardless of shear strain. Extrapolation of these results suggests that spatial variations in fault width and hydraulic characteristics will cause a heterogeneous stress drop and fault slip over the failure surface, explaining many of the features of active faulting (e.g., barriers, non uniform slip, rupture stoppage, random ground accelerations, strong motions, and frequency-magnitude relations).

TABLE OF CONTENTS

TABLE OF CONTENTS (continued)

LIST OF TABLES

LIST OF ILLUSTRATIONS

LIST OF ILLUSTRATIONS (continued)

ACKNOWLEDGMENTS

I wish to express my gratitude to my advisor, Leslie Smith, for his encouragement, assistance, and generous support in the research and preparation of this disseration. I am particularly indebted to him for the day-to-day interactions that we have shared.

I am grateful to the members of my committee, Scott Dunbar, Al Freeze, and John Ross, for the reviews and constructive criticisms of this manuscript. Special thanks to Lorie Cahn, Craig Forster, Keith Loague, Joel Massmann, and Al Woodbury for the many hours of discussions we have shared.

I am also grateful for the scholarship support provided by the University of British Columbia through a University Graduate Fellowship.

This research was funded by a grant to Leslie Smith from the Natural Sciences and Engineering Research Council of Canada (NSERC). Computations were carried out on an FPS 164 Array Processor supported by an NSERC Major Installation Grant to the University of British Columbia.

CHAPTER I

OVERVIEW OF THE STUDY

Most rocks within and adjacent to fault zones are porous and, under crustal conditions the pores are likely to contain water. Because the pressure of pore waters influences the mechanical properties of rock, stresses and strains are coupled to fluid flow within the porous medium. Furthermore, shear heating within a fault zone during deformation can lead to thermal expansion, pressurization and flow of pore fluids, thereby coupling the thermal field to the fluid-pressure field and, consequently, to the stress and strain fields. This coupling can lead to decreases or increases in the strength of a fault as well as in the strength of the adjacent medium. Thus the behavior of pore waters is of considerable importance in the mechanics of fault zone processes.

Numerous models have been proposed to explain how pore fluids might affect deformation processes. The majority of these models have been concerned with dilatancy in the presence of pore fluids. In this context, dilatancy is the process whereby the pore volume expands because of an applied differential stress. Nur and Booker (1972) discussed possible changes in fluid pressure arising from earthquake-induced stress drops, and the potential of these changes to act as triggering mechanisms for aftershocks. Scholz *et al.* (1973) suggested dilatancy could delay seismic failure by reducing

fluid pressure on a fault, and then trigger failure when the pore pressure is recovered. Rice and Simons (1976) examined how the coupling of dilatancy with pore-pressure diffusion could provide a mechanism by which a propagating shear fault could be stabilized against seismic failure. In this case the decrease in fluid pressure caused by dilatancy would tend to inhibit further inelastic deformation. In additional work, Rice and Rudnicki (1979) and Rudnicki (1979, 1980) examined the precursory creep behavior that such coupling could lead to. Simpson (1976) and Nur and Bell (1978) suggested that increases in fluid pressures induced by reservoir loading could act as a mechanism triggering increased seismic activity. These studies have examined the role of pore fluids either before or after seismic failure. Melosh (1979) suggested that during a seismic event a transient increase in fluid pressure could occur due to acoustic fluidization.

Hubbert and Rubey (1959) have discussed the importance of pore-fluid pressures in the mechanics of slip for low-angle overthrust faults. They suggested that the movement of a large thrust sheet posed a serious mechanical problem because friction along the base would seem to require either impossibly high shear stresses in the sheet or an unreasonably steep slope. Their hypothesis that high fluid pressures can reduce the frictional resistance along fault surfaces to near-zero values is a major contribution to fault mechanics. According to the Hubbert-Rubey hypothesis, the frictional resistance to motion is given by a simple modification of the

friction law. For this modification the shear stress required for slip is given by the product of the coefficient of friction and the effective normal stress acting across the fault surface. Because the coefficient of friction is reasonably constant for a variety of rock types and a wide range of normal stresses (Byerlee, 1978; Morrow *et al.*, 1982), the resistive shear stress can be reduced to very small values only by lowering the effective normal stress across the fault. Because the effective stress is equal to the total stress minus the fluid pressure, a requirement for low shear strength is that the fluid pressures adjacent to the fault surface must be close to lithostatic values. Hubbert and Rubey concluded that high fluid pressures play a vital role in low-angle thrust faulting. If overthrusting and other styles of faulting are initiated and sustained by abnormally high fluid pressures, then a mechanism for generating and maintaining that pressure poses a fundamental problem in fault mechanics. One such mechanism, a transient increase in fluid pressure due to thermal expansion of pore fluids caused by frictional heating within a fault zone, is the subject of this thesis.

Assuming that the failure surface is established and that the shear stress required for slip is given by the friction law, many investigators have shown that shear heating could play an important role in the dynamics of fault processes. Jaeger (1942), McKenzie and Brune (1972), Richards (1976), Cardwell *et al.* (1978), Scholz (1980), and Sibson (1980) suggested frictional heating could lead to partial melting on

the fault surface with a subsequent reduction in dynamic shear strength. These studies have neglected the presence and possible effect of pore water. If water is present, the dynamics are more complicated. The response of fluid pressures to shear heating can be described by the following two extreme cases. If the hydraulic diffusivity is much greater than the thermal diffusivity, then the thermal expansion of pore fluids is accomodated by fluid flow from the heated region. In this case the fluid pressure and dynamic shear strength remain unchanged during slip. Because the advection of heat is generally small, the fault is a large source of frictional heat and partial melting may occur. This is the response expected for high-permeability material. If the hydraulic diffusivity is less than the thermal diffusivity and if the medium is rigid, then there is no appreciable loss of fluid mass within the heated region due to transport from, or pore dilatation within, that region. In this case the heating process takes place at constant fluid mass and substantial increases in fluid pressure can occur during deformation. The resulting thermal pressurization causes the effective compressive stress to decrease, promoting inelastic deformation mechanisms such as frictional sliding past grain boundaries and microcracking. If fluid pressures approach lithostatic values the dynamic shear strength will become small, and the material within the fault zone will lose cohesion and deform as a viscous fluid. This is the response expected for media with low permeability that have undergone

an initial phase of consolidation. In addition, dilatancy recovery due to shear strain release in the region adjacent to the fault zone can further enhance increases in fluid pressures (Sibson, 1973; Scholz *et al.*, 1973; Rice and Rudnicki, 1979).

Sibson (1973; 1977) showed that if water is present in interconnected pores adjacent to a fault surface, the temperature rise cause by frictional heating can result in a rapid increase in fluid pressure. The thermal pressurization of pore-fluids would cause the two sliding surfaces to lose cohesion, and consequently, reduce the dynamic shear strength and the rate of frictional heating to virtually zero. In such a case the maximum temperature attained on the fault surface would be substantially less than that required for partial melting. In additional work, Sibson (1975) presented evidence for frictional melting on the outer Hebrides thrust zone and suggested such contrast in behavior might depend upon whether slip occurred under "wet" or "dry" conditions.

Without attempting to solve the coupled equations, Lachenbruch (1980) wrote down the governing equations for heat and fluid flow, and analyzed for special cases the interaction of controlling parameters and their critical range of values. The concepts discussed in this work form the basis and starting point for this study. For his analysis he assumed that the width and relative slip velocity across the fault zone are constant during deformation, that the strain is

independent of position in the fault zone, and that the shear stress required for slip is given by a friction law. Lachenbruch showed that a reduction in fault strength due to thermal pressurization requires the tandem operation of three processes: shear heating must cause a significant temperature rise, the temperature rise must cause a significant fluid-pressure increase, and the fluid-pressure increase must cause a significant reduction in shear strength. Failure of any of these conditions can lead to decoupling of the thermal, pore fluid pressure and stress fields, and thereby a failure to reduce the shear strength of a fault. He concluded that if permeability or pore-dilatational rate exceed 10^{-13} m^2 or 2%, respectively, then coupling of thermal, hydrologic, and mechanical effects could probably be neglected, with fluid pressure and dynamic shear strength remaining constant during slip. Raleigh and Everden (1981), assuming no transport of fluid or heat, calculated the maximum fluid pressure increase for various displacements, displacement velocities, and fault zone widths. They used these calculations as evidence for low ambient shear stresses in the crust.

While these studies have served to illustrate pertinent features of the response, they have considered only a fault zone of constant width and fixed strain rate, for the following two limiting cases: those cases where the fluid transport is so large it nullifies thermal pressurization, and those cases where the transport of heat or fluid, or both, are so small they can be neglected. In addition, changes in the

pore-dilatation rate during slip have not been considered. For these cases, it is possible to analyze the system using simple analytical models. For intermediate conditions, these studies do not provide an adequate description of the transient increase in temperature within a fault zone during slip, and its effect on the fluid pressure and stress fields.

By assuming a friction law to describe the shear stress required for slip, it is not possible to examine the evolution of inelastic deformation across a fault zone. Since this law describes only the gross resistance between two sliding surfaces, the shear stress is only influenced by the effect that the strain rate has on the rate of heat generation and, consequently, on the fluid pressure and effective stress. This approach decouples the equations describing motion within a fault zone from the equations describing the fluid pressure and temperature. Thus it is necessary to make *a priori* assumptions about the width of deformation and the strain rate across the fault zone to calculate the fluid-pressure and temperature fields. In order to solve for deformations a rheological law is needed to define the way in which shear stress is related to strain rate, effective stress, and temperature for the material within a fault zone. By considering the rheology of fault-zone material, no arbitrary assumptions are invoked with respect to any of its mechanical characteristics.

For the purposes of this thesis a fault zone is defined as a region of intensely deformed material that is flanked on both sides by relatively undeformed material. The fault zone, perhaps a few centimeters to tens of meters wide, undergoes strains that are finite and largely irrecovable. The surrounding crustal rocks experience infinitesimal strains which store the elastic energy that has risen slowly because of long-term tectonic movement. During deformation this strain energy is primarily released by transfer to the fault zone where it is dissipated into heat and the kinetic energy of motion. Because deformation may not occur across the entire fault zone, a distinct fault zone boundary is an artifice. Conceivably the boundary will vary both in time and space. During slip, deformation across the fault zone resembles the flow of a viscous fluid under an applied shear stress. In this case, inelastic shear deformations dominate the elastic response and the fault zone can be described with a rheology that is dependent on the effective stress and temperature. For a constant shear stress, this formulation implies that fault material behaves as a visco-plastic material which at failure yields and undergoes inelastic deformation.

Such fluid-mechanical formulations exist for non-porous, single-constituent materials with a temperature-dependent rheology. Turcotte and Oxbaugh (1968) modeled the deep structure of dip-slip fault zones using a fluid dynamical theory which included shear heating and a temperature-dependent rheology. Sukanek and Laurence (1974)

discussed the rate of heat dissipation within some simple shear flows. Yuen *et al.* (1978) presented a time-dependent analytical model of temperature, velocity, viscosity, and shear stress in a fault zone. For their analysis a kinematic model was adopted where the relative slip velocity across the zone is constant. Because their model consisted of two-half spaces sliding past each other on a thin planar surface, it is independent of the style of faulting. The model was applied to a hypothetical fault zone, and to fault zones located along descending oceanic slabs and along major transform faults. They showed that an initially planar fault zone would widen as slip progresses, eventually stabilizing at a width that is dependent on the ambient temperature conditions. The maximum temperatures associated with shear heating were always less than those required for partial melting. They concluded that thermomechanical coupling, through shear heating, a strongly temperature-dependent viscosity and the diffusion of heat, are the principal factors controlling fault zone structure. Similiar results have been obtained by Fleitout and Froideaux (1979), Lockett and Kusznir (1982), and Brun and Cobbold (1982).

These studies on deformation across a fault zone have also neglected the presence and possible effect of pore waters. If pore waters are present, thermal pressurization can cause the porous medium to loose cohesion, promoting a net reduction in the shear strength of the region adjacent to the failure surface. This loss of shear strength could cause an

initially planar zone to broaden as slip progesses. Conversely, an initially broad zone would tend to contract about the region where the initial strain rate and, consequently, fluid pressure and temperature rise happened to be the greatest. Whether or not the zone will widen (or contract) to halt (or enhance) the thermal pressurization process, or stabilize at a certain width and shear strength, depends upon the rheological relation which links the shear strength to the deformation rate, effective stress and temperature.

Currently, very little is known about the rheological behavior of a fault zone at any depth. For disaggregated fault gouge it is probable the rheology would follow a friction law behavior; that is the shear strength approaches zero as the fluid pressures appoach lithostatic values (e.g., Handin *et al.*, 1963; Jaeger and Cook, 1969; Savage, 1977; Lachenbruch, 1980; Hanes and Inman, 1985). It is assumed that the shear stress required for slip across the fault is given by the friction law

$$\tau_r = \mu_d(\tau_n - P) \qquad (1.1)$$

where τ_r is the resistive shear stress, μ_d is the dynamic coefficient of friction, τ_n is the total normal stress acting across the fault, and P is the pore-fluid pressure. A principal motivation for using this law is its wide-spread applicability in describing the results of laboratory

experiments for a variety of rock types. For most rocks μ_d is insensitive to composition and hardness, and has values between 0.4 and 1.0 (Byerlee, 1978). For surfaces separated by a thin clay-rich layer of fault gouge, Morrow *et al.* (1982) reported values for μ_d that ranged from 0.2 to 0.6. In general, the coefficient of friction is dependent on the effective normal stress and deformation history of the fault zone (e.g., Dietrich, 1979a, 1979b; Rice, 1983; Ruina, 1983, 1984; Rice and Tse, 1986). Because this law describes the gross resistance between two sliding blocks, the shear stress is influenced only by the effect that frictional heating has on the fluid pressure and slip rate. This approach decouples the equations describing motion within the fault zone from the equations describing fluid pressure and temperature. Thus it is not possible to examine the evolution of inelastic deformation, and *a priori* assumptions about the width of deformation and the strain rate across the zone must be made to calculate the fluid-pressure and temperature fields. Whatever the rheological relation may be, however, it is likely that it follows a friction law behavior (1.1). If that were so, then initially broad zone would tend to contract about the plane where the fluid pressure rise was the greatest. Without a rheological law relating the shear strength to effective stress, temperature and deformation rate, it is simply noted when these calculations imply that deformation would expand or contract about the edges of the zone.

Thermal pressurization has been considered in several other geologic situations. Habib (1976), Voight and Faust (1982), and Anderson (1980) examined frictional heat generation within the fluid-saturated basal zones of large landslides. Modeling of this problem resembles the analysis of of pore-pressures changes due to fault generated frictional heating. Barker (1972) and Bradley (1972) examined thermal pressurization within an isolated volume of sediments that are subjected to a temperature rise during burial. Domenico and Palciauskas (1979a; 1979b) examined how high geothermal gradients in combination with a rapid rate of sedimentation could lead to excess pore pressures. They showed that thermal pressurization of pore fluids could be of a sufficient magnitude to initiate inelastic deformation, and thereby, the development of fracture porosity in compacting basins. Palciauskas and Domenico (1982) examined the hydromechanical response of crystalline rock to heating, and showed that the response can be characterized by the four isothermal elastic parameters of Biot (1941), in combination with nonisothermal parameters related to the fluid and solid phases, and the thermal expansivity of the medium. Delaney (1982) carried out a detailed analysis of fluid flow and heat transfer induced by heating along the contact with a planar intrusion. Parameter values for material properties were identified for which substantial increases in pore pressures could be generated.

The objectives of this thesis are threefold. First, the equations governing fluid pressure, temperature, and stress

are developed to explicitly include expansion or contraction of the fluid and solid phases due to changes in fluid pressure and temperature. This development is necessary to examine the parameters that govern the rate of fluid pressurization and pore dilatation due to an arbitrary rise in temperature, and to examine their critical range of values where thermal pressurization is significant. Second, using both analytical and numerical models, an examination was made of how the thermal expansion of pore fluids due to frictional heating on a fault surface affects the temperature and dynamic shear strength of the fault during slip. Third, this model is expanded to account for fault zones of finite width and a variable resistive stress. The aim of this thesis is to examine the full nonlinear behavior of fault motion, and to determine limits to fault behavior for various ranges of the controlling parameters. Generalizations are formed describing the importance of thermal and hydrologic effects during fault motion, dimensionless measures of their importance, and characteristics time scales for thermal pressurization. In addition, an examination is made of how thermal pressurization affects the shear strength of the adjacent medium and thereby the style of deformation. The results are independent of the style of faulting and can be applied to strike-slip, thrust and normal fault zones. The analysis presented here removes some of the limitations of previous studies, and develops a better understanding of the role of frictional heating and thermal pressurization in the physics of fault zone processes.

The text of this thesis is divided in three main parts. Each part consists of a paper written to be published in a scientific journal. Consequently, each chapter is self-contained, with an introduction, text, appendices, references, tables, and figures.

Chapter II outlines the derivations of the field equations and discusses the material properties that are necessary for a quantatitive study of fault processes. The theory in Chapter II is not new. The purpose of the derivations is four fold. First, the requirement for conservation of solid mass is used to develop a compatibility constraint for porosity. This constraint determines the pore-dilatation rate arising from deformations caused by changes in pore-fluid pressure, temperature and total stresses. Second, the fluid flow equation is developed to explicitly include expansion or contraction of the fluid phase due to changes in fluid pressure and temperature. This development is necessary to examine the parameters that govern the rate of fluid pressurization due to an arbitrary rise in temperature and examine their critical range of values where thermal pressurization is significant. Third, previous studies for porous media have assumed that the rate of heat generation due to mechanical work is negligible. For fault processes, however, a significant amount of heat can be generated by mechanical deformation of the solid matrix. Consequently, mechanical forms of energy must be considered. Fourth, the equations set out here form the foundation for examining the

thermal, hydrologic and mechanical response of a fault zone during deformation. These equations are developed in three dimensions, however, in Chapters III and IV the fault zone is assumed to deform by simple shear. In this case, heat and fluid flow occur at right angles to the centerline of the faiult zone. Thus only the one-dimensional forms of these equations are used in subsequent chapters.

In Chapter III, the effects of frictional heating and fluid flow on the thermal, hyrologic, and mechanical response of a fault surface are examined. The results of this chapter illustrate how the effects of heat transfer and fluid flow influence the thermohydromechanical response of a fault surface during slip, and lead to the following conclusions:

i) For rigid media with low permeability, only a small temperature increase is required for the thermal expansion of pore fluids to pressurize the fluids and to maintain the fluid pressure on the fault surface at near-lithostatic values. This result is in agreement with the earlier analysis by Lachrnbruch (1980). For media with greater permeabilities or porous medium compressibilities, or both, large temperature rises are required on the fault surface for the thermal pressurization of pore fluids to overcome fluid losses due to fluid flow or fluid-volume changes due to pore dilatation, or both. Temperatures on the fault plane stabilize at the point where there is a dynamic balance between the temperature and pressure fields, with the increase in fluid volume due to

thermal expansion equal to fluid loss due to flow and fluid-volume changes due to pore dilatation.

ii) The dynamic shear strength remains close to its initial value until the fault surface is heated to a temperature required for thermal expansion of pore fluids to exceed substantially fluid losses due to flow and fluid-volume changes due to pore dilatation. Once this condition is established, the shear strength diminishes rapidly to a value sufficient to maintain the thermal pressurization process. For media with greater permeability or compressibility, or both, the shear strength will remain close to its initial value over greater displacements. If either the permeability exceeds 10^{-15} m^2 or the porous medium compressibility exceeds 10^{-8} Pa^{-1}, then frictional melting may reduce the dynamic shear strength before the effects of thermal pressurization become significant.

iii) The main effect of varying the depth to the fault surface is to change the initial conditions at the onset of slip. Because increases in the initial effective stress lead to an increase in the maximum fluid pressure, the temperature required to sustain fluid pressures at near-lithostatic values depends on the initial effective stress. If fluid pressures are initially hydrostatic, then the final temperature attained on the fault surface increases with depth. However, because the transient rate of decrease of the shear strength depends primarily on the material properties of the porous medium, and on the coefficent of friction and the slip velocity on the

fault surface, changes in initial conditions do not significantly change the rate of decrease in shear strength.

iv) The coefficient of friction and slip velocity determine the rate at which thermal pressurization proceeds, but not the final outcome. However, if the coefficient of friction is less than 10^{-1} and if the slip velocity is less than 10^{-2} ms^{-1}, then it is doubtful that either thermal pressurization or frictional melting could reduce the dynamic shear strength of the fault surface. In these conditions frictional heating is small, and the temperature rise would be minimal for an earthquake event with realistic displacement.

Chapter IV examines the effect of fault width, the dynamics of a variable resistive stress, and the physical parameters that control the thermal and hydrologic fields. A one-dimensional model is formulated for an earthquake which incorporates the effects of frictional heating on the thermal, hydrologic, and mechanical response of a fault. This model has been used to examine the parameters that control the fault response, and to determine their critical range of values where thermal pressurization is significant. In addition, an important parameter, the thermal pressurization coefficient, is discussed. This parameter controls the rates of pore dilatation and fluid pressurization due to a temperature rise. The main conclusions of this chapter are:

i) Motion of the fault blocks can be characterized by two time scales, a characteristic slip duration for the release of

elastic strain energy and a characteristic time for thermal pressurization due to frictional heating. These time scales depend primarily on the fault geometry, and the hydraulic characteristics of the fault zone and adjacent medium. Because of the wide variations in these parameters, a wide variety of fault behavior is possible.

ii) For earthquakes occurring across narrow zones comprised of stiff material with low permeability ($<10^{-18}$ m^2), the characteristic time for thermal pressurization is much less than the characteristic slip duration. Consequently, during slip the resistive stress decreases more rapidly than the shear stress applied by the elastic region, and the fault blocks rapidly accelerate. This behavior would lead to earthquakes of relatively short durations with large stress drops, accelerations and displacements, and provide an explanation for strong motions.

iii) For earthquakes occurring across zones where shear strains are less than one, or the porous medium compressibility and permeability exceeds 10^{-8} Pa^{-1} and 10^{-14} m^2, the characteristic time for thermal pressurization is much greater than the slip duration. Because thermal pressurization would be negligible, the fault would retain its initial shear strength and resist further motion. This behavior would lead to earthquakes with relatively small stress drops, accelerations and displacements, and provide an explanation for the presence of barriers along faults.

iv) The style of deformation across a fault zone may be controlled by the hydraulic characteristics of the zone and adjacent wall rock. If the hydraulic diffusivity of the wall rock is greater than that of the fault zone, deformation would tend to contract about the central region where the fluid pressure rise and, consequently, the decline in shear strength is greatest. In this case it is not unreasonable to expect very narrow deformation zones for large earthquakes. Conversely, if the hydraulic diffusivity of the wall rock is less than that of the zone, the wall rock acts to confine the excess fluid pressure within the zone. In this case the diffusion of excess pore pressures from the fault could cause a progressive weakening of the adjacent wall rock, and thereby a widening of the deformation zone.

v) The spatial variations in fault width and hydraulic characteristics could readily explain a heterogenous stress drop, and thereby an irregular rupture propagation and slip rate over the fault. Because these parameters can endure through many earthquake cycles, earthquakes recurrent on a given fault may have the same set of characteristic displacements and magnitudes. Variations within the set would depend on the relative magnitudes of the fault length, and the characteristic length scales for the fault width and hydraulic characteristics. If the characteristic length scales for these parameters are much less than the fault length, then variations in the displacements and magnitudes would be large. If, however, the characteristic length for these parameters is

on the order of the fault length, then the fault block model would apply and the variations would be small. This scale dependency would conform to the frequency-magnitude relations observed for many faults (e.g., Nur, 1978; Aki 1984; Stuart *et al.*, 1985). Thus the spatial distribution of these parameters may play an important role in the dynamics and statistical characteristics of earthquakes.

The results of this thesis suggest that the nature of fault motion depends critically upon the characteristic time scales for thermal pressurization and slip duration. In turn, these parameters depend upon the fault geometry, and the hydraulic characteristics of the fault zone and the adjacent medium. Because of the wide variations possible in these parameters, a wide variety of fault behavior is possible. Knowledge of these parameters appears essential to understanding the dynamics of fault motion, and to open the possibility of quantitative prediction of earthquake behavior.

CHAPTER II

FIELD EQUATIONS

A quantitative framework for studying fault processes can be built on the differential equations describing conservation of mass, energy, and momentum. The development of these equations in porous media requires a continuum approach where the solid and fluid phases are regarded as coexisting continua, with the field variables and medium parameters representing average values over a representative elementary volume of the porous medium. This approach is justified provided that the pore spaces and fractures through which the flow takes place are much smaller than the distance over which there is a resolvable change in fluid pressure, temperature and stress.

The theory presented here is not new. The heat-transfer equations for a fluid continuum (e.g.; Landau and Lifshitz, 1959; Slattery, 1972; White, 1974; Plattern and Legros, 1984) and a thermoelastic solid continuum (e.g.; Nowacki, 1975; Nowinski, 1978) are well known. For porous media numerous papers on heat and mass transfer can be found in the literature (e.g.; Stallman, 1960, 1963; Brownell *et al.*, 1977; Faust and Mercer, 1979; O'Neil and Pinder, 1981; Bear and Corapcioglu, 1981; Sharp, 1983). For isothermal flow Biot (1941), Cooper, 1966; De Weist (1966), Bear (1972), and Rice and Cleary (1976) have examine deformation of porous media due

to changes in effective stress. Detailed and extended discussions can be found in the work by Bear (1972). The purpose of the derivations presented here is four fold. First, we shall use the requirement for conservation of solid mass to develop a compatibility constraint for porosity. This constraint determines the pore-dilatation rate arising from deformations caused by changes in pore-fluid pressure, temperature and total stresses. Second, the fluid flow equation is developed to explicitly include expansion or contraction of the fluid phase due to changes in fluid pressure and temperature. This development is necessary to examine the parameters that govern the rate of fluid pressurization due to an arbitrary rise in temperature and examine their critical range of values where thermal pressurization is significant. Third, previous studies for porous media have assumed that the rate of heat generation due to mechanical work is negligible. For fault processes, however, a significant amount of heat can be generated by mechanical deformation of the solid matrix. Consequently, mechanical forms of energy must be considered. Fourth, the equations set out here form the foundation for examining the thermal, hydrologic and mechanical response of a fault zone during deformation. These equations are developed in three dimensions, however, in subsequent chapters we assume that heat and fluid flows only at right angles to the failure surface. Thus only the one-dimensional forms of these equations are used in subsequent chapters.

Two different methods are widely used to describe the mechanics of motion in a continuum. The first is the Eulerian approach where motion is described with respect to a fixed spatial reference frame. The second is the Lagrangian approach where the history of a particular particle, or group of particles, that is specified by its original position at some reference time is followed. Because we wish to express fluid and heat motion in terms of volume-averaged fluxes and have little interest in describing them as particle displacement fields, the Eulerian approach has the advantage of allowing one to work with independent variables that are natural for interpreting fluid and heat transport. For this reason the differential equations for conservation of mass, energy, and momentum are conceptually simpler to develop using an Eulerian description. That is the framework we shall adopt for their development. For solution of the field equations, however, it is mathematically simpler to use a Lagrangian description to characterize the deformations of the solid matrix. That is the framework we shall adopt when solving the field equations.

All equations in this chapter, and subsequent chapters, are developed with respect to a Cartesian coordinate system (x_1, x_2, x_3). In addition, boldface symbols are used to indicate vector fields (e.g., $\mathbf{U}_s$, $\mathbf{V}_f$), the tilde to denote tensor fields (e.g., $\tilde{\mathbf{k}}$, $\tilde{\tau}$), and subscripts to designate vector and tensor components (e.g., V_{s_i}, τ_{ij}). The gradient operator ∇ is defined as $\partial/\partial x_i \hat{\mathbf{x}}_i$, where the circumflex is used to denote a

unit vector. Scalar products are given as $\nabla \cdot \mathbf{V}_f$. Overdots are used to indicate time derivatives (e.g., $\dot{e}_{ij} = d_s e_{ij}/dt$). The summation convention for repeated subscripts is followed throughout (e.g., $e_{ii} = e_{11}+e_{22}+e_{33}$), and frequent use is made of the Kronecker delta function δ_{ij}, where $\delta_{ij}=0$ for $i \neq j$ and $\delta_{ij}=1$ for $i=j$.

CONSERVATION OF SOLID MASS

The Eulerian form of the mass balance equation for the solid phase of a porous medium is given by

$$\nabla \cdot [(1-n)\rho_s \mathbf{V}_s] + \frac{\partial}{\partial t}[(1-n)\rho_s] = 0 \qquad (2.1)$$

where $\mathbf{V}_s$ is the velocity vector for the solid matrix with respect to a fixed coordinate system, ρ_s is the density of the solid phase, and n is porosity. Employing the Eulerian form of the material derivative for following the motion of the solid matrix, defined as

$$\frac{d_s}{dt} = \frac{\partial}{\partial t} + \mathbf{V}_s \cdot \nabla \qquad (2.2)$$

yields the following form of the continuity equation:

$$\frac{1}{(1-n)} \left(\frac{d_s}{dt} n\right) = \nabla \cdot \mathbf{V}_s + \frac{1}{\rho_s} \left(\frac{d_s}{dt} \rho_s\right) \qquad (2.3)$$

Because the density of the solids is related to temperature

and pressure we may decompose the second term on the righthand side to obtain

$$\frac{1}{\rho_s}\frac{d_s}{dt}\rho_s = \frac{1}{\rho_s}\frac{\partial}{\partial\bar{\tau}}\rho_s\Big|_T \frac{d_s}{dt}\bar{\tau} + \frac{1}{\rho_s}\frac{\partial}{\partial T}\rho_s\Big|_{\bar{\tau}} \frac{d_s}{dt}T \qquad (2.4a)$$

$$= \beta_s \frac{d_s}{dt}\bar{\tau} - \gamma_s \frac{d_s}{dt}T \qquad (2.4b)$$

where β_s and γ_s represent the coefficients of isothermal volumetric compressibility and isobaric volumetric thermal expansivity of the solid phase, respectively, $\bar{\tau}$ is the average value of effective normal stress acting on the solid grains, and T is temperature.

Combining equations (2.3) and (2.4) yields the following compatibility equation for porosity:

$$\frac{d_s}{dt}n = (1-n)\left[\nabla\cdot\mathbf{v}_s + \beta_s \frac{d_s}{dt}\bar{\tau} - \gamma_s \frac{d_s}{dt}T\right] \qquad (2.5)$$

where $\nabla\cdot\mathbf{v}_s$ represents the volumetric dilatation rate ($d_s e/dt$), which is a function of the evolving stress field and the constitutive equations relating stress to strain rate (Biot, 1941; De Wiest, 1966; Rice and Cleary, 1976). Equation (2.5) states that the pore-dilatation rate ($\partial n/\partial t$) is given by the rate at which solids are leaving a unit volume minus the rate at which they are expanding due to decreases in the average effective normal stress or increases in the temperature within

the volume. Equation (2.5) provides an important relationship for determining the change in porosity due to deformations induced by changes in effective stress and temperature. The inclusion of this porosity constraint is necessary because a porous medium is not a simply connected body; it is a multiply connected body with cavities. These cavities represent porosity, and they may either increase or decrease in volume as deformation progresses.

CONSERVATION OF FLUID MASS

Assuming the pores are fully saturated with a single phase fluid, and that the solid and fluid phases are mechanically separate and distinct, the Eulerian form of the fluid mass balance equation is

$$\nabla\cdot(n\rho_w\mathbf{V}_f) + \frac{\partial}{\partial t}(n\rho_w) = 0 \qquad (2.6)$$

where $\mathbf{V}_f$ is the pore-fluid velocity with respect to a fixed coordinate frame (Eulerian coordinates), and ρ_w is the density of water. Because we wish to express fluid velocity in terms of the volume-flux density (Darcy flux)

$$\mathbf{q}_f = n(\mathbf{V}_f - \mathbf{V}_s) \qquad (2.7)$$

defined as the relative flux of pore fluids with respect to the solid matrix, we rewrite equation (2.6) as

$$\nabla\cdot[n(\mathbf{V}_f-\mathbf{V}_s)] + n\nabla\cdot\mathbf{V}_s + \frac{d_s}{dt}n + \frac{n}{\rho_w}\frac{d_f}{dt}\rho_w = 0 \qquad (2.8)$$

where

$$\frac{d_f}{dt} = \frac{\partial}{\partial t} + \mathbf{V}_f\cdot\nabla \qquad (2.9a)$$

$$= \frac{d_s}{dt} + \frac{\mathbf{q}_f}{n}\cdot\nabla \qquad (2.9b)$$

is the Eulerian form of the material derivative for following the motion of the pore fluid. Substitution of the pore-dilatation rate (2.5) into equation (2.8) yields the Eulerian form of the mass-balance equation

$$\nabla\cdot\mathbf{q}_f + \nabla\cdot\mathbf{V}_s + (1-n)\left(\beta_s\frac{d_s}{dt}\bar{\tau} - \gamma_s\frac{d_s}{dt}T\right) + \frac{n}{\rho_w}\frac{d_f}{dt}\rho_w = 0 \qquad (2.10)$$

Because the density of water is related to fluid pressure and temperature through equations of state, we may decompose the last term of equation (2.10) to obtain

$$\frac{n}{\rho_w}\frac{d_f}{dt}\rho_w = n\left(\frac{1}{\rho_w}\frac{\partial}{\partial P}\rho_w\Big|_T\frac{d_f}{dt}P + \frac{1}{\rho_w}\frac{\partial}{\partial T}\rho_w\Big|_P\frac{d_f}{dt}T\right) \qquad (2.11a)$$

$$= n\left(\beta_w\frac{d_f}{dt}P - \gamma_w\frac{d_f}{dt}T\right) \qquad (2.11b)$$

where β_w and γ_w are the coefficients of isothermal volumetric

compressibility and isobaric thermal expansivity for water, respectively, P is the pore-fluid pressure, and T is temperature. Equation (2.11) shows that increased pore pressure compresses fluid into the pores, while increased temperature expands fluid out of the pores.

Combining equations (2.10) and (2.11), and expanding the material derivative with respect to the fluid, yields the final form of the continuity equation for fluid mass in Eulerian coordinates,

$$-\nabla\cdot\mathbf{q}_f - \mathbf{q}_f\cdot(\beta_w\nabla P - \gamma_w\nabla T) + [n\gamma_w + (1-n)\gamma_s]\frac{d_s}{dt}T = \nabla\cdot\mathbf{v}_s + \left[n\beta_w\frac{d_s}{dt}P + (1-n)\beta_s\frac{d_s}{dt}\bar{\tau} \right] \qquad (2.12)$$

The terms on the lefthand side are, in order, the rate of fluid transport, the change in fluid mass due to pressure contraction or thermal expansion of fluids along the flow path, and the change in fluid mass due to the difference in thermal expansivities of the fluid and solid phases. The terms on the righthand side are the change in fluid mass due to volumetric dilatation of the porous medium, and the change in fluid mass due to the difference in the compressibilities of the fluid and solid phases or changes in total stress. We can see from the last term on the lefthand side that changes in temperature act as a source of fluid. In particular, increases in temperature will expand fluid out of the pores and tend to

increase fluid pressure, while decreases will contract fluid into the pores and tend to decrease fluid pressures. Because the thermal expansion of water is large, a temperature increase can cause a significant increase in fluid pressure. For isothermal conditions and incompressible solid grains, equation (2.12) takes the familiar form of Biot's (1941) equation.

Equation (2.12) is completed by expression of the volume-flux density (Bear, 1972)

$$\mathbf{q}_f = -\frac{\tilde{\mathbf{k}}}{\mu_w} \cdot (\nabla P + \rho_w \mathbf{g}) \qquad (2.13)$$

where $\tilde{\mathbf{k}}$ is the permeability tensor of the porous medium, μ_w is the dynamic viscosity of water, and $\mathbf{g}$ is the gravitational acceleration field. The form of equation (2.13) reflects the assumption that there will be no fluid flow when the pressure gradient is hydrostatic (i.e., $\nabla P = -\rho_w \mathbf{g}$). For equation (2.13) to be valid fluid flow through the pores must be laminar. This constraint is satisfied provided that inertial forces and slip phenomena are negligible, and the Reynolds number for fluid flow is small (i.e., $Re = d\rho_w |\mathbf{q}_f| / n\mu_w << 1$, where d is a characteristic grain diameter).

HEAT TRANSFER EQUATION

The Eulerian form of the energy balance equation for a saturated porous medium is

$$\nabla\cdot[\mathbf{q}_h + n\rho_w\mathbf{V}_f\epsilon_f + (1-n)\rho_s\mathbf{V}_s\epsilon_s] + \frac{\partial}{\partial t}[n\rho_w\epsilon_f + (1-n)\rho_s\epsilon_s] =$$

$$\tilde{\tau}'\cdot\nabla\mathbf{V}_s + \mu_w\Phi + \frac{nP}{\rho_w}\frac{d_f}{dt}\rho_w \qquad (2.14)$$

where $\mathbf{q}_h$ is the conductive heat-flux vector, ϵ_f and ϵ_s represent the internal thermal energy of the fluid and solid phases, respectively, $\tilde{\tau}'$ is the total stress tensor, and Φ is a viscous dissipation function for the fluid. For details on the development of equation (2.14) see Appendix 2A. In equation (2.14) thermal forms of energy appear on the lefthand side and mechanical forms of energy on the righthand side. The terms on the lefthand side are, in order, the rate of heat transport by conduction and convection of the fluid and solid phases, and the rate of internal heat storage in the fluid and solid phases. The terms on the righthand side are the rate of heat generation due to deformation of the solid matrix, viscous heat dissipation within the pore fluids, and the rate of heat addition due to pressurization of the pore fluids.

Applying the chain rule to the lefthand side we can rewrite equation (2.14) as

$$\nabla\cdot\mathbf{q}_h + n\rho_w(\frac{\partial}{\partial t}\epsilon_f + \mathbf{V}_f\cdot\nabla\epsilon_f) + (1-n)\rho_s(\frac{\partial}{\partial t}\epsilon_s + \mathbf{V}_s\cdot\nabla\epsilon_s) +$$

$$\epsilon_f[\nabla\cdot(n\rho_w\mathbf{V}_f) + \frac{\partial}{\partial t}(n\rho_w)] + \epsilon_s\{\nabla\cdot[(1-n)\rho_s\mathbf{V}_s] + \frac{\partial}{\partial t}[(1-n)\rho_s]\} =$$

$$\tilde{\tau}' \cdot \nabla \mathbf{V}_s + \mu_w \Phi + \frac{nP}{\rho_w} \frac{d_f}{dt} \rho_w \qquad (2.15)$$

The last two expressions on the lefthand side are identically zero by the conservation equations for fluid and solid mass. Expressing the second and third terms on the lefthand side in terms of their respective material derivatives, equation (2.15) can be written as

$$-\nabla \cdot \mathbf{q}_h + \tilde{\tau}' \cdot \nabla \mathbf{V}_s + \mu_w \Phi + \frac{nP}{\rho_w} \frac{d_f}{dt} \rho_w = n\rho_w \frac{d_f}{dt} \epsilon_f + (1-n)\rho_s \frac{d_s}{dt} \epsilon_s \qquad (2.16)$$

We now replace the internal thermal energy of the fluid and solid phases with the enthalpy per unit mass of fluid h_f and solid h_s, where

$$h_f = \epsilon_f + \frac{P}{\rho_w} \qquad (2.17a)$$

$$h_s = \epsilon_s + \frac{\bar{\tau}}{\rho_s} \qquad (2.17b)$$

Using equation (2.17), the rate of change in internal energy is

$$\frac{d_f}{dt} \epsilon_f = \frac{d_f}{dt} h_f - \frac{1}{\rho_w} \frac{d_f}{dt} P + \frac{P}{\rho_w} \frac{1}{\rho_w} \frac{d_f}{dt} \rho_w \qquad (2.18a)$$

$$\frac{d_s}{dt}\,\epsilon_s = \frac{d_s}{dt}\,h_s - \frac{1}{\rho_s}\frac{d_s}{dt}\,\bar{\tau} + \frac{\bar{\tau}}{\rho_s}\frac{1}{\rho_s}\frac{d_s}{dt}\,\rho_s \qquad (2.18b)$$

These equations are a convenient form when solving problems that involve two phases (liquid and steam) of the fluid component (see e.g.; Faust and Mercer, 1979). Usually, however, we must write them in terms of temperature so that boundary conditions given in terms of temperature can be incorporated into the solution.

For a pure substance in the absence of surface tensions and motion, there are only two independent properties, pressure and temperature. Hence,

$$\frac{dh}{dt} = \left.\frac{\partial h}{\partial P}\right|_T \frac{dP}{dt} + \left.\frac{\partial h}{\partial T}\right|_P \frac{dT}{dt} \qquad (2.19)$$

Substituting the specific heat at constant pressure, defined as

$$c_p = \left.\frac{\partial h}{\partial T}\right|_P \qquad (2.20)$$

into equation (2.19) yields

$$\frac{dh}{dt} = \left.\frac{\partial h}{\partial P}\right|_T \frac{dP}{dt} + c_p \frac{dT}{dt} \qquad (2.21)$$

The first term on the righthand side can be evaluated by means of the thermodynamic relation

$$dh = Tds + \frac{dP}{\rho} \tag{2.22}$$

where s is entropy. We can rewrite this relation as

$$\frac{dh}{dP} = T\frac{ds}{dP} + \frac{1}{\rho} \tag{2.23}$$

We now apply this relation to a representative elementary volume at thermodynamic equilibrium. Since thermodynamic equilibrium implies constant temperature, equation (2.23) yields

$$\left.\frac{\partial h}{\partial P}\right|_T = \left.\frac{\partial s}{\partial P}\right|_T T + \frac{1}{\rho} \tag{2.24}$$

Recall from the Maxwell relations of thermodynamics that

$$\left.\frac{\partial s}{\partial P}\right|_T = \frac{1}{\rho}\left(\frac{1}{\rho}\frac{\partial \rho}{\partial T}\right) = -\frac{\gamma}{\rho} \tag{2.25}$$

where γ is the thermal expansivity of the material. Insertion of equation (2.25) into (2.21) yields the relationship for enthalpy as a function of pressure and temperature

$$\frac{dh}{dt} = c_p\frac{dT}{dt} + \frac{(1-\gamma T)}{\rho}\frac{dP}{dt} \tag{2.26}$$

Employing equation (2.26) we can rewrite the equations for the internal thermal energy of the fluid and solid phases as a function of pressure and temperature, where

$$\frac{d_f}{dt}\epsilon_f = c_w \frac{d_f}{dt} T - \frac{\gamma_w T}{\rho_w} \frac{d_f}{dt} P + \frac{P}{\rho_w}\left(\frac{1}{\rho_w} \frac{d_f}{dt} \rho_w\right) \tag{2.27a}$$

$$\frac{d_s}{dt}\epsilon_s = c_s \frac{d_s}{dt} T - \frac{\gamma_s T}{\rho_s} \frac{d_s}{dt} \bar{\tau} + \frac{\bar{\tau}}{\rho_s}\left(\frac{1}{\rho_s} \frac{d_s}{dt} \rho_s\right) \tag{2.27b}$$

where c_s and c_w are the isobaric specific heat of the solid and fluid phases, respectively. These equations indicate that the change in internal thermal energy is equal to the change in internal heat storage plus the rate of heat addition due to pressurization of the fluid or solid phase. In equation (2.27) local thermal equilibrium between the pore fluids and the solid grains is assumed. This approximation is satisfied if the pore spaces and fractures through which heat transport takes place are much smaller than the distance over which there is a significant temperature change. A significant temperature change may be 10^{-1} or 10 °C depending on the nature of the problem.

In applications to solid-earth physics the heat addition due to pressurization of the solid phase is likely to be unimportant. With that assumption, combining equations (2.16) and (2.27), and expanding the material derivatives for the convective terms we can rewrite the energy balance equation in terms of temperature as

$$-\nabla\cdot\mathbf{q}_h - [n\rho_w c_w \mathbf{V}_f + (1-n)\rho_s c_s \mathbf{V}_s]\cdot\nabla T +$$

$$\tilde{\tau}'\cdot\nabla\mathbf{V}_s + \mu_w\Phi + n\gamma_w T\frac{d_f}{dt}P = (\rho c)_{sf}\frac{\partial T}{\partial t} \qquad (2.28)$$

where $(\rho c)_{sf}$ is the heat capacity of the solid-fluid composite, defined as

$$(\rho c)_{sf} = n\rho_w c_w + (1-n)\rho_s c_s \qquad (2.29)$$

Because we need to express fluid motion in terms of the Darcy flux $\mathbf{q}_f$ we rewrite the convective terms of equation (2.28) as

$$[n\rho_w c_w \mathbf{V}_f + (1-n)\rho_s c_s \mathbf{V}_s]\cdot\nabla T =$$

$$\{\rho_w c_w[n(\mathbf{V}_f-\mathbf{V}_s)] + (\rho c)_{sf}\mathbf{V}_s\}\cdot\nabla T \qquad (2.30)$$

Replacing the convective terms of equation (2.28) with (2.30) and insertion of the Darcy flux yields

$$-\nabla\cdot\mathbf{q}_h - \rho_w c_w \mathbf{q}_f\cdot\nabla T + \tilde{\tau}'\cdot\nabla\mathbf{V}_s + \mu_w\Phi + n\gamma_w T\frac{d_f}{dt}P =$$

$$(\rho c)_{sf}\left(\frac{\partial T}{\partial t} + \mathbf{V}_s\cdot\nabla T\right) \qquad (2.31)$$

Expanding the material derivative using equation (2.9b), and noting that the term within the brackets on the righthand side can be written as the Eulerian form of the material derivative

of temperature with respect to the solid matrix, yields the final form of the equation describing heat transfer in Eulerian coordinates

$$-\nabla\cdot\mathbf{q}_h - \rho_w c_w \mathbf{q}_f\cdot\nabla T + n\gamma_w\left(\frac{d_s}{dt}P + \frac{\mathbf{q}_f}{n}\cdot\nabla P\right)T + \tilde{\tau}'\cdot\nabla\mathbf{v}_s + \mu_w\Phi = (\rho c)_{sf}\frac{d_s}{dt}T \qquad (2.32)$$

The terms on the the lefthand side are, in order, the rate of conductive heat transfer, the rate of convective heat transport by the fluid phase, the rate of heat addition due to pressurization of the pore fluid, heat generation due to deformation of the solid matrix, and viscous heat dissipation within the fluid. The righthand term represents the rate of internal heat storage and the rate of convective heat transport by the solid. For groundwater flow problems viscous heat dissipation within the fluid is negligible, provided that the conditions for use of the Darcy flux are satisfied (e.g.; Garg and Pritchett, 1977; Brownell *et al.*, 1977). Hence, we will neglect that term in subsequent use of the heat transfer equation. In Appendix 2B, we summarize the conditions where heat addition due to pressurization of the pore fluid is negligible.

Equation (2.32) is completed by expressing the conductive heat flux by Fourier's law

$$q_h = -\tilde{K}_{sf} \cdot \nabla T \tag{2.33}$$

where $\tilde{K}_{sf}$ is the thermal-conductivity tensor of the solid-fluid composite.

THE EQUATIONS OF MOTION

Deformation of the porous medium is governed by the effective stress τ_{ij} (Biot, 1941), which is defined as

$$\tau_{ij} = \tau'_{ij} - \xi P \delta_{ij} \tag{2.34}$$

where stresses are defined as positive when compressive, ξ is a proportionality constant between pore and bulk volume changes, and δ_{ij} is the Konecker delta function. This law states that the strain response of a saturated medium is identical to that of a solid continuum if one uses the effective stress τ_{ij} instead of the total stress τ'_{ij}. To apply equation (2.34) the effective stress is defined as an average over some finite area that is sufficient to cover a number of grains and pores. In addition, deformation of the porous medium can be described by the strain of the solid matrix e_{ij}.

From stress-strain measurements Biot and Willis (1957), and Nur and Byerlee (1971) have suggested that

$$\xi = \frac{k_{sf} - k_s}{k_{sf}} \tag{2.35}$$

where k_s and k_{sf} are the bulk moduli of the solid grains and porous medium, respectively. From equation (2.35), ξ is the ratio of fluid volume expelled to the volumetric dilatation for drained conditions at constant temperature. For media with appreciable porosity, $k_s/k_{sf}<<1$, with $\xi\simeq 1$, and the fluid volume expelled is equal to the volumetric dilatation. This is the conventional assumption in compaction theory. In this case, equation (2.34) reduces to Terzaghi's simple effective stress law.

The components of the total stress tensor τ'_{ij} at a point within the porous medium satisfy the equations of motion

$$\frac{\partial}{\partial x_j}\tau'_{ij} + \rho_{sf}F_i = \rho_{sf}\frac{d_s}{dt}V_{s_i} \qquad (2.36)$$

where **F** is the body force per unit mass, ρ_{sf} is the density of the solid-fluid composite, and the summation convention is invoked. Expressing equation (2.36) in terms of the effective stress yields

$$\frac{\partial}{\partial x_j}\tau_{ij} + \rho_{sf}F_i + \frac{\partial}{\partial x_i}(\xi P) = \rho_{sf}\frac{d_s}{dt}V_{s_i} \qquad (2.37)$$

If the effects of inertia are neglected, then equation (2.37) reduces to the well-known stress equlibrium equations for a porous media (Biot, 1941; Verruijt, 1969). Equation (2.37) alone is not sufficient to establish unique relations between stress, deformation rate, fluid pressure, and temperature. In

addition, some description of the medium which defines the way that stress is related to deformation, fluid pressure, and temperature is essential. Such a relation is expressed by the constitutive equations for the porous medium. The weakest link in the application of equation (2.37) is the constitutive equations relating stress to strain.

The strain response of a porous medium consists of both elastic and inelastic responses. For example, a fault zone consists of a region of intensely deformed material that is flanked on both sides by relatively undeformed material. The fault zone, perhaps a few centimeters to tens of meters wide, undergoes strains that are finite and largely irrecoverable. During deformation the fault zone behaves as a visco-plastic material. The surrounding crustal rocks, however, experience infinitesimal strains which store the elastic energy that has risen slowly because of long-term tectonic movement. During deformation this strain energy is primarily released by transfer to the fault zone where it is dissipated into heat and the kinetic energy of motion. Thus the region surrounding the fault zone behaves as a linear-elastic body. Because deformation may not occur across the entire fault zone, a distinct fault zone boundary is an artifice. Conceivably the fault-zone width and, consequently, the boundary between visco-plastic and elastic deformation will vary both in time and space. Furthermore, the fault-zone material may behave elastically in hydrostatic compression and as a viscous fluid in shear. In such a case, if the shear stress across the zone

exceeds the yield strength, the zone will constantly creep. Changes in fluid pressure, however, may cause an elastic consolidation or extension perpendicular to the zone.

For a thermoelastic porous medium the stress-strain relationships are

$$\tau_{ij} = C_{ijkl} e_{kl} + \gamma_{sf_{ij}} \Theta \tag{2.38}$$

where e_{kl} are the strains of the solid matrix, C_{ijkl} is a tensor of elastic coefficients, $\gamma_{sf_{ij}}$ are the thermal expansion coefficients of the solid-fluid matrix, and Θ is the incremental temperature increase from the initial value. In employing equation (2.38) we have assumed that these coefficients, which are strictly valid for a solid continuum, are also valid for a saturated porous medium. Thus the elastic coefficients represent coefficients of the porous medium to be determined experimentally. In general, they are dependent on total stresses, fluid pressure, and temperature. For a linear isotropic elastic medium equation (2.38) reduces to (after Biot and Willis, 1957)

$$\tau_{ij} = -(\lambda e_{kk}\delta_{ij} + 2\mu e_{ij}) + \frac{1}{(\lambda+2\mu)} \gamma_{sf} \Theta \delta_{ij} \tag{2.39}$$

where λ and μ are the Lame´ constants, and γ_{sf} is the volumetric thermal expansion coefficient of the porous medium. Note the sign change on the strain term in equation (2.39). This change arises because in equation (2.34) stresses were

defined as positive when compressive, that is, in the negative directions of the axes. To have solid-matrix displacements follow the convention that positive displacements correspond to positive stresses, displacements must be positive when in the negative direction. This is the conventional sign notation used in continuum (Jaeger and Cook, 1979, pg. 10). In the equations for pore dilatation, fluid flow, and heat transfer, however, displacements are positive in the positive directions of the axes. Thus to retain that convention the signs on the strain terms in equation (2.38) and the inertial terms in equations (2.36) and (2.37) have to be changed. This change of convention leaves all formulae unaltered, but when comparing displacements to stress it should be remembered that positive displacements correspond to decreases in the compressive stress. Using the relationship between the strain e_{ij} and the solid-matrix displacement $\mathbf{U}_s$

$$e_{ij} = \frac{1}{2}\left(\frac{\partial}{\partial x_i} U_{s_j} + \frac{\partial}{\partial x_j} U_{s_i}\right) \qquad (2.40)$$

equation (2.37) can be solved in terms of the solid-matrix displacements U_{s_i} (Biot, 1941; Verruijt, 1969; Rice and Cleary, 1976).

During slip, deformation within the fault zone resembles the flow of a viscous fluid under an applied shear stress. In this case, inelastic shear deformations dominate the elastic response and the porous medium can be described effectively as a viscous fluid. Thus deformations within a fault zone can be

described by a rheology that is dependent on the effective stress, deformation rate and history, and temperature. For constant shear stress, this formulation implies that fault material behaves as a visco-plastic material which at failure yields and undergoes deformation at a constant rate.

Such fluid-mechanical formulations exist for single-constituent, non-porous material with a temperature dependent rheology. For instance, thermal softening in ductile shear zones (Turcotte and Oxburgh, 1968; Yuen *et al.*, 1978; Fleitout and Froidevaux, 1980; Lockett and Kusznir, 1980; Brun and Cobbold, 1982), and asthenosphere and mantle convection (Weertman and Wertman, 1975; Melosh, 1976; Murrell *et al.*, 1976; Yuen and Schubert, 1979) have been described sucessfully with this formulation. These studies suggest that the behavior of porous media within the fault zone during slip under shear can be written in terms of a rheological law relating the deformation rate tensor $\dot{e}_{ij}$ to the effective stress:

$$\tau_{ij} = -(\kappa_{sf}\dot{e}_{kk}\delta_{ij} + 2\mu_{sf}\dot{e}_{ij}) \qquad (2.41)$$

where μ_{sf} and κ_{sf} are the dynamic and second coefficients of viscosity for the porous medium, respectively. Since κ_{sf} is associated only with volume expansion, it is customary to call it the coefficient of bulk viscosity. The terms μ_{sf} and κ_{sf} are analogous to the Lame´ coefficients μ and λ for linear elasticity. In general, the dynamic and bulk viscosities are non-linear functions of the deformation rate, effective

stress, and temperature. For example, as fluid pressures increase the effective stress decreases in compression promoting inelastic deformation mechanisms such as frictional sliding past grain boundaries and microcracking. If the fluid pressures approach lithostatic values, the solid grains will lose frictional cohesion and the shear strength will decrease. This behavior would be similiar to that of a material with a temperature dependent rheology (Weertman and Weertman, 1975; Yuen *et al.*, 1978). Using equations (2.40) and (2.41) the equations of motion can be solved in terms of the solid-matrix velocities V_{s_i}.

EULERIAN VERSUS LAGRANGIAN COORDINATES

In the previous sections the Eulerian approach has been used to discuss field variables (P, T, τ_{ij}, $\mathbf{V}_s$, and $\mathbf{U}_s$) as a function of position $\mathbf{x}$ and time t . The displacement $\mathbf{U}_s$ is taken to be the displacement of a solid particle at $\mathbf{x}$ and time t from its initial position at $\mathbf{x}_0$ and time t_0, and P, T, τ_{ij} and $\mathbf{V}_s$ to be the pore-fluid pressure, temperature, effective stress and solid-matrix velocity at $(\mathbf{x},t)$. Because we wish to express fluid and heat motion in terms of volume-averaged fluxes and have little interest in describing them as particle displacement fields, this approach offers the advantage of allowing one to work with independent variables that are natural for interpreting fluid and heat transport phenomena. This approach, however, has the disadvantage of cumbersome expressions for the rate of change of material properties with

respect to the solid matrix. For example, the solid-matrix velocity $\mathbf{V}_s$ at $(\mathbf{x},t)$ is difficult to express in terms of the solid-matrix displacement field $\mathbf{U}_s(\mathbf{x},t)$. Consideration of the distance traveled in time δt yields

$$V_{s_i}(\mathbf{x},t)\ \delta t \;=\; U_{s_i}(\mathbf{x}+\mathbf{V}_s\delta t\,,t+\delta t) \;-\; U_{s_i}(\mathbf{x},t) \tag{2.42}$$

Taking the Taylor series expansion of the first term on the righthand side, dividing by δt, and taking the limit as δt approaches zero yields the solid-matrix velocity

$$V_{s_i}(\mathbf{x},t) \;=\; \frac{\partial}{\partial t} U_{s_i}(\mathbf{x},t)\Big|_{\mathbf{x}} + V_{s_j}(\mathbf{x},t)\ \frac{\partial}{\partial x_j} U_{s_i}(\mathbf{x},t)\Big|_{t} \tag{2.43}$$

which is an implicit equation to be solved for $V_{s_i}(\mathbf{x},t)$, where components of $\mathbf{V}_s$ appear on both sides of the equation. One can readily see that insertion of equation (2.43) into the field equations will yield cumbersome expressions for the material derivative with respect to the solid matrix.

For numerical solution of the field equations, we adopt a Lagrangian description of the porous medium, where the features of the deformed solid matrix are described with respect to the original undeformed state. The distinction between Eulerian and Lagrangian approaches, however, is not necessary if the spatial variations in the pore-fluid pressure, temperature, and stress fields have length scales much greater than the magnitude of solid-matrix displacements.

In this case, it makes no practical difference whether a spatial gradient is evaluated at a fixed position (Eulerian) or for a solid-particle (Lagrangian). The Lagrangian description is now adopted because it yields simple relationships for the solid-matrix displacement, the material derivative with respect to the solid matrix, and the solid-matrix velocity, given as

$$\mathbf{U}_s(\mathbf{x}_s,t) = \mathbf{x}_s(t) - \mathbf{x}_{s_0}(\mathbf{x}) \tag{2.44a}$$

$$\frac{d_s}{dt} = \frac{\partial}{\partial t} \tag{2.44b}$$

$$\mathbf{V}_s(\mathbf{x}_s,t) = \frac{\partial}{\partial t}\,\mathbf{U}_s(\mathbf{x}_s,t) \tag{2.44c}$$

where $\mathbf{x}_{s_0}$ and $\mathbf{x}_s$ are the position of a particular solid particle at time $t=0$ and time t. Note that once the particle has been chosen and labeled, $\mathbf{x}_s$, $\mathbf{U}_s$ and $\mathbf{V}_s$ are functions of time only. Thus in Lagrangian coordinates the convective terms with respect to the solid matrix are dropped from the Eulerian forms. Furthermore, the Lagrangian approach has the advantage for following the history and process of deformation from the undeformed to the deformed state, whereas the Eulerian approach is most useful in removing the effects of deformation processes. For example, in the Lagrangian approach we allow the fault zone to deform and track the motion of the deforming solid-matrix as illustrated in Figure 2.1 for a fault zone where the deformations are described by progressive simple

shearing. For this illustration the solid-matrix displacement is measured with respect to the centerline of the fault zone and is constant for any line parallel to the centerline. From Figure 2.1 we can see that deformation of the porous medium produces a convection-like effect in the field variables and medium properties, and introduces moving boundary conditions. For simple shear within the fault zone, we assume that heat and fluid flow occurs at right angles to the centerline of the fault zone. Thus in subsequent chapters, we consider the one-dimensional problem, and model fluid and heat transport along a line perpendicular to the centerline of the fault zone.

LANGRANGIAN FORM OF THE FIELD EQUATIONS

We now summarize the Lagrangian form of the field equations. These equations are outlined below. All equations are expressed in a Lagrangian reference frame with respect to the solid matrix of the porous medium. The Lagrangian form of the heat transfer equation is obtained from the Eulerian form (2.32) by replacing the material derivative with respect to the solid matrix by equation (2.44b). Thus the equation describing the transient temperature distribution in a saturated porous medium is given by

$$\nabla\cdot(K_{sf}\nabla T) - \rho_w c_w \mathbf{q}_f\cdot\nabla T + n\gamma_w\left(\frac{\partial P}{\partial t} + \frac{\mathbf{q}_f}{n}\cdot\nabla P\right)T +$$

$$\tilde{\tau}'\cdot\nabla\mathbf{v}_s = (\rho c)_{sf}\frac{\partial T}{\partial t} \qquad (2.45)$$

The terms on the lefthand side of (2.45) are, in order, the rate of conductive heat transport, the rate of advective heat transport, the rate of heat addition due to pressurization of the fluid, and the rate of shear heating within the fault zone. The term on the righthand side represents the rate of internal heat storage. Local thermal equilibrium between the solid matrix and the fluid is assumed.

The Lagrangian form of the fluid flow equation is obtained form the Eulerian form (2.12) by replacing the material derivative with respect to the solid matrix by equation (2.44b). Thus the equation describing the transient fluid flow within a saturated porous medium is given by

$$\nabla\cdot\left[\frac{\tilde{\mathbf{k}}}{\mu_w}\cdot\nabla(P + \rho_w g)\right] + \mathbf{q}_f\cdot(\beta_w\nabla P - \gamma_w\nabla T) + [n\gamma_w + (1-n)\gamma_s]\frac{\partial T}{\partial t} =$$

$$\nabla\cdot\mathbf{v}_s + \left[n\beta_w\frac{\partial P}{\partial t} + (1-n)\beta_s\frac{\partial \bar{\tau}}{\partial t}\right] \qquad (2.46)$$

The terms on the lefthand side of (2.46) are, in order, the rate of fluid transport, the change in fluid mass due to pressure contraction or thermal expansion of fluids along the flow path, and the change in fluid mass due to the difference in thermal expansivities of the fluid and solid phases. The

terms on the righthand side are the change in fluid mass due to volumetric dilatation of the porous medium and the change in fluid mass due to the difference in the compressibility of the fluid and solid phases. For water the density ρ_w, compressibility β_w, thermal expansivity γ_w, and dynamic viscosity μ_w coefficients are strongly temperature dependent. This dependence is shown in Figure 2.2.

The Lagrangian form of the equations describing motion of the soild matrix is obtained form the Eulerian form (2.37) by replacing the material derivative with respect to the solid matrix by equation (2.44b). Thus the equations describing motion of the solid matrix are given by

$$\frac{\partial}{\partial x_j}\tau_{ij} + \rho_{sf}F_i + \frac{\partial}{\partial x_i}(\xi P) = -\rho_{sf}\frac{\partial}{\partial t}V_{s_i} \qquad (2.47)$$

where stresses are defined as positive when compressive and displacements are defined as positive in the positive directions of the axes. For equation (2.47), the solid matrix displacements and velocities are as given by equations (2.44a) and (2.44c).

In addition the porosity in equations (2.45) through (2.47) must satisfy the Lagrangian form of the compatibility equation:

$$\frac{\partial n}{\partial t} = (1-n)\left[\nabla\cdot\mathbf{v}_s + \beta_s \frac{\partial \bar{\tau}}{\partial t} - \gamma_s \frac{\partial T}{\partial t} \right] \qquad (2.48)$$

For these equations the dependent variables and media parameters represent average values over a representative elementary volume of the porous medium. As seen from above, the field equations governing heat transfer, fluid flow, and motion are coupled through the dependent variables of temperature and fluid pressure, the constitutive equations relating stress to solid-matrix displacement (or velocity), the compatibility equation for porosity, and the equations of state for water. These equations along with initial and boundary conditions provide the mathematical framework for studying the physics of fault zone processes.

TEMPERATURE AND PRESSURE DEPENDENT PARAMETERS

Solution of the field equations requires that the density, dynamic viscosity, thermal conductivity, and specfic heat of water be expressed as state functions of pressure and temperature. These properties are illustrated for pure water as a function of temperature for selected pressures in Figure 2.2. For the density of liquid water at tempertures less than the critical temperature (374.15 °C) the analytic expression of Myer *et al.* (1967) is used. The derivatives of density with respect to temperature and pressure for that region are obtained directly from differentiation of the analytic expression. For temperatures greater than the critical

temperature and for the steam field, the analytic expression of Keenan *et al.* (p. 128, 1978) is solved for density by means of a Newton-Raphson iterative technique. The iterative technique is employed until the normalized density change between sucessive iterations is less than a specified tolerance (10^{-7}). The compressibility and thermal expansivity are calculated using the finite-difference approximations:

$$\beta_w \simeq \frac{1}{\rho_w(P,T)} \frac{\rho_w(P+\Delta P,T) - \rho_w(P,T)}{\Delta P} \tag{2.49a}$$

$$\gamma_w \simeq \frac{-1}{\rho_w(P,T)} \frac{\rho_w(P,T+\Delta T) - \rho_w(P,T)}{\Delta T} \tag{2.49b}$$

where $\Delta P = 10^{-1}$ MPa, and $\Delta T = 10^{-2}$ °C for Figure 2. Once the density is determined for a specific temperature and pressure, the dynamic viscosity, thermal conductivity and specific heat are calculated as state functions of density and temperature using the analytic expressions given by Keenan *et al.* (p. 130, 1978) for isobaric specfic heat, Watson *et al.* (1981) for viscosity, and Kestin (1978) for thermal conductivity.

Figures 2.2a through 2.2f are useful for determining when the variations in the thermodynamic and transport properties of water are an important consideration in solution of the field equations. For example, for liquid water at temperatures less than 250 °C the variation in water properties with respect to pressure is negligible. For that temperature range we may treat the compressibility, specfic heat and thermal

conductivity as constants, and the density, thermal expansivity and viscosity as functions of temperature only. In such a case the simplified expressions of Sorey (1978) for density, and Huykorn and Pinder (1977) for viscosity could be used. In addition, if the change in temperature is not significant (<10%), then it is possible to linearize the equations by assuming constant water properties. If the temperatures exceed 250 °C, however, we can readily see from these figures that consideration of the variation in water properties with pressure and temperature is essential. For example, the compressibility of water can change by almost two orders of magnitude between 250 °C and 400 °C depending on pressure. While variations in other water properties are not as large, they are significant. Furthermore, the influence of pressure on water properties in this temperature range is quantitatively smaller than that of temperature but nonetheless it is far from negligible. For temperatures greater than 400 °C the influence of pressure is more important than that of temperature. A further evaluation of the effects of pressure- and temperature-dependent properties of water on the thermal convection of water in porous media is discussed by Straus and Schubert (1977).

Because the range of values for the density, compressibility, expansivity, thermal conductivity, and specific heat of the solid grains is considerably smaller than that of variations in water properties and the hydraulic characteristics of porous media, they are approximated as

constants. The thermal conductivity of the solid-fluid composite K_{sf} may be approximated by (Woodside and Messmer, 1961; Sass *et al.*, 1971)

$$K_{sf} = K_s^{(1-n)} K_w^{n} \tag{2.50}$$

where K_s and K_w are the thermal conductivity of the solid and water, respectively. In equation (2.50), the thermal conductivity of the solid matrix is assumed to be isotropic.

We finally need to describe the way in which permeability changes during deformation. Permeability is generally considered to be a function of effective stress and, to a lesser extent, temperature. Because there is no one permeability for a given temperature or effective stress, there exists no equation of state which relates them. It follows that a parameter must be determined which has a one-to-one correspondence with permeability. It seems reasonable that permeability should increase (or decrease) as porosity increases (or decreases). Numerous relations have been either proposed or derived (e.g.; Snow, 1968; Brace, 1977; Bear, 1979, p. 67; Bernabe *et al.*, 1982) to explain how porosity affects permeability. One such relationship is given by Walder and Nur (1984):

$$k = k_0 \frac{n^m - n_c^m}{n_0^m - n_c^m} \tag{2.51}$$

where k_0 is the initial value of permeability, n_0 is the initial value of porosity, n_c is the critical porosity for fluid flow, and m is some exponent. The advantage of this formulation is that as porosity becomes vanishingly small so does permeability. With m=3, Nur and Walder point out that equation (2.51) is similiar to the Kozeny-Carmen equation, which describes the relationship between k and n for some porous media. In cases where permeability is allowed to vary with effective stress and temperature equation (2.51) is used.

SUMMARY

The mathematical framework for modelling the evolution of temperature, fluid pressure, and deformation across a fault zone is complete. The field equations outlined above are complex and must be solved numerically in terms of the dependent variables temperature, fluid pressure and solid-matrix displacement (or velocity). For the Lagrangian approach there are both moving boundary conditions and a deforming grid. The numerical approach to solve the field equations is to use a finite element grid which deforms during simulation. The displacement $\mathbf{U}_s$ of any point in the grid is governed by the simultaneous solution of the field equations for temperture, porosity, fluid pressure, and motion. Large deformations and deformation rates can, therefore, be accomodated. This strategy is not perfectly general. There may be simulations which lead to unacceptable grid deformations, at which time rezoning of the grid is required. This solution

method enables the simulation of configurations where the character of the displacements cannot be specified conveniently beforehand.

To model temperature, fluid pressure, and stress within a fault zone during simple shear, we neglect the three-dimensional effects of inhomogeneities and assume that the transfer of fluid and heat occurs at right angles to the fault surface. In this framework the mathematical problem involves finding solutions to the one-dimensional equations describing heat transfer, fluid flow, and stress. This is the framework adopted in subsequent chapters.

APPENDIX 2A: DERIVATION OF THE EULERIAN FORM OF THE ENERGY EQUATION

In this appendix we will develop the differential equation describing heat transfer in a deforming porous medium. We start from the first law of thermodynamics and proceed to develop the Eulerian form of the energy equation where mechanical forms of energy are included. For this development we assume a continuum approach where the fluid and solid phases are regarded as coexisting continua, with the field variables and medium parameters representing average values over a representative elementary volume of the porous medium.

The differential equation describing energy transfer in a porous medium is a statement of the first law of thermodynamics. Its expression can be derived as soon as all forms of energy and work are listed. In mathematical terms the first law of thermodynamics, expressed as a time rate of change, is given by

$$\frac{d}{dt} U_T + \frac{d}{dt} U_K = \frac{dQ}{dt} + \frac{dW}{dt} \qquad (2.A1)$$

where U_T and U_K are the internal thermal and kinetic energy, respectively, Q the net rate of heat transfer into a volume, and W the rate of work done on the volume. No heat sources due to radioactive decay or chemical reactions are considered, and the energy consumed in creating new failure surfaces is

assumed to be negligible (see e.g.; Richards, 1976; Lachenbruch and Sass, 1980). Because the potential energy due to the presence of a body force (e.g. gravity) is considered to be the result of work done by the body force, it does not appear explicitly in equation (2.A1). In addition, stored strain energy is implicitly included in the coupling between the rate of work done on the volume and the equations of motion.

The rate at which the internal thermal energy of a fixed volume of porous medium changes can be expressed as

$$\frac{d}{dt} U_T = \frac{\partial}{\partial t} \iiint_v [n\rho_w \epsilon_f + (1-n)\rho_s \epsilon_s] dv \qquad (2.A2)$$

where ϵ_f and ϵ_s are the internal thermal energy per unit mass of the fluid and solid phases, respectively. The rate of change in kinetic energy within the volume is

$$\frac{d}{dt} U_K = \frac{d}{dt} \iiint_v [\tfrac{1}{2}\rho_{sf} \mathbf{V}_s \cdot \mathbf{V}_s + \tfrac{1}{2} n\rho_w (\mathbf{V}_f - \mathbf{V}_s) \cdot (\mathbf{V}_f - \mathbf{V}_s)] dv \qquad (2.A3)$$

where the second term within the brackets represents the excess kinetic energy of the fluid phase with respect to the motion of the solid matrix. The net rate of heat transfer into the volume is the sum of the conductive heat flux through the solid-fluid composite plus the convective flux of the fluid and solid phases. It can be expressed as

$$\frac{dQ}{dt} = -\iint_S [\mathbf{q}_h + n\rho_w \epsilon_f \mathbf{V}_f + (1-n)\rho_s \epsilon_s \mathbf{V}_s] \cdot \hat{\mathbf{n}} ds \qquad (2.A4)$$

where $\hat{\mathbf{n}}$ denotes a unit normal vector to the surface element ds. The divergence theorem permits the surface integral to be cast as a volume integral, giving

$$\frac{dQ}{dt} = -\iiint_V \nabla \cdot [\mathbf{q}_h + n\rho_w \epsilon_f \mathbf{V}_f + (1-n)\rho_s \epsilon_s \mathbf{V}_s] dv \qquad (2.A5)$$

The second term on the righthand side of equation (2.A1) represents the rate at which work is done by surface tractions and interior body forces in deforming the solid-fluid composite and in moving the fluid through the pores relative to the solid matrix. For the solid-fluid composite the force acting on a surface element and an interior volume element are, respectively,

$$\tilde{\tau}' \cdot \hat{\mathbf{n}} ds \qquad (2.A6a)$$

$$\rho_{sf} \mathbf{F} dv \qquad (2.A6b)$$

The rate of work is given by

$$(\tilde{\tau}' \cdot \hat{\mathbf{n}} ds) \cdot \left(\frac{d}{dt} \mathbf{x}_s\right) \qquad (2.A7a)$$

$$(\rho_{sf} \mathbf{F} dv) \cdot \left(\frac{d}{dt} \mathbf{x}_s\right) \qquad (2.A7b)$$

where $\mathbf{x}_s$ is the position of a particular solid-matrix particle at time t. Hence, the rate at which work is done on the

solid-fluid composite of the volume is

$$\frac{d}{dt} W_{sf} = \iint_S (\tilde{\tau}' \cdot \mathbf{V}_s) \cdot \hat{\mathbf{n}} ds + \iiint_v \rho_{sf} \mathbf{F} \cdot \mathbf{V}_s dv \qquad (2.A8)$$

Applying the divergence theorem to the surface integral we obtain

$$\frac{d}{dt} W_{sf} = \iiint_v [\nabla \cdot (\tilde{\tau}' \cdot \mathbf{V}_s) + \rho_{sf} \mathbf{F} \cdot \mathbf{V}_s] dv \qquad (2.A9)$$

Similiarly, we can show that the rate at which work is done in moving the fluid relative to the solid matrix is

$$\frac{d}{dt} W_f = \iiint_v n[\nabla \cdot (\tilde{\tau}_f \cdot \mathbf{V}_r) + \rho_w \mathbf{F} \cdot \mathbf{V}_r] dv \qquad (2.A10)$$

where $\tilde{\tau}_f$ is the stress tensor within the moving fluid, and $\mathbf{V}_r = \mathbf{V}_f - \mathbf{V}_s$ is the relative velocity of the fluid with respect to the solid matrix.

Combining equations (2.A3), (2.A9) and (2.A10) we obtain the rate of change of work done on the volume minus the rate of change in kinetic energy of the volume

$$\frac{dW}{dt} - \frac{d}{dt} U_K = \iiint_v \{ \nabla \cdot (\tilde{\tau}' \cdot \mathbf{V}_s) + \rho_{sf} \mathbf{F} \cdot \mathbf{V}_s + \rho_{sf} \frac{d}{dt} \frac{\mathbf{V}_s \cdot \mathbf{V}_s}{2} +$$

$$n[\nabla \cdot (\tilde{\tau}_f \cdot \mathbf{V}_r) + \rho_w \mathbf{F} \cdot \mathbf{V}_r + \rho_w \frac{d}{dt} \frac{\mathbf{V}_r \cdot \mathbf{V}_r}{2}] \} dv \qquad (2.A11)$$

which we rewrite as

$$\frac{dW}{dt} - \frac{d}{dt} U_K = \iiint_v \{ \tilde{\tau}' \cdot \nabla \mathbf{V}_s + n\tilde{\tau}_f \nabla \cdot \mathbf{V}_r +$$

$$\mathbf{V}_s \cdot [\nabla \cdot \tilde{\tau}' + \rho_{sf} \mathbf{F} - \rho_{sf} \frac{d}{dt} \mathbf{V}_s] +$$

$$n\mathbf{V}_r \cdot [\nabla \cdot \tilde{\tau}_f + \rho_w \mathbf{F} - \rho_w \frac{d}{dt} \mathbf{V}_r] \} dv \qquad (2.A12)$$

The last two terms within the brackets are identically zero by the equations of motion for the solid-fluid composite and the fluid with respect to the solid matrix. Physically this means that part of the work done on the volume by tractions on the surface and body forces is converted into kinetic energy with the remainder dissipated into thermal energy. Hence, the rate of energy addition due to mechanical work is

$$\frac{dW}{dt} - \frac{d}{dt} U_K = \iiint_v [\tilde{\tau}' \cdot \nabla \mathbf{V}_s + n\tilde{\tau}_f \cdot \nabla \mathbf{V}_r] dv \qquad (2.A13)$$

Since the fixed volume is arbitrary, the resultant integrand obtained by substitution of equations (2.A2), (2.A5) and (2.A13) into equation (2.A1) must be equal to zero for any point within the volume. Thus we obtain the differential equation describing energy transfer within a porous medium

$$\frac{\partial}{\partial t}[n\rho_w \epsilon_f + (1-n)\rho_s \epsilon_s] + \nabla \cdot [\mathbf{q}_h + n\rho_w \mathbf{V}_f \epsilon_f + (1-n)\rho_s \mathbf{V}_s \epsilon_s] =$$

$$\tilde{\tau}' \cdot \nabla \mathbf{V}_s + n\tilde{\tau}_f \cdot \nabla \mathbf{V}_r \qquad (2.A14)$$

For a Newtonian fluid we can rewrite the last term of equation

(2.A14) as (Landau and Lifschitz, 1959)

$$\tilde{n\tau}_f \cdot \nabla \mathbf{V}_r = n\mu_w \left[\frac{\partial}{\partial x_j} V_{r_i} \left(\frac{\partial}{\partial x_j} V_{r_i} + \frac{\partial}{\partial x_i} V_{r_j} \right) - \frac{2}{3} (\nabla \cdot \mathbf{V}_r)^2 \right] - nP \nabla \cdot \mathbf{V}_r \qquad (2.A15)$$

The first term of equation (2.A15) is always positive and hence always acts as a thermal source. In contrast $nP\nabla \cdot \mathbf{V}_r$ represents the rate of heat addition due to pressure work done by expanding, or contracting, the fluid mass inside the pore volume. From the fluid continuity equation (2.8) we may write

$$\nabla \cdot \mathbf{V}_r = \nabla \cdot \mathbf{V}_s + \frac{1}{n} \frac{\mathrm{d}_f}{\mathrm{d}t} n + \frac{1}{\rho_w} \frac{\mathrm{d}_f}{\mathrm{d}t} \rho_w \qquad (2.A16)$$

Substitution of equation (2.A16) into (2.A15) yields

$$\tilde{n\tau}_f \cdot \mathbf{V}_r = \mu_w \Phi + \frac{nP}{\rho_w} \frac{\mathrm{d}_f}{\mathrm{d}t} \rho_w \qquad (2.A17)$$

where Φ is defined as

$$\Phi = n \left[\frac{\partial}{\partial x_j} V_{r_i} \left(\frac{\partial}{\partial x_j} V_{r_i} + \frac{\partial}{\partial x_i} V_{r_j} \right) - \frac{2}{3} (\nabla \cdot \mathbf{V}_r)^2 \right] + \frac{1}{\mu_w} \left(n \nabla \cdot \mathbf{V}_s + \frac{\mathrm{d}_f}{\mathrm{d}t} n \right) \qquad (2.A18)$$

and is referred to as the viscous dissipation function for the fluid. This term characterizes the irreversible conversion of mechanical energy into thermal energy as the fluid flows through the pores. Insertion of equation (2.A17) into (2.A14)

yields the Eulerian form of the energy balance equation for a saturated porous media

$$\frac{\partial}{\partial t}[n\rho_w\epsilon_f + (1-n)\rho_s\epsilon_s] + \nabla\cdot[\mathbf{q}_h + n\rho_w\mathbf{V}_f\epsilon_f + (1-n)\rho_s\mathbf{V}_s\epsilon_s] =$$

$$\tilde{\tau}'\cdot\nabla\mathbf{V}_s + \mu_w\Phi + \frac{nP}{\rho_w}\frac{d_f}{dt}\rho_w \qquad (2.A19)$$

where thermal forms of energy appear on the lefthand side and mechanical forms on the righthand side. This is equation (2.14) in Chapter 2. If mechanical forms of energy are negligible, then the righthand side of equation (2A.19) is zero.

APPENDIX 2B: CONDITIONS WHERE HEAT ADDITION DUE TO PRESSURIZATION OF WATER ARE SIGNIFICANT

To evaluate the rate of heat addition due to the pressurization of pore water, we rewrite its contribution to the heat transfer equation (2.31) as

$$n\gamma_w T \frac{d_f}{dt} P = n\gamma_w T \left(\frac{\partial P}{\partial T}\right) \frac{d_f}{dt} T \qquad (2.B1)$$

Since the maximum fluid-pressure increase occurs for undrained conditions (k=0), if pressure work is negligible for those conditions, then it must also be negligible for drained conditions (k>0). For undrained conditions where there is no transport of pore fluids (k=0) it can be shown from equation (2.46) that

$$\left.\frac{\partial P}{\partial T}\right|_{k=0} = \frac{n\gamma_w + (1-n)\gamma_s - \gamma_{sf}}{n\beta_w - (1-n)\xi\beta_s + \beta_{sf}} \qquad (2.B2a)$$

$$= \Gamma \qquad (2.B2b)$$

where Γ is defined as the thermal pressurization coefficient of the porous medium, and β_{sf} is the compressibility of the porous medium. The term β_{sf} characterizes the volumetric dilatational strain that will take place for a unit change in effective stress in a freely dilatating medium (e.g., Biot, 1941; Gambolati, 1974). The term Γ characterizes the increase in fluid pressure per unit change in temperature for undrained conditions. Substituting equations (2.B1) and (2.B2) into

equation (2.32) yields the heat transfer equation for undrained conditions

$$\nabla \cdot K_{sf} \nabla T + \tilde{\tau}' \cdot \nabla \mathbf{v}_s = (1-\zeta_w)(\rho c)_{sf} \frac{d_s}{dt} T \qquad (2.B3)$$

where ζ_w is defined as the pressure-work coefficient for water and is given by

$$\zeta_w = \frac{n\gamma_w \Gamma T}{(\rho c)_{sf}} \qquad (2.B4)$$

This term characterizes the ratio of the rate of heat addition by pressurization of water to the rate of heat storage within the porous medium. If $\zeta_w << 1$, then heat addition due to pressurization of pore water is negligible. For the porous medium properties listed in Table 2.1, Figure 2.3 illustrates the pressure-work coefficient ζ_w as a function of temperature for selected fluid pressures and porous medium compressibilities β_{sf}. These figures show that for compressibilities less than 10^{-7} Pa^{-1} heat addition due to pressurization of water is not negligible, in general. In such a case the temperature and compressibility must be considered before the thermal effects of pressurization can be neglected. For example, if temperatures are less than 250 °C or greater than 600 °C, then the thermal effects of pressurization may be neglected. If temperatures lie between 250 °C and 600 °C, however, then heat addition due to pressurization of water is not negligible. In addition, the variation in ζ_w with pressure

and temperature must be considered. For media with compressibilities greater than 10^{-7} Pa^{-1} the pressure-work term can be neglected.

Furthermore, if the permeability exceeds 10^{-16} m^2, then the hydraulic diffusivity is much greater than the thermal diffusivity and the heating of water is accomodated by fluid expansion and flow instead of fluid pressurization. In such a case the fluid pressure rise with temperature will be small. Hence, for drained conditions with permeabilities greater than 10^{-16} m^2 heat addition due to pressurization of water is negligible irregardless of the temperature and porous medium compressibility. For permeabilities less than 10^{-16} m^2 the nature of the problem to be solved, and the range in permeability, compressibility, temperature and pressure must be considered before deciding whether the heat addition due to the pressurization of water can be neglected.

NOTATION

C_{ijkl}	coefficients of elasticity.
c_p	specific heat at constant pressure
c_s	isobaric specific heat of the solid grains.
c_w	isobaric specific heat of water.
e	volumetric strain (dilatation) $e_{11}+e_{22}+e_{33}$.
e_{ij}	solid matrix strain.
$\dot{e}_{ij}$	solid matrix strain rate.
f	as a subscript denotes fluid.
$\mathbf{F}$	body force acting on the porous medium.
$\mathbf{g}$	gravitational acceleration.
h_f	fluid enthalpy.
h_s	solid enthalpy.
k	porous medium permeability.
$\underset{\sim}{\mathbf{k}}$	permeability tensor.
k_o	initial permeability.
k_s	bulk modulus of the solid grains.
k_{sf}	bulk modulus of the porous medium.
K_s	thermal conductivity of the solid grains.
K_w	thermal conductivity of water.
$\underset{\sim}{\mathbf{K}}_{sf}$	thermal conductivity of the solid-fluid composite.
n	porosity.
n_o	initial porosity.
n_c	critical porosity for fluid flow.
p	fluid pressure increase above ambient conditions.
P	pore fluid pressure.
Q	rate of heat transfer into a region.
$\mathbf{q}_f$	fluid specific discharge relative to the solid matrix.
$\mathbf{q}_h$	conductive heat flux.
s	as a subscript denotes solid.
t	time.
T	thermodynamic temperature.
U_K	internal kinetic energy
$\mathbf{U}_s$	solid-matrix displacement relative to a fixed coordinate system.

U_{s_i} components of the solid-matrix displacement.

U_T internal thermal energy

$\mathbf{V}_f$ fluid velocity relative to a fixed coordinate system.

V_{f_i} components of the fluid velocity.

$\mathbf{V}_r$ fluid velocity relative to the solid matrix $\mathbf{V}_f - \mathbf{V}_s$.

V_{r_i} components of the fluid velocity relative to the solid matrix.

$\mathbf{V}_s$ solid-matrix velocity with respect to a fixed coordinate system.

w as a subscript denotes water.

W rate of work done on a system.

W_f rate of work done in moving the pore fluid relative to the solid matrix.

W_{sf} rate of work done on the solid-fluid matrix.

$\mathbf{x}$ fixed coordinate position (x_1, x_2, x_3).

$\mathbf{x}_s$ solid particle position with respect to a fixed coordinate system.

Γ thermal pressurization coefficient of the porous medium.

β_s isothermal compressibility of the solid grains.

β_{sf} porous medium compressibility.

β_w isothermal compressibility of water.

∇ gradient operator $\hat{\mathbf{x}}_i \partial/\partial x_i$.

δ_{ij} Kronecker delta function.

ϵ_f fluid internal thermal energy per unit mass.

ϵ_s solid internal thermal energy per unit mass.

γ_s isobaric thermal expansivity of the solid grains.

γ_{sf} linear thermal expansion coefficient of the porous medium.

γ_w isobaric thermal expansivity of water.

κ_{sf} bulk viscosity of the porous medium.

λ a Lame' constant.

μ shear modulus.

μ_{sf} dynamic viscosity of the porous medium.

μ_w dynamic viscosity of water.

Φ viscous heat dissipation function for the fluid.

ρ_s density of the solid grains.

ρ_{sf} density of the solid-fluid composite.

ρ_w density of water.

$\rho_w c_w$ heat capacity of water.

$\rho_s c_s$ heat capacity of the solid.

$(\rho c)_{sf}$ heat capacity of the solid-fluid composite.

$\tilde{\tau}'$ total stress tensor.

$\tilde{\tau}$ effective stress tensor.

τ_f stress tensor within the moving fluid.

$\bar{\tau}$ average effective normal stress $(\tau_{11}+\tau_{22}+\tau_{33})/3$.

τ_{ij} components of the effective stress tensor.

τ'_{ij} components of the total stress tensor.

Θ temperature increase over ambient conditions.

ξ proportionality constant between pore and bulk volume changes.

ζ_w pressure-work coefficient for water.

$\hat{}$ over a letter, denotes unit vector.

$\cdot$ between two vectors or two tensors, denotes scalar dot product; between a tensor and a vector, denotes vector dot product.

$\sim$ over a letter, denotes tensor quantity.

REFERENCES

Bear, J., *Hydraulics of Groundwater*, McGraw-Hill Inc., New York, 1979.

Bear, J., *Dynamics of Fluids in Porous Media*, 764 pp., American Elsevier, New York, 1972.

Bear, J., and M.Y. Corapcioglu, A mathematical model for consolidation in a thermoelastic aquifer due to the hot water injection, *Water Resour. Res.*, 17(3), 723-736, 1981.

Bernabe, Y., B. Evans, and W.F. Brace, Permeability, porosity, and pore geometry of hot pressed clacite, *Mech. Mater.*, 1, 173-183, 1982.

Biot, M. A., General theory of three dimensional consolidation, *J. Appl. Phys.*, 12, 155-164, 1941.

Biot, M. A. and D. G. Willis, The elastic coefficients of the theory of consolidation, *J. Appl. Mech.*, 24, 594-601, 1957.

Brace, W.F., Permeability from resistivity and pore shape, *J. Geophys. Res.*, 82, 3343-3349, 1977.

Brownell, Jr., D.H., S.K. Garg, and J.W. Pritchett, Governing equations for geothermal reservoirs, *J. Geophys. Res.*, 6, 929-934, 1977.

Brun, J.P., and P.R. Cobbold, Strain heating and thermal softening in continental shear zones: a review, *J. Struct. Geol.*, 2, 149-158, 1980.

Cooper, H.H., Jr., The equation of groundwater flow in fixed and deforming coordinates, *J. Geophys. Res.*, 71, 4785-4790, 1966.

Faust, C.R., and J.W. Mercer, Geothermal reservoir simulation 1. Mathematical models for liquid- and vapor dominated hydrothermal systems, *J. Geophys. Res.*, 15, 23-30, 1979.

Fleitout, L., and C. Froidevaux, Thermal and mechanical evolution of shear zones, *J. Struct. Geol.*, 2, 159-164, 1980.

Gambolati, G., Second-order theory of flow in 3D deforming media, *Water Resour. Res.*, 10(6), 1217-1228, 1974.

Garg, S.K., and J.W. Pritchett, On pressure-work, viscous dissipation, and the energy balance equation for geothermal reservoirs, *Adv. Water Resources*, 1, 41-47, 1977.

Huyakorn, P.S., and G.F. Pender, A pressure-enthalpy finite element model for simulating hydrothermal reservoirs, Second

International Symposium on Computer Methods for Partial Differential Equations, Lehigh Univ., Bethlehem, Pa., June 22-24, 1977.

Keenan, J.H., F.G. Keyes, P.G. Hill, and J.G. Moore, **Steam Tables**, 162pp., John Wiley, New York, 1978.

Kestin, J., Thermal conductivity of water and steam, *Mech. Eng.*, 100(8), 1255-1258, 1978.

Lachenbruch, A.H., and J.H. Sass, Heat flow and energetics of the San Andreas fault, *J. Geophys. Res.*, 80, 6185-6221, 1980.

Landau, L.D., and E.M. Lifshitz, **Fluid Mechanics**, Pergamon Press, New York, 1959.

Lockett, J.M., and N.S. Ksuznir, Ductile shear zones: some aspects of constant slip velocity and constant shear stress models, *Geophys. J. R. Astr. Soc.*, 69, 477-494, 1982.

Melosh, H.J., Plate motion and thermal instability in the astenosphere, *Tectonophysics*, 35, 363-390, 1976.

Murrell, S.A.F., D.L. Turcotte, and K.E. Torrance, Studies of finite amplitude non-Newtonian convection with application to convection in the earth's mantle, *J. Geophys. Res.*, 81, 1939-1946, 1976.

Myer, C.A., R.B. McClintoch, G.J. Silvestri, and R.C. Spencer, **ASME Steam Tables - Thermodynamic and Transport Properties of Steam**, ASME, New York, 1967.

Nowacki, W., **Dynamic Problems of Thermoelasticity**, Noordhoff, Leyden, The Netherlands, 1975.

Nowinski, J.L., **Theory of Thermoelasticity with applications**, Sijthoff & Noordhoff, Leyden, The Netherlands, 1978.

O'Neil, K., and G.F. Pinder, A derivation of the equations for transport of liquid and heat in three dimensions in a fractured medium, *Adv. Water Resources*, 4, 150-164, 1981.

Platten, J.K., and J.C. Legros, **Convection in Liquids**, Springer-Verlag, New York, 1984.

Rice, J.R. and M.P. Cleary, Some basic stress diffusion solutions for fluid-saturated elastic porous media with compressible constituents, *Rev. Geophys. Space Phys.*, 14, 227-241, 1976.

Richards, P.G., Dynamic motions near an earhquake fault: a three dimensional solution, *Bull. Seis. Soc. Am.*, 66, 1-32, 1976.

Sass, J.H., A.H. Lachenbruch, and R.J. Munroe, Thermal conductivity of rocks from measurements on fragments and its application to heat-flow determinations, *J. Geophys. Res.*, 76, 3391-3401, 1971.

Sharp, J.M., Jr., Permeability controls on aquathermal pressuring, *Am. Assoc. Pet. Geol. Bull.*, 67, 2057-2061, 1983.

Slattery, J.C., **Momentum, Energy, and Mass Transfer in Continua**, McGraw-Hill, New York, 1972.

Snow, D., Fracture deformation and changes of permeability and storage upon changes in fluid pressure, **Colo. Sch. Mines Q.**, 63, 201-244, 1969.

Sorey, M.L., Numerical modeling of liquid geothermal systems, *U.S. Geol. Surv. Prof. Pap., 1044-D*, 1978. Stallman, R.W., Notes on the use of temperature data for computing velocity, paper presented at 6th Assembly on Hydraulics, Soc. Hydrotech. France, Nancy, June 28-30, 1960.

Stallman, R.W., Computation of groundwater velocity from temperature data, *U.S. Geol. Surv. Water Supply Pap. 1544-H*, H36-H40, 1963.

Straus, J.M., and G. Schubert, Thermal convection of water in a porous medium: effects of temperature- and pressure-dependent thermodynamic and transport properties, *J. Geophys. Res.*, 82(2), 325-333, 1977.

Turcotte, D.L. and E.R. Oxbaugh, A fluid theory for the deep structure of dip-slip fault zones, *Phys. Earth Planet. Interiors*, 1, 381-387, 1968.

Verruijt, A., Elastic storage of aquifers, in **Flow Through Porous Media**, edited by R.J.M DeWeist, Academic Press, New York, 1969.

Walder, J. and A. Nur, Porosity reduction and crustal pore pressure, *J. Geophys. Res.*, 89, 11539-11548, 1984.

Watson, J.T.R., R.S. Basu, and J.V. Sengers, An improved representative equation for the dynamic viscosity of water substance, *J. Phys. Chem. Ref. Data*, 9(3), 1255-1279, 1980.

Weertman, J. and J.R. Weertman, High temperature creep of rock and mantle viscosity, *Annu. Rev. Earth Planet. Sci.*, 3, 293-315, 1975.

White, F.M., **Viscous Fluid Flow**, McGraw-Hill, New York, 1974.

Woodside, W. and J.H. Messmer, Thermal conductivity of porous media, *J. Appl. Phys.*, 32, 1688, 1961.

Yuen, D.A., L. Fleitout, G. Schubert, and C. Froideaux, Shear deformation zones along major transform faults and subducting slabs, *Geophys. J. R. Astr. Soc.*, 54, 93-119, 1978.

Yuen, D.A. and G. Schubert, On the stability of frictionally heated shear flows in the asthenosphere, *Geophys. J. R. Astr. Soc.*, 57, 189-207, 1979.

TABLE 2.1. Parameter Values for Porous Medium Properties Held Constant for Calculation of ζ_w.

Property	Value
Porosity n	0.20
ξ	1.0
Thermal expansivity of the porous medium γ_{sf}	10^{-5} °C^{-1}
Density of the solid ρ_s	2.6×10^3 kg m^{-3}
Specific heat of the solid c_s	10^3 J kg^{-1} °K^{-1}
Thermal conductivity of the solid K_s	2.5 W m^{-1} °K^{-1}
Compressibilty of the solid β_s	10^{-11} Pa^{-1}
Thermal expansivity of the solid γ_s	2.5×10^{-5} °C^{-1}

FIGURE CAPTIONS

Figure 2.1. Lagrangian description of a fault zone where the deformations are describe by progressive simple shearing. For a homogeneous medium, the transport of heat and fluid occurs perpendicular to the centerline of the fault zone. Thus it is necessary to consider only the one-dimensional problem along a line perpendicular to the centerline of the fault zone.

Figure 2.2. Thermodynamic properties of pure water as a function of temperature T for selected fluid pressures P: (a) density ρ_w based upon the the analytic expressions by Myer *et al.* (p. 23, 1967) and Keenan *et al.* (p. 128, 1978); (b) isothermal volumetric compressibility β_w; (c) isobaric thermal expansivity γ_w; (d) dynamic viscosity μ_w (Watson *et al.*, 1980); (e) thermal conductivity K_w (Kestin, 1978); and (f) isobaric specific heat c_w (Keenan *et al.*, p. 130, 1978). The fluid pressure increment between curves is 5 MPa for 5-20 MPa, 10 MPa for 20-40 MPa, and 20 MPa for 40-100 MPa. The liquid-steam transition is indicated by the dashed lines. For further explanation see text.

Figure 2.3. The pressure-work (PW) coefficient for water ζ_w calculated as a function of temperature T for selected fluid pressures P and porous medium compressibilities β_{sf} using the porous medium properties summarized in Table 2.1. The fluid pressure increment between curves is 5 MPa for 5-20 MPa, 10

MPa for 20-40 MPa, and 20 MPa for 40-100 MPa. The liquid-steam transition is indicated by the dashed lines. For further explanation see text.

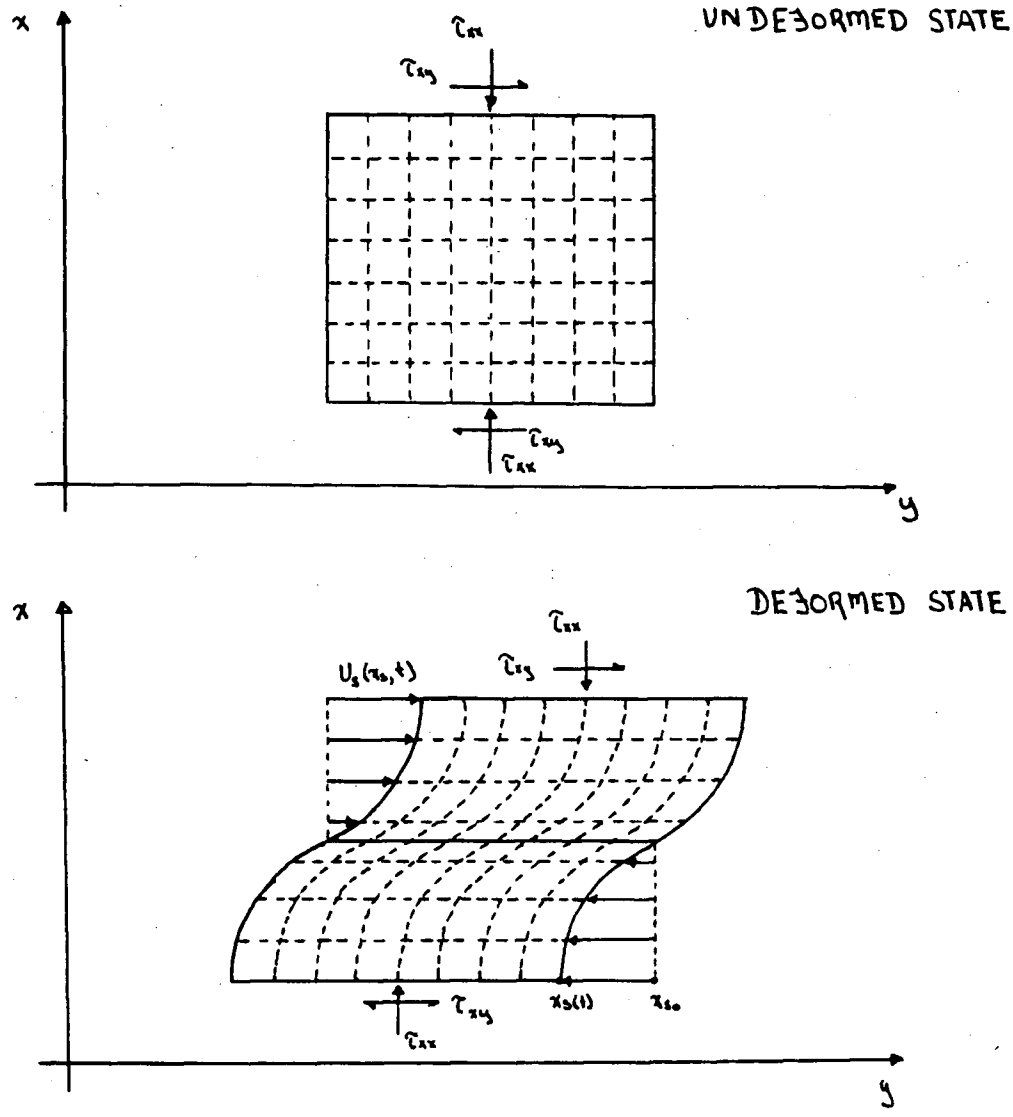

Figure 2.1

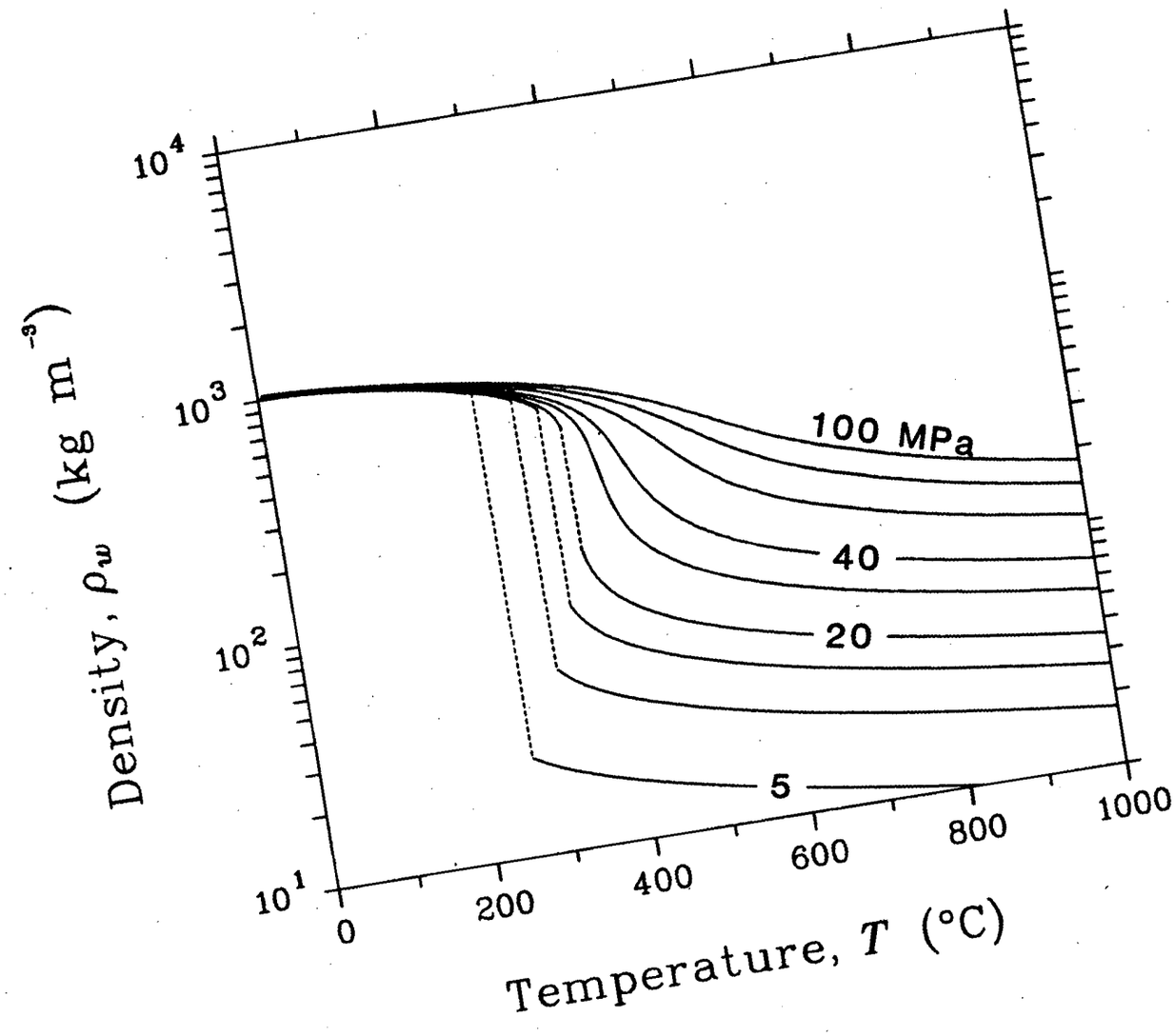

Fig. 2.2a. Density.

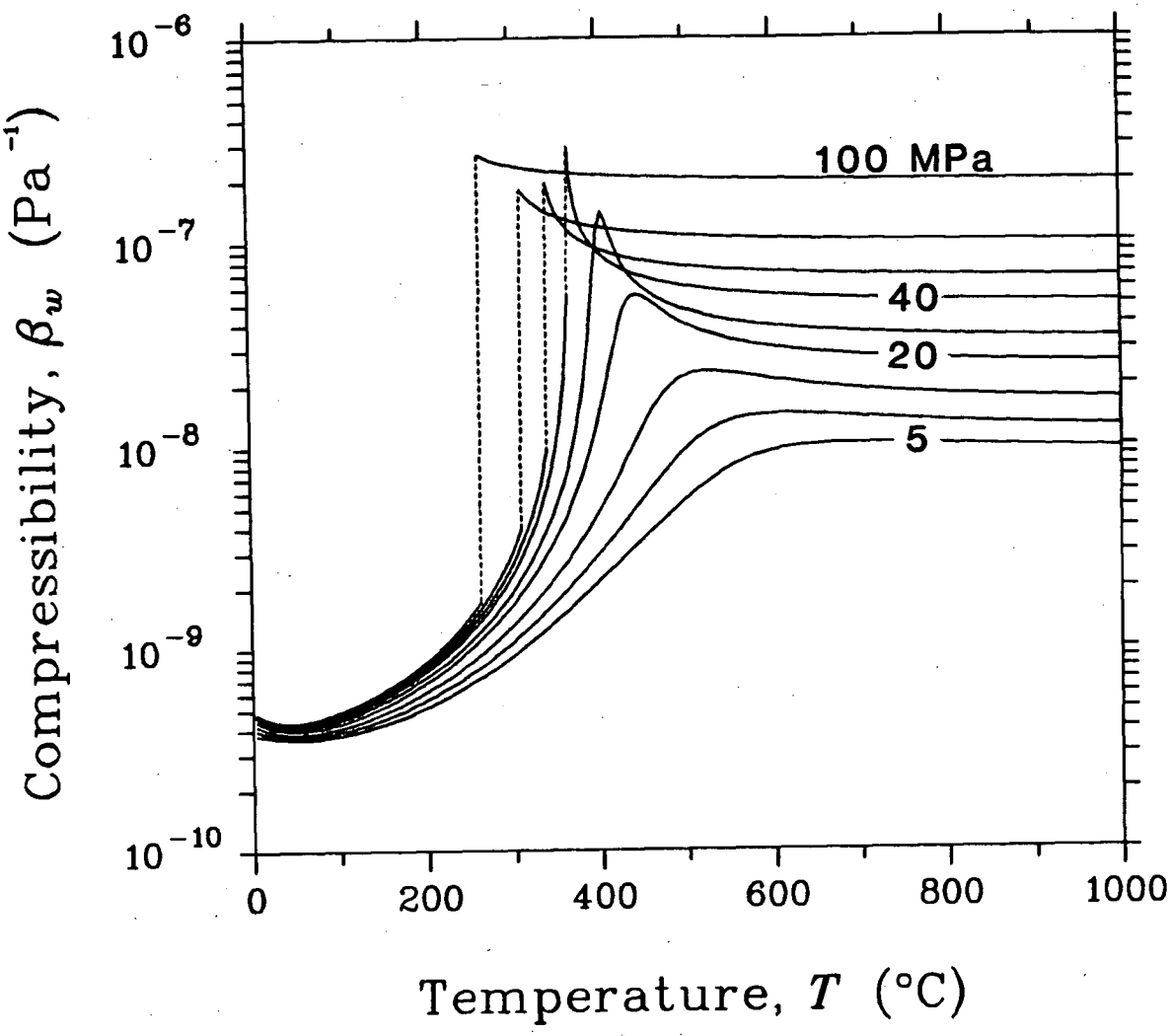

Fig. 2.2b. Isothermal compressibility.

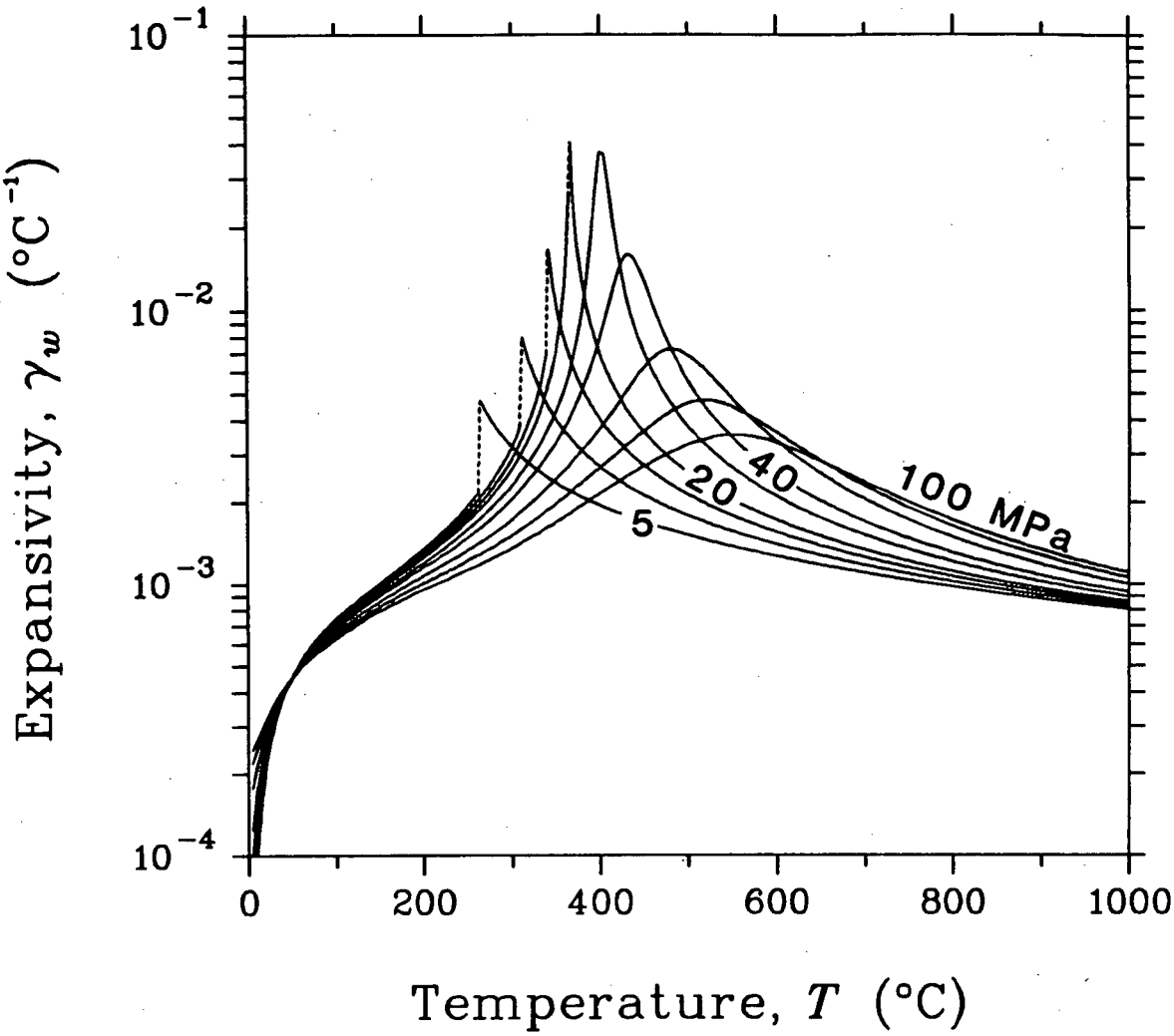

Fig. 2.2c. Isobaric thermal expansivity.

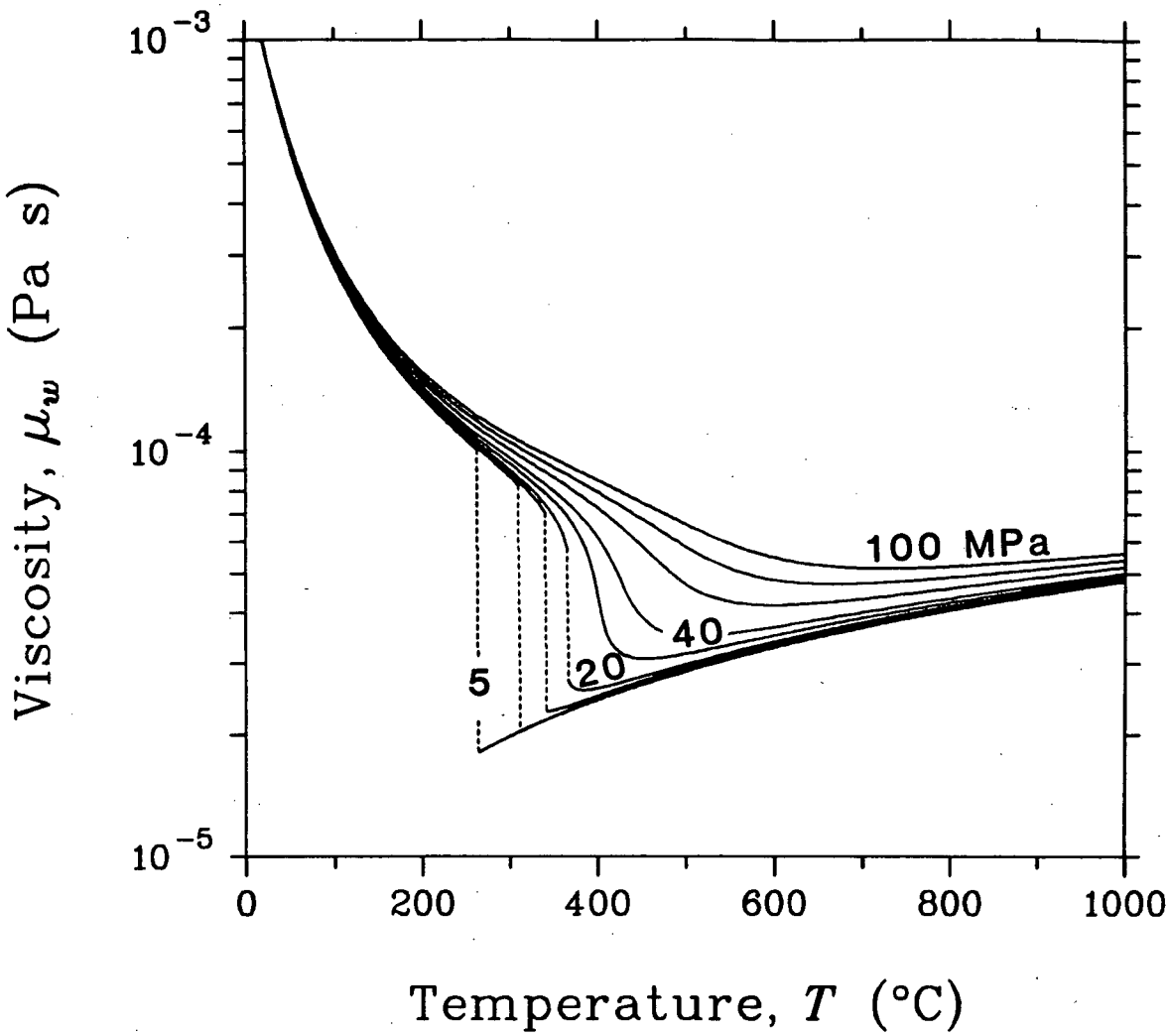

Fig. 2.2d. Dynamic viscosity.

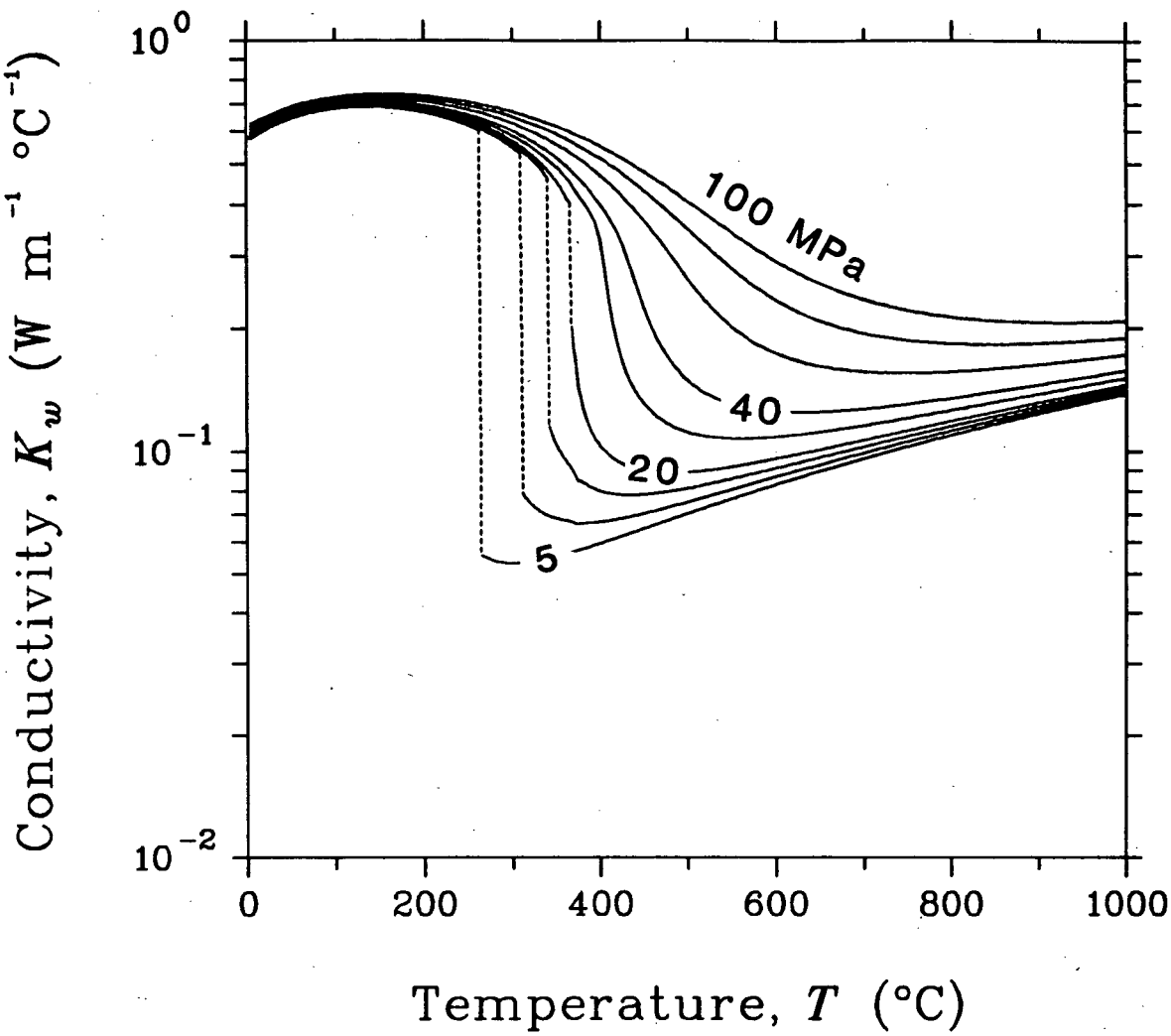

Fig. 2.2e. Thermal conductivity.

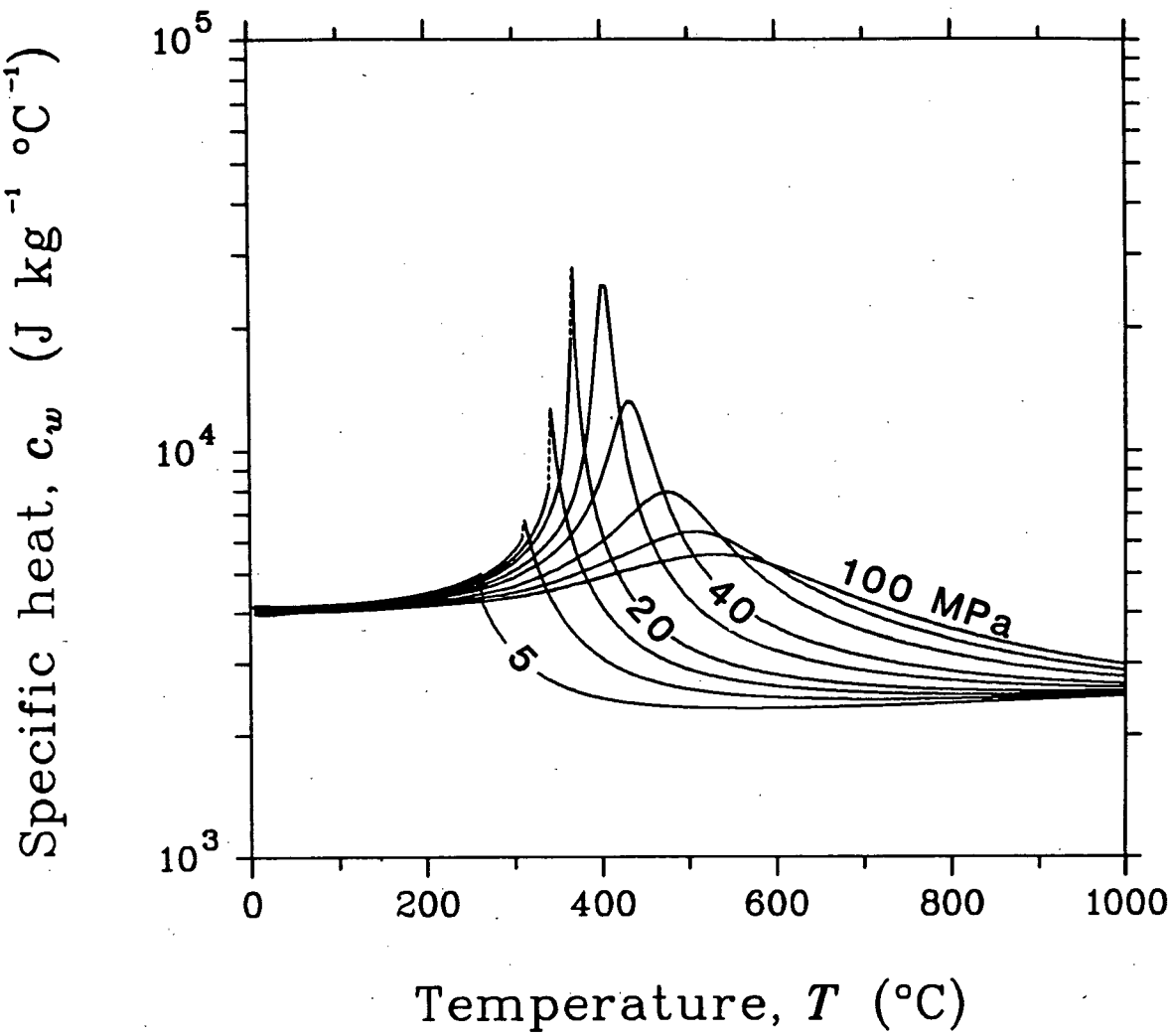

Fig. 2.2f. Isobaric specific heat.

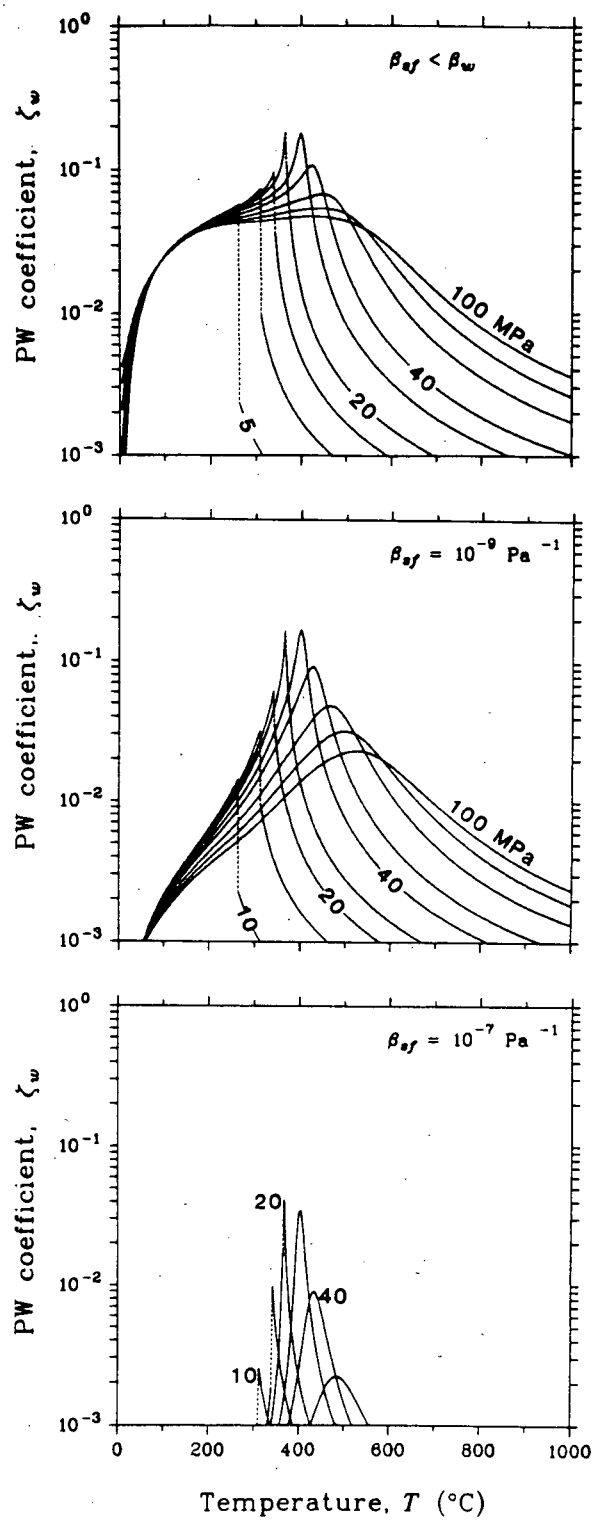

Fig. 2.3. Pressure–work coefficient for water.

CHAPTER III

PORE-FLUID PRESSURES AND FRICTIONAL HEATING ON A FAULT SURFACE

Most rocks within the vicinity of shallow earthquakes are porous and, within the upper crust, the pores are likely to contain water. Because the pressure of pore waters influences the mechanical properties of rock, stresses and strains are coupled to fluid flow within the porous medium. This coupling can decrease or increase the strength of a fault as well as the strength of the adjacent medium. Furthermore, frictional heating on a fault surface can lead to thermal expansion, pressurization, and flow of pore waters, coupling the thermal field with the stress, strain, and fluid fields. Consequently, the behavior of pore waters before and during slip is of considerable importance in the mechanics of earthquake processes.

Assuming the fault surface is established and that the shear stress required for slip is given by the friction law, many investigators have shown that frictional heating could play an important role in the dynamics of fault processes. Jaeger (1942), McKenzie and Brune (1972), Richards (1976), Cardwell *et al.* (1978), Scholz (1980), and Sibson (1980) suggested that shear heating could lead to partial melting on the fault surface with a subsequent reduction in the shear strength. These studies have neglected the presence and

possible effect of pore water. If water is present, the dynamics are more complicated. The response of fluid pressures to frictional heating can be described by the following two extreme cases. If the hydraulic diffusivity of the adjacent medium is much greater than the thermal diffusivity, the thermal expansion of pore fluids is accomodated by fluid flow from the heated region adjacent to the fault surface. In such a case the fluid pressure and dynamic shear strength remain unchanged during slip. Consequently, the fault surface is a large source of frictional heat and partial melting may occur. This is the response we would expect for high-permeability material. If the hydraulic diffusivity is less than the thermal diffusivity and if the medium is rigid, then there is no appreciable fluid explusion from the heated region during slip and the heating process takes place at constant fluid mass. In this case the resulting thermal pressurization causes the effective stress to decrease, promoting a net reduction in the dynamic shear strength of the fault surface. If fluid pressures approach lithostatic values the two sliding surfaces will loose cohesion, and the rate of frictional heating and the dynamic shear strength will approach zero (Sibson, 1973; 1977). For this case the maximum temperature attained on the fault surface would be substantially less than that required for frictional melting. This is the response we would expect for media with low permeability that have undergone an initial phase of consolidation.

Without attempting to solve the coupled equations, Lachenbruch (1980) wrote down the governing equations for heat and fluid flow, and analyzed for special cases the interaction of controlling parameters and their critical range of values. He concluded that if permeability exceeds 10^{-13} m^2 then coupling of thermal, hydrologic, and mechanical effects could probably be neglected, with fluid pressure and dynamic shear strength remaining constant during slip. Raleigh and Everden (1981), assuming no transport of fluid or heat, calculated the maximum fluid pressure increase for various displacements, displacement velocities, and fault zone widths. While these studies have served to illustrate pertinent features of the response they have considered only two limiting cases: those where fluid transport is so large it nullifies thermal pressurization, and those where the transport of heat or fluid, or both, are so small they can be neglected. For these cases, it is possible to analyze the system using analytical models. For intermediate conditions, these studies do not provide an adequate description of the transient increase in temperature on a fault surface during slip, and its effect on the fluid pressure and stress fields. In addition, changes in the pore-dilatation rate during slip were not considered.

The purpose of this paper is to bridge that gap in existing work. Using a numerical model, we examine how the thermal expansion of pore fluids due to frictional heating on a fault surface affects the temperature and dynamic shear strength of a fault during slip. This approach permits

consideration of the fully coupled behavior of the thermal, fluid pressure, and stress fields. Variations in the thermodynamic properties of water and pore-dilatation rates are incorporated in a straightforward manner. The analysis presented here removes some of the limitations of previous studies, and develops a better understanding of the role of frictional heating and thermal pressurization in the physics of fault processes.

A MATHEMATICAL MODEL FOR SLIP ON A NARROW FAULT

Figure 3.1 shows a simplified geometry for a narrow fault zone. The model consists of two elastic blocks which slide past each other on a planar surface. The width of the elastic blocks is determine by width of the thermal and hydrologic fields caused by frictional heating during slip (of the order of a few centimeters to several meters). A kinematic model is assumed where the slip velocity across the fault surface remains constant with time. This approach has the advantage of allowing us to characterize the response in terms of average slip velocities. The fluid-pressure changes that might arise from effects at the propagating ends of the failure surface (e.g.; Rice and Simons, 1976; Rice and Rudnicki, 1979) are assumed to be negligible in comparison to changes in fluid pressure arising from frictional heating on the failure surface. This assumption is reasonable for events where the propagation velocities of the fault tips are several orders of magnitude greater than the relative slip velocities across the

failure surface.

The shear stress required for slip on a fault surface is given by the friction law

$$\tau_r = \mu_d(\tau_n'-P) \tag{3.1}$$

where τ_n' represents the total normal stress acting on the sliding surface, τ_r is the resistive shear stress, μ_d is the dynamic coefficient of friction, and P is the pore-fluid pressure. The principal motivation for using this law is its wide spread applicability in describing the results of laboratory measurments for a variety of rock types. For most rocks μ_d is insensitive to composition and hardness, and has values between 0.4 and 1.0 (Byerlee, 1978). According to Byerlee, frictional sliding is well described by μ_d=0.85 for effective normal stresses in the range 5-200 MPa. For surfaces separated by a thin clay-rich layer of fault gouge, Morrow *et al*. (1982) reported values for μ_d that ranged from 0.2 to 0.6. From equation (3.1) the average rate of frictional heating on the fault surface is given by

$$\mu_d(\tau_n'-P)\cdot V_{sv} \tag{3.2}$$

where V_{sv} is the relative slip velocity across the fault. For the case where pore pressure remains constant, equation (3.2) has been used to predict high temperatures during slip (McKenzie and Brune, 1972; Richards, 1976; Cardwell, 1978;

Lachenbruch, 1980).

The large scale mechanical response of the fault is determined by the average temperature over the failure surface. Presumably the frictional heat represented by equation (3.2) is not generated uniformly over the fault surface but is localized to asperity contacts. During stable sliding experiments, at rates of 10^{-4} ms^{-1} and confining pressures of 50 MPa, Teufel and Logan (1978) and Logan(1979) measured maximum temperatures at asperity contacts in excess of 1000 °C. However, the average surface temperature did not exceed 125 °C. Measurements of frictional heating in granite by Lockner and Okubo (1983) suggest that equation (3.2) gives a good representation of the average temperature generated on the fault surface, but yields little information about local maxima at asperity contacts. If these results can be extended to crustal conditions, they support the assumption that a significant amount of frictional heat should be generated on an active fault surface and that (3.2) can be used to determine the thermohydromechanical behavior of the fault.

To model the system shown in Figure 3.1, we neglect the three-dimensional effects of inhomogeneities and assume that the transfer of fluid and heat occurs at right angles to the fault surface. In this framework the mathematical problem involves finding solutions to the one-dimensional equations describing heat transfer, fluid flow, and stress. These equations are outlined below. All equations are expressed in a

Lagrangian reference frame with respect to the solid matrix of the porous medium.

Heat Transfer Equation

The equation of heat transfer describing the transient temperature distribution in a saturated porous medium is given by

$$\frac{\partial}{\partial x}(K_{sf}\frac{\partial T}{\partial x}) - \rho_w c_w q_x(\frac{\partial T}{\partial x}) + n\gamma_w[\frac{\partial P}{\partial t} + \frac{q_x}{n}(\frac{\partial P}{\partial x})]T + \mu_d(\tau_n'-P)V_{sv}\delta(x) = (\rho c)_{sf}\frac{\partial T}{\partial t} \qquad (3.3)$$

where T is temperature, K_{sf} and $(\rho c)_{sf}$ the thermal conductivity and heat capacity of the solid-fluid composite, respectively, $\rho_w c_w$ and γ_w the heat capacity and thermal expansivity of water, respectively, n the porosity, q_x the Darcy flux, and $\delta(x)$ the Dirac delta function. For mathematical convenience the position of the fault is fixed at x=0. The terms on the lefthand side are, in order, the rate of conductive heat transport, the rate of convective heat transport, the rate of heating addition due to pressurization of the fluid and the rate of frictional heating on the fault surface. The term on the righthand side represents the rate of internal heat storage. No heat sources or sinks are considered other than frictional heating on the fault surface, and local thermal equilibrium between the solid matrix and the fluid is assumed. The thermal conductivity of the solid grains is

assumed to be independent of pressure and temperature. The thermal conductivity of the solid-fluid composite is given by a geometric mean where $K_{sf} = K_s^{(1-n)} K_w^n$ (Woodside and Messmer, 1961).

Fluid and Solid Mass Conservation Equations

Assuming the pores are fully saturated with water, and that the solid and fluid phases are separate and distinct, the equation for conservation of fluid mass is

$$-\frac{\partial}{\partial x}(q_x) - q_x[\beta_w(\frac{\partial P}{\partial x}) - \gamma_w(\frac{\partial T}{\partial x})] + [n\gamma_w + (1-n)\gamma_s]\frac{\partial T}{\partial t} =$$

$$\frac{\partial e}{\partial t} + [n\beta_w \frac{\partial P}{\partial t} + (1-n)\beta_s \frac{\partial \bar{\tau}}{\partial t}] \qquad (3.4)$$

where q_x is the Darcy flux, n and e the porosity and volumetric dilatation of the porous medium, β_w and γ_w the compressibility and thermal expansivity of water, β_s and γ_s the compressibilty and thermal expansivity of the solid phase, and $\bar{\tau}$ the average value of effective normal stress acting on the solid grains. The terms on the lefthand side are, in order, the rate of fluid transport, the change in fluid mass due to pressure contraction or thermal expansion of fluids along the flow path, and the change in fluid mass due to the difference in thermal expansivities of the fluid and solid phases. The terms on the righthand side are the change in fluid mass due to volumetric dilatation of the porous medium and the change in fluid mass due to the difference in the

compressibility of the fluid and solid phases. Equation (3.4) is completed by expression of the Darcy flux,

$$q_x = -\frac{k}{\mu_w}\frac{\partial P}{\partial x} \tag{3.5}$$

where k is the permeability and μ_w is the dynamic viscosity of water. In equation (3.5) fluid flow due to gravitational forces is assumed to be negligible over the time scale of interest.

The condition for conservation of the solid mass requires the following compatibility constraint for porosity:

$$\frac{\partial n}{\partial t} = (1-n)\left[\frac{\partial}{\partial x}(V_x) + \beta_s \frac{\partial \overline{\tau}}{\partial t} - \gamma_s \frac{\partial T}{\partial t}\right] \tag{3.6}$$

where V_x is the velocity of the solid matrix, and $\partial V_x/\partial x$ represents the volumetric-dilatation rate ($\partial e/\partial t$). Equation (3.6) states that the pore-dilatation rate ($\partial n/\partial t$) is given by the rate at which solids are leaving a unit volume minus the rate at which they are expanding due to decreases in the average effective normal stress or increases in temperature within the volume.

Equilibrium Equations for Stress

Deformation of the porous medium is governed by the effective stress τ_{ij}, which is defined as

$$\tau_{ij} = \tau'_{ij} - \xi P \delta_{ij} \tag{3.7}$$

where stresses are defined as positive when compressive. This law states that the strain response of a saturated medium is identical to that of a solid continuum if one uses the effective stress τ_{ij} instead of the total stress τ'_{ij} (Biot, 1941). From stress-strain measurements Biot and Willis (1957), and Nur and Byerlee (1971) have suggested that

$$\xi = 1 - k_s/k_{sf} \tag{3.8}$$

where k_s and k_{sf} are the bulk moduli of the solid grains and porous medium, respectively. Hence, ξ is a proportionality constant between pore and bulk volume changes for drained conditions at constant temperature. It is the ratio of fluid volume expelled to volumetric dilatation. For media with appreciable porosity, $k_s/k_{sf} \ll 1$, with $\xi \simeq 1$, and the fluid volume expelled is equal to the volumetric dilatation. This is the conventional assumption in compaction theory. In this case, equation (3.7) reduces to Terzaghi's simple effective stress law. With equation (3.7) the equilibrium equations for a one-dimensional system are

$$\frac{\partial}{\partial x}(\tau_{xx}) + \frac{\partial}{\partial x}(\xi P) = 0 \tag{3.9a}$$

$$\frac{\partial}{\partial x}(\tau_{xy}) = 0 \tag{3.9b}$$

Equilibrium in the absence of body forces requires that τ_{xy} is independent of x and is a function of time only. If total stresses remain constant, then changes in fluid pressure are responsible for all deformations of the porous medium.

The weakest link in the application of equation (3.9) is the stress-strain relationships. The strain response of porous media consists of elastic and inelastic responses which can be divided into two components: compaction or extension of the medium in response to changes in effective stress, and dilatation arising from shear deformation. Because we have assumed a kinematic model and have confined shear deformation to the fault surface, shear deformation adjacent to the fault must be zero. Consequently, only compaction or extension can occur in the adjacent region. Most of the inelastic deformation probably occurs during the initial stages of compaction. After the initial cycle of compaction-extension, the medium follows an elastic hysteretic response (Holcomb, 1977, 1981; Jorgensen, 1981). As most earthquakes occur in regions where other earthquakes have occurred, the medium will have been repeatedly loaded and unloaded. We assume the region surrounding the fault surface has undergone an initial compaction cycle and thus its response to changes in effective stress can be approximated as elastic.

For a linear-elastic porous medium the constitutive equation for stress and strain is (after Biot and Willis, 1957)

$$\tau_{ij} = -2\mu\left[\frac{\nu}{(1-2\nu)}e_{kk}\delta_{ij} + e_{ij}\right] + \gamma_{sf}(T-T_0)\delta_{ij} \qquad (3.10)$$

where μ is the shear modulus, ν Poisson's ratio, and γ_{sf} the linear thermal expansion coefficient of the porous medium. In employing a linear stress-strain relationship we have assumed that these coefficients, which are strictly valid for a solid continuum, are also valid for a saturated porous medium. Thus the elastic coefficients represent coefficients of the porous medium to be determined experimentally. In general, they are dependent on total stress, fluid pressure, and temperature. Substitution of equation (3.10) into (3.9) and integration over the flow domain, with the position of the fault fixed at $x=0$, yields

$$U_x(x,t) = \int_0^x \left[\frac{(1-2\nu)\xi}{2\mu(1-\nu)}\, p(\eta,t) + \gamma_{sf}\,\Theta\,(\eta,t)\right] d\eta \qquad (3.11)$$

where U_x is the extension or consolidation of the region exterior to the fault, $p=(P-P_0)$ is the fluid pressure increase above the initial value P_0, and $\Theta=(T-T_0)$ is the temperature increase above the initial value T_0. The corresponding volumetric-dilatation rate is

$$\frac{\partial e}{\partial t} = \frac{\partial}{\partial t}\left[\frac{(1-2\nu)\xi}{2\mu(1-\nu)}\, p + \gamma_{sf}\,\Theta\right] \qquad (3.12)$$

Because the quantity in front of the pressure term has units of compressibility, it is identified as

$$\beta_{sf} = \frac{(1-2\nu)\xi}{2\mu(1-\nu)} \tag{3.13}$$

where β_{sf} is the compressibility of the porous medium. This parameter measures the relative volumetric reduction that will take place as the medium is compressed and the fluid allowed to drain. Because μ, ν, ξ, p, γ_{sf} , and Θ are nonlinear functions of U_x and e, equations (3.11) and (3.12) represent implicit equations for U_x and e.

Solution Technique

Substituting the Darcy flux and the volumetric strain rate into equations (3.3) and (3.4), and assuming that the total stresses remain constant during slip yields the final form of the equations governing the temperature increase,

$$\frac{\partial}{\partial x}(K_{sf}\frac{\partial\Theta}{\partial x}) + (\rho_w c_w \frac{k}{\mu_w})(\frac{\partial p}{\partial x})(\frac{\partial\Theta}{\partial x}) + n\gamma_w[\frac{\partial p}{\partial t} - \frac{k}{n\mu_w}(\frac{\partial p}{\partial x})^2](\Theta+T_o) +$$

$$\mu_d(\tau_n'-P_o-p)V_{sv}\delta(x) = (\rho c)_{sf}\frac{\partial\Theta}{\partial t} \tag{3.14}$$

and the pressure increase,

$$\frac{\partial}{\partial x}(\frac{k}{\mu_w}\frac{\partial p}{\partial x}) + \frac{k}{\mu_w}[\beta_w(\frac{\partial p}{\partial x})^2 - \gamma_w(\frac{\partial\Theta}{\partial x})(\frac{\partial p}{\partial x})] + [n\gamma_w + (1-n)\gamma_s]\frac{\partial\Theta}{\partial t} -$$

$$\frac{\partial}{\partial t}(\gamma_{sf}\Theta) = n\beta_w\frac{\partial p}{\partial t} - (1-n)\beta_s\frac{\partial}{\partial t}(\xi p) + \frac{\partial}{\partial t}(\beta_{sf}p) \tag{3.15}$$

In addition, the porosity in equations (3.14) and (3.15) must

satisfy the compatibility equation:

$$\frac{\partial n}{\partial t} = (1-n)\,\frac{\partial}{\partial t}[(\beta_{sf}-\xi\beta_s)p + (\gamma_{sf}-\gamma_s)\Theta] \qquad (3.16)$$

Equation (3.14) to (3.16) can be solved by a Galerkin finite-element technique to give an approximate solution to this coupled system of equations. Details of the approach are summarized in the Appendix.

For all simulations, we assume a uniform temperature T_0 and fluid pressure P_0 for the initial conditions, and that the solutions remain bounded as $|x|$ approaches infinity. The latter condition is satisfied by placing the boundaries of the finite element mesh far enough from the fault surface so that they experience no temperature or fluid pressure perturbations. For all simulations of the fault plane model, the permeability and porous medium compressibility are assumed to be independent of changes in fluid pressure and temperature, and to be uniform and equal on both sides of the fault. Although these assumptions may be relaxed easily, they are retained in order to clarify their separate effects in the thermal-pressurization process.

RESULTS

Presentation of Results

In general, it is convenient to solve a problem and present its results in terms of dimensionless parameters and variables; but because of the strong cross-coupling and nonlinearity of the equations, and because the parameters are solution dependent, superposition is not applicable in this thermal pressurization problem. In addition, any attempt to linearize or scale the equations with parameters taken at some initial value, or intermediate fluid pressure and temperature values, will fail because of product terms. This behavior poses a dilemma for presenting results in a manner that can be readily generalized for a variety of parameters and initial conditions.

This situation is exemplified by means of the fluid-flow equation (3.15). From that equation, the fluid pressure increase is governed by a diffusion equation where the balance between pressurization and flow is determined by the hydraulic diffusivity,

$$a_h = \frac{k}{\mu_w[n\beta_w - (1-n)\xi\beta_s + \beta_{sf}]} \tag{3.17}$$

When the porous medium is homogenous, the solution can be expressed in terms of a characteristic diffusion length $\eta = x/\sqrt{4a_h t}$ (Lachenbruch *et al.*, 1976; Lachenbruch, 1980;

Delaney, 1982). Expressing the solution in terms of η generalizes the results for the full range of possible values of a_h. For frictional heating, however, the thermal pressurization and flow of pore fluids are driven by the term

$$\Gamma = \frac{n\gamma_w + (1-n)\gamma_s - \gamma_{sf}}{n\beta_w - (1-n)\xi\beta_s + \beta_{sf}} \tag{3.18}$$

where Γ is defined as the coefficient of thermal pressurization for the porous medium. This term characterizes the increase in fluid pressure per unit change in temperature for undrained conditions. The numerator and denominator represent the rate of fluid volume expansion due to changes in temperature and fluid pressure, respectively. From equations (3.17) and (3.18), it is apparent that an increase in β_{sf} will cause a decrease in both a_h and Γ. The decrease in Γ results in a decrease in the rate of thermal pressurization, and thereby a reduction in the rate of fluid-pressure increase. The decrease in a_h, however, suggests an enhancement in the rate at which thermal pressurization occurs. Furthermore, if we increase β_{sf}, it is possible to manipulate k such that a_h remains constant as Γ decreases, or increases. This behavior implies that for a fixed value of a_h there is a range of possible responses in the fluid pressure, and that a_h, by itself, is insufficient to characterize them. The competing effects between the rate of thermal pressurization and the balance between pressurization and flow make it is necessary to specify explicitly the permeability, compressibility, and

expansivity of the porous medium, to characterize fully the fluid-pressure response. Because of this behavior we must examine the influence of porous-medium properties for a set of initial conditions representative of a given depth.

Solutions for Limiting Cases

The numerical solutions have been compared with analytical solutions for two limiting cases. First, for large permeabilities or compressibilities thermal pressurization is nullified by the transport of pore fluids or by pore dilatation, respectively. In this case, the fluid pressure and shear strength remain unchanged during slip, and the temperature increase is as given by (McKenzie and Brune, 1972)

$$\Theta(x,t) = \frac{\mu_d(\tau_n'-P_0)V_{sv}}{2K_{sf}} \left[\frac{\sqrt{4a_t t}}{\sqrt{\pi}} \exp\left(\frac{-x^2}{4a_t t}\right) - |x| \operatorname{erfc}\left(\frac{|x|}{\sqrt{4a_t t}}\right) \right] \qquad (3.19)$$

where $a_t = K_{sf}/(\rho c)_{sf}$ is the thermal diffusivity. Second, for permeabilities less than 10^{-20} m^2 there is no appreciable transport of pore fluids and the fluid pressure increase is

$$p(x,t) = \Gamma\, \Theta(x,t) \qquad (3.20)$$

The temperature increase Θ is obtained by considering the equivalent half-space problem and by assuming that heating due to pressurization of the fluid is negligible. In this case,

the rate of frictional heating enters the solution by the boundary condition,

$$-K_{sf}\frac{\partial\Theta}{\partial x} = \frac{1}{2}\mu_d[(\tau_n'-P_0) - \Gamma\Theta]V_{sv} \qquad \text{at } x=0 \tag{3.21}$$

which can be regarded as a boundary with linear heat transfer into a medium at temperature $(\tau_n'-P_0)/\Gamma$. The solution is given by (after Carslaw and Jaeger, 1959, p. 72)

$$\Theta(x,t) = \frac{(\tau_n-P_0)}{\Gamma}\left[\operatorname{erfc}\left(\frac{x}{\sqrt{4a_t t}}\right) - \exp(\phi x + \phi^2 a_t t)\operatorname{erfc}\left(\frac{x}{\sqrt{4a_t t}} + \phi\sqrt{a_t t}\right)\right] \tag{3.22}$$

where

$$\phi = \frac{\mu_d V_{sv}}{2K_{sf}}\Gamma \tag{3.23}$$

The dynamic shear strength of the fault surface is given by

$$\tau_r(d) = \tau_{r_0}\exp(\phi^2 a_t d/V_{sv})\operatorname{erfc}(\phi\sqrt{a_t d/V_{sv}}) \tag{3.24}$$

where τ_{r_0} is the initial shear strength and d is the displacement across the fault surface. For intervening values of permeability, the numerical solutions will lie between these two limits. If the compressibility exceeds 10^{-9} Pa^{-1}, however, then the thermal pressurization coefficient is

proportional to the ratio of the thermal expansivity of water to the compressibility of the medium. In this case large temperature increases cause large increases in the thermal pressurization coefficient (see Figure 3.2), and equation (3.22) will overestimate the maximum temperature obtained on the fault surface and equation (3.24) will underestimate the rate of reduction in shear strength. Furthermore, the rate of heat addition due to pressurization of pore waters can significantly enhance the rate of thermal pressurization (see Appendix 2B and Figure 2.3).

Fault Surface Depth of 2 km

To illustrate several basic effects attributable to thermal pressurization, we first consider frictional heating on a fault surface at a depth of 2 km. For this example we have assumed the following parameter values: a dynamic coefficient of friction, μ_d, of 0.6, a slip velocity V_{sv} of 1 ms^{-1}, a porosity n of 0.2, and a initial temperature T_0 of 80 °C. The total normal stress τ_n' acting on the fault surface is 45 MPa, due solely to the lithostatic pressure for a rock column with a specific bulk density of 2.3. The ambient fluid pressure P_0 is 19 MPa, equal to the hydrostatic head. For these conditions, the initial effective normal stress $\tau_n'-P_0$ acting on the fault is 26 MPa, and the initial resistive shear strength τ_r of the fault surface is 15.6 MPa.

Figure 3.2 shows the transient increase in temperature on the fault surface as a function of displacement for media with

various permeabilities. Each of the four diagrams corresponds to a different value of porous medium compressibility. If the compressibility is less than 10^{-11} Pa^{-1}, the medium is essentially rigid ($\beta_{sf}=0$) and fluid flow is the only mechanism for accomodating the thermal expansion of pore fluids. For permeabilities less than 10^{-20} m^2 there is essentially no transport of fluid during the slip event, and the response occurs at constant fluid mass. In this case the coefficient of thermal pressurization is approximated by the ratio of the thermal expansivity to the compressibility of water. Because the rate at which water pressurizes is large ($\gamma_w/\beta_w \simeq 1.6$ MPa $°C^{-1}$), only a small temperature increase is required for the thermal expansion of pore fluids to pressurize the fluids and to maintain the fluid pressure on the fault surface at near-lithostatic values. For media with greater permeability, there is an increase in the rate of fluid loss due to transport. If the fluids are to pressurize, there must be an increase in the fluid-expansion rate in the porous medium adjacent to the fault surface. For this to occur, there must be a greater temperature increase on the fault surface. If permeabilities exceed 10^{-15} m^2, however, the hydraulic diffusivity greatly exceeds the thermal diffusivity and the movement of fluid away from the fault surface can nullify thermal pressurization of the fluids. In such case the slip event occurs at constant fluid pressure and the large temperature rise reflects frictional heating due to the large resistive shear strength.

Similarly, if the medium is compressible, thermal pressurization will initiate a pore-volume expansion, providing a second mechanism for accomodating the thermal expansion of pore fluids. The greater the compressibility of the porous medium, the larger the temperature rise that is required for the thermal expansion of pore fluids to exceed substantially fluid volume changes due to pore dilatation, and thus pressurize the fluid. As shown in Figure 3.3, when there is no transport of fluid (k=0), a larger temperature rise occurs with a given displacement in a medium which is more compressible. For larger permeability values even greater temperature increases are required to overcome fluid losses due to flow and pore-volume changes due to dilatation.

The response shown in Figure 3.2 indicates the fault surface stabilizes at a constant temperature that is dependent on the transport and pore-dilatation characteristics of the porous medium. This behavior can be explained by examining the rate of frictional heating and its relation to fluid pressurization. At the initiation of slip the fault surface is a strong frictional heat source; this leads to a rapid increase in temperature. As slip progresses, the region adjacent to the fault surface is heated until the rate of thermal expansion of pore fluids substantially exceeds the loss of the fluid due to transport and volume changes due to pore dilatation. Once this condition is achieved, the pore fluids start to pressurize, causing the shear strength and frictional heating to diminish rapidly and the fault surface

to stabilize at a constant temperature. At this point there is a dynamic balance between the temperature and pressure fields, where the rate of fluid-volume increase due to thermal expansion equals the loss of fluids due to transport and fluid-volume changes due to pore dilatation. The temperature increase necessary to sustain fluid pressures at near-lithostatic values and to maintain this balance is dependent primarily on the fluid and thermal transport properties and the pore-dilatation characteristics of the adjacent medium.

Figure 3.3 shows the shear strength of the fault surface as a function of displacement. Note that the shear strength has been normalized by its initial value (τ_f/τ_{f_0}) and that each of the four figures correspond to the same values of porous medium compressibility as in Figure 3.3. The 1000 °C isotherm is shown in Figure 3.4 to delineate the region where partial melting may occur. If the medium is rigid ($\beta_{sf} \leq 10^{-11}$ Pa^{-1}), then for permeabilities less than 10^{-20} m^2 the total displacement needed to cause a significant reduction in shear strength is small ($<10^{-3}$ m). This behavior can be explained in terms of the frictional heat source acting on the fault surface. From equation (3.2), frictional heat is directly proportional to the shear strength of the fault surface. Large reductions in shear strength coincide with large reductions in frictional heating. For low permeabilities the strong initial source is maintained only for a short displacement before the thermal expansion of pore fluids substantially exceeds fluid

loss due to transport and pressurizes the fluids. Once thermal pressurization of pore fluid starts, the fault surface stabilizes at a constant temperature and the shear strength diminishes rapidly to a level that is necessary only to maintain the temperature required to sustain thermal pressurization of pore fluids at near-lithostatic values. For higher permeabilities, the temperature rise needed to overcome the loss of pore fluids due to transport increases. The shear strength will remain at its initial value, creating a strong frictional heat source until the thermal expansion of fluids substantially exceeds the loss of fluids due to transport. If the permeability exceeds 10^{-15} m^2, then frictional melting on the fault surface may reduce the dynamic shear strength before the effects of thermal pressurization become significant (McKenzie and Brune, 1972).

Similarly, for the case where there is no transport of fluids, increases in porous medium compressibility require the initial shear strength to be maintained over a greater total displacement. Once the fault surface is heated to the temperature required for the thermal expansion of pore fluids to exceed substantially the pore dilatation rate, the shear strength diminishes rapidly. As the compressibility increases, the rate at which the shear strength decreases is enhanced. This behavior occurs because for compressibilities that exceed 10^{-9} Pa^{-1}, the coefficient of thermal pressurization is given approximately by $\Gamma \simeq n\gamma_w/\beta_{sf}$. If the porous medium compressibility is independent of changes in fluid pressure,

then large temperature increases lead to large increases in the thermal expansivity of water and thereby large increases in the thermal pressurization coefficient. Thus, for large compressibilities when the temperature rises rapidly, the thermal pressurization coefficient will also rise rapidly.

The results from Figures 3.2 and 3.3 indicate that if the permeability exceeds 10^{-15} m^2, then, regardless of the porous medium compressibility, thermal expansion of pore fluids is accomodated by the transport of fluids from the heated region adjacent to the fault surface. Conversely, if the porous medium compressibility exceeds 10^{-8} Pa^{-1}, then, regardless of the permeability, pore dilatation accomodates the thermal expansion of pore fluids. In both cases the pore fluids expand at constant pressure. Hence, there is no feedback of fluid pressure into the reduction of shear strength, and the fault acts as a strong source of frictional heat.

For undrained conditions ($k \leq 10^{-20}$ m^2) the temperature increase on the fault surface is obtained by setting $x=0$ in equation (3.22) and is given as a function of displacement by

$$\Theta_f(d) = \frac{(\tau_n - P_0)}{\Gamma} \left[1 - \exp(\phi^2 a_t d/V_{sv}) \operatorname{erfc}(\phi\sqrt{a_t d/V_{sv}}) \right] \qquad (3.25)$$

For large displacements the second term within the brackets vanishes and the maximum temperature rise is as given by the

ratio of the initial effective stress to the thermal pressurization. Thus the maximum temperature rise needed to sustain fluid pressures at near-lithostatic values is independent of the coefficient of friction, μ_d, and the slip velocity V_{sv}, and thereby independent of the rate of frictional heating on the fault surface. This behavior implies that the coefficient of friction and slip velocity determine only the rate at which thermal pressurization proceeds, but not the final outcome. If either μ_d or V_{sv} decrease, then the total displacement required for an equivalent reduction in shear strength is increased. Furthermore, if either the coefficient of friction or the slip velocity deviates from its initial value during slip and such deviation is small in comparsion with the average value over the slip event, then the rate of thermal pressurization will not be altered significantly.

It is possible to extend this argument to drained conditions ($k>10^{-20}$ m^2). To balance fluid-volume loss due to pressurization and flow by the thermal expansion of pore fluids, there must be an additional temperature rise on the fault surface. The magnitude of the temperature rise will depend on the fluid and thermal transport properties of the porous medium, but not on the rate at which this temperature increase is achieved. This behavior will be discussed in further detail in Chapter 4. Suffice it to say here that under the conditions just discussed as fluid pressures approach lithostatic values the fault surface stablizes at a

near-constant temperature. Once the temperature has stabilized, fluid pressures are maintained at lithostatic values by the diffusion of heat from a constant temperature fault surface into the adjacent medium. Thus the maximum temperature for drained conditions is also independent of the coefficient of friction and the slip velocity. On the other hand, the rate of temperature increase and the rate of shear strength reduction, are dependent on μ_d or V_{sv}. The results of Figures 3.2 and 3.3 can be generalize for other values of μ_d and V_{sv}, provided we maintain the same initial porosity and thermal properties of the solids. For other values of μ_d and V_{sv}, the displacement scales in Figures 3.2 and 3.3 can be adjusted by multiplying by

$$\frac{\mu_d^2}{\mu_d'^2}\ \frac{V_{sv}}{V'_{sv}} \tag{3.26}$$

where the primed values denote the new values, and the unprimed values represent the reference values μ_d=0.6 and V_{sv} =1 ms^{-1}. For example, consider an event with 1 m displacement in a rigid medium. For μ_d=0.6 and V_{sv}=1 ms^{-1} permeabilities less than 10^{-15} m^2 are required for a significant reduction in shear strength, but for μ_d=0.19 and V_{sv}=10^{-1} ms^{-1} the displacement scales are be multiplied by 100, and permeabilities less than 10^{-17} m^2 are required for an equivalent reduction in shear strength to occur. Furthermore, if μ_d is much smaller than 10^{-1} or $V_{sv}$is much less than 10^{-2} ms^{-1}, then it is doubtful thermal pressurization could reduce

significantly the dynamic shear strength of a fault during an earthquake event unless the porous medium were rigid.

Effect of Depth

The results presented in the previous section apply for a fault surface at a depth of 2 km. The effect of locating the fault at any other depth will be to change the initial conditions on the fault (i.e., total normal stress, ambient fluid pressure, and background temperature). If the initial fluid pressures are hydrostatic, then as the depth of the fault surface is increased the initial effective stress $\tau_n'-P_o$ on the fault surface will increase. An increase in effective stress leads to a corresponding increase in the maximum possible fluid pressure, and thereby, an increase in the temperature needed to sustain fluid pressures at near-lithostatic values.

For undrained conditions, equation (3.25) shows that there is a linear relationship between the maximum temperature rise and the initial effective stress. The rate at which the maximum temperature is achieved is independent of the initial effective stress and depends only on the coefficient of friction, slip velocity, thermal pressurization coefficient and thermal transport properties. If these values remain fixed, then we can scale the temperature in Figure 3.2 by the ratio of the new value for initial effective stress to the reference value (24 MPa). For example, if the initial effective stress is 12 MPa and the fluid pressure is

hydrostatic, then the temperature scale would be halved. For drained conditions and compressibilities that exceed 10^{-10} Pa^{-1}, this scaling factor holds provided the initial value of the thermal pressurization coefficient Γ is equal to the value for the figure. When this is not the case, this scaling factor cannot be used. Although equation (3.25) suggests we could scale linearly with respect to the thermal pressurization coefficient, this is not the case, because of the temperature and pressure dependency of the thermal expansivity and compressibility of water.

Similarly, equation (3.24) shows that for undrained conditions the transient decrease in the normalized shear strength (τ_f/τ_{f_o}) is independent of the initial effective stress. Thus Figure 3.3 is representative of the transient decrease in shear strength for any given depth. For drained conditions and compressibilities that exceed 10^{-10} Pa^{-1}, this behavior holds provided the initial thermal pressurization coefficient is equal to the value for the figure. The position of the 1000 °C isotherm is, however, dependent on the initial effective stress. If the initial effective stress is increased (or decreased), then the isotherm will shift towards decreased (or increased) displacements.

For a further illustration of such results, consider the temperature rise and reduction in shear strength for a fault at a depth of 1 km. In this case the total stress and initial hydrostatic fluid pressure are halved, and the temperature

scale in Figure 3.2 is multiplied by 0.5. For a 10^{-1} m displacement event, occurring in a medium with a permeability of 10^{-17} m^2 and a compressibility of 10^{-10} Pa^{-1}, the temperature rise is approximately 150 °C and the final normalized shear strength is approximately 0.20. Recall that the displacement scales in Figures 3.2 and 3.3 can be adjusted for other values of the coefficient of friction and slip velocity by using equation (3.26). If we change the coefficient of friction μ_d, and slip velocity V_{sv} from their reference values, 0.6 and 1 ms^{-1}, to 0.19 and 10^{-1} ms^{-1}, respectively, then the displacement scales in Figures 3.3 and 3.3 are multiplied by 100. For the new values the same event at a depth of 1 km would have a temperature rise of 50 °C and a final normalized shear strength of 0.80.

Because the transient decrease in shear strength depends on the material properties of the porous medium and on the coefficient of friction and slip velocity on the fault surface, changes in the initial conditions do not change the rate of decrease in shear strength. The temperature required to sustain fluid pressures at near-lithostatic values, however, is dependent on the initial conditions because changes in the initial effective stress lead to changes in the maximum fluid pressure. Thus the primary effect of changes in depth is to increase (or decrease) the final temperature obtained on the fault surface.

DISCUSSION

These results suggest that the permeability and compressibility of the porous medium are the most important parameters controlling the thermohydromechanical response of the fault. This result is in agreement with the earlier analysis by Lachenbruch (1980) and is comparable with the results obtained by Delaney (1982). If the values of these parameters are small, then the thermal expansion of pore fluids caused by frictional heating during an earthquake event can result in thermal pressurization and a subsequent decrease in the dynamic shear strength of the fault surface. In Figure 3.4 we summarize the conditions of permeability and compressibility which lead to a substantial reduction in the shear strength of the fault surface. The shaded region of Figure 3.4 represents the region where large reductions will occur for events with a total displacement greater than 10^{-1} m, a slip velocity V_{sv} of 1 ms^{-1}, and a coefficient of friction, μ_d, of 0.6. For permeability and compressibility values lying outside the shaded region the thermal expansion of pore fluids is not effective in reducing the shear strength of the fault surface. For $V_{sv}=10^{-1}$ ms^{-1}, or $\mu_d=0.2$, the boundary of the shaded region moves inward to curve (*i*); for $V_{sv}=10^{-1}$ ms^{-1} and $\mu_d=0.2$ to (*ii*).

Figure 3.4 shows that the upper limit of permeability required for a substantial reduction in shear strength is lower than the value of 10^{-13} m^2 suggested by Lachenbruch

(1980). The results presented here indicate that 10^{-15} m^2 is a better estimate of the upper limit for a rigid medium. If the medium is compressible, then this limit must be lowered even further. This discrepency can be explained by considering the various assumptions on which these two analyses are based. In obtaining a first estimate of the upper permeability limit, Lachenbruch neglected the effect of an increase in fluid pressure on the reduction of shear strength and, consequently, on the frictional heat source. Furthermore, he assumed a fault zone of finite width, so that thermal transport could be neglected. With these assumptions, fluid-volume increases due to thermal expansion remain constant during slip, creating a favorable environment for a large increase in temperature and fluid pressure.

This numerical analysis incorporates both thermal transport (conductive and convective) and the feedback of pore pressures in the reduction of shear strength and frictional heating. If pore pressures increase, the rate of frictional heating decreases, and the fluid volume increase due to thermal expansion decreases. This behavior requires a lower permeability to limit fluid flow and to sustain pressurization of the pore fluids. In addition, in estimating an upper limit for the permeability, Lachenbruch allowed the central temperature in the fault zone to increase linearly with displacement. This analysis shows that the fault would stabilize at a constant temperature, with the rate of fluid-volume expansion decreasing to near-zero values. At this

point thermal pressurization is maintained by diffusion of heat from the constant temperature fault surface into the surrounding medium.

Four major assumptions may limit the generality of these results. First, we have simplified the physical situation by assuming the transfer of fluid and heat occurs at right angles to the fault surface. This approach requires uniformity of material properties along the fault and leads to a temperature increase and reduction in shear strength that is uniform over the fault surface; but if there are lateral variations in material properties , especially those of permeability and porous medium compressibility, then the temperature increase and reduction in shear strength will not be uniform over the fault surface. In such case the slip velocity will not be uniform in time or space and will lead to oscillatory slip behavior (e.g.; Nur,1978). The influence of spatial variations in material properties will probably be of second order, and the velocities used earlier represent the average of the oscillatory slip velocity. In addition, because geologic formations are non-uniform, it is doubtful that a complete reduction in shear strength, as suggested by Figure 3.4, could occur.

Second, a kinematic description is incomplete if a rapid decrease in shear strength occurs. The onset of such a reduction will act as a mechanism triggering the release of strain energy stored in the region exterior to the fault,

causing the slip velocity to increase. In this case inertial terms in the stress equations cannot be neglected. The dynamic problem must be considered to understand how slip across the fault relieves strain energy that has risen slowly because of long-term tectonic movement. In addition, the recovery of dilatancy accompanying the release of shear strain can cause a net decrease in pore volume in the adjacent medium and inhibit the migration of fluid from the fault (Scholz *et al.*, 1973; Sibson, 1973; Lachenbruch, 1980). The combination of these two effects would cause a further enhancement in the rate of thermal pressurization.

Third, deformation has been confined to a planar surface, so that the friction law can be used to describe frictional heat generation. In fact, as the thermal pressurization of the adjacent region progresses, the effective stress will decrease in compression and thereby promote inelastic-deformation mechanisms such as frictional sliding past grain boundaries and microfracturing. As microfracturing generally occurs at fluid pressures below the minimum principle stress, some sort of inelastic response would occur prior to a complete reduction in shear strength. This behavior will cause a loss of cohesion and a net reduction in the shear strength of the porous medium adjacent to the fault surface. The loss of cohesion could cause an initially planar zone to broaden as slip progresses.

Fourth, we have assumed that fluid pressures could approach lithostatic values. However, if the least principle stress is less than the lithostatic stress, then hydrofracturing may intervene and act to stabilize the fluid pressure at the value of the least principle stress. In such case, the shear strength of the fault surface will not be reduced to near-zero values but will asymptotically approach the value

$$\mu_d(\tau_n'-\tau_3') \tag{3.27}$$

where τ_3' is the least principle stress. The temperature rise will no longer approach a maximum value but will continue to rise at a reduced rate determine by equation (3.27). This behavior could lead to extensive fracturing of the region adjacent to the fault surface. It is not clear, however, whether such hydrofracturing could be important on the time scale of an earthquake event (Lachenbruch, 1980). In any case, the influence of microfracturing will probably not change the conditions required for thermal pressurization to reduce the initial shear strength.

The third and fourth assumptions pose the greatest limit on using the results presented here. For low values of permeability ($<10^{-19}$ m^2) high pore pressures will be confined to a narrow zone. For high values of permeabilities ($>10^{-15}$ m^2), the pore pressure rise will be insufficient to affect the strength of the adjacent medium. Thus, for these two extremes

the approximation of a planar fault surface should hold, provided that the surface was initially planar. For intermediate permeabilities, however, the migration of pore fluids will cause a progressive weakening of the region adjacent to the fault surface and a widening of the zone of deformation. Lachenbruch (1980) showed that if the fault zone width is greater than the displacement, or if the pore-dilatation strain exceeds 2 or 3% of the shearing strain, then coupling of thermal, hydrologic, and mechanical effects is unimportant. Whether or not the zone will widen sufficiently to halt the thermal pressurization process, or to stabilize at a certain width and shear strength, depends upon the constitutive relation between shear strength and effective stress. Furthermore, the formation of new microfractures and improved interconnectivity of these fractures can lead to a substantial increase in permeability. This behavior leads to enhanced fluid flow, which may arrest the thermal pressurization process and cause a restoration of the shear strength.

CONCLUSIONS

This paper illustrates how the effects of heat transfer and fluid flow influence the thermohydromechanical response of a fault surface during slip. The analysis leads to the following conclusions:

1. For rigid media with low permeability, only a small

temperature increase is required for the thermal expansion of pore fluids to pressurize the fluids and to maintain the fluid pressure on the fault surface at near-lithostatic values. This result is in agreement with the earlier analysis by Lachrnbruch (1980). For media with greater permeabilities or porous medium compressibilities, or both, large temperature rises are required on the fault surface for the thermal pressurization of pore fluids to overcome fluid losses due to fluid flow or fluid-volume changes due to pore dilatation, or both. Temperatures on the fault plane stabilize at the point where there is a dynamic balance between the temperature and pressure fields, with the increase in fluid volume due to thermal expansion equal to fluid loss due to flow and fluid-volume changes due to pore dilatation.

2. The dynamic shear strength remains close to its initial value until the fault surface is heated to a temperature required for thermal expansion of pore fluids to exceed substantially fluid losses due to flow and fluid-volume changes due to pore dilatation. Once this condition is established, the shear strength diminishes rapidly to a value sufficient to maintain the thermal pressurization process. For media with greater permeability or compressibility, or both, the shear strength will remain close to its initial value over greater displacements. If either the permeability exceeds 10^{-15} m^2 or the porous medium compressibility exceeds 10^{-8} Pa^{-1}, then frictional melting may reduce the dynamic shear strength before the effects of thermal pressurization become

significant.

3. The main effect of varying the depth to the fault surface is to change the initial conditions at the onset of slip. Because increases in the initial effective stress lead to an increase in the maximum fluid pressure, the temperature required to sustain fluid pressures at near-lithostatic values depends on the initial effective stress. If fluid pressures are initially hydrostatic, then the final temperature attained on the fault surface increases with depth. However, because the transient rate of decrease of the shear strength depends primarily on the material properties of the porous medium, and on the coefficent of friction and the slip velocity on the fault surface, changes in initial conditions do not significantly change the rate of decrease in shear strength.

4. The coefficient of friction and slip velocity determine the rate at which thermal pressurization proceeds, but not the final outcome. However, if the coefficient of friction is less than 10^{-1} and if the slip velocity is less than 10^{-2} ms^{-1}, then it is doubtful that either thermal pressurization or frictional melting could reduce the dynamic shear strength of the fault surface. In these conditions frictional heating is small, and the temperature rise would be minimal for an earthquake event with realistic displacement.

APPENDIX: NUMERICAL SOLUTION OF EQUATIONS

Equations (3.14) and (3.15) are solved numerically using a Galerkin finite-element technique with linear basis functions and deforming coordinates. Temperature, fluid pressure, and material and fluid properties vary linearly across each of the elements. Time derivatives are approximated by a fully implicit backward difference scheme. The thermodynamic properties of water are incorporated as state functions of fluid pressure and temperature using relations given by Keenan *et al.* (1978) for density and specific heat, Watson *et al.* (1981) for dynamic viscosity, and Kestin (1978) for thermal conductivity.

The heat flux from the fault surface can be considered as a surface discontinuity in the heat flux across the region, giving rise to a Dirac delta function. Thus frictional heating on a fault surface at an arbitrary location x_f can be described as

$$Q|_{x_f} = \mu_d(\tau_n'-P)\, V_{sv}\delta(x-x_f) \qquad (3.A1)$$

This equation is handled easily using finite element techniques. Because of the properties of the Dirac delta function, the frictional heat flux is simply added to the righthand side of the finite-element equation for node x_f. This approach has the advantage of allowing non-uniform material properties on either side of the fault surface or

multiple faults with varying coefficients of friction and slip velocities, or both.

For all simulations the grid spacing increases with distance from the fault surface, with the smallest grid spacing adjacent to the fault. For problems that are symmetric about the fault surface, the equivalent half-space problem is modeled. The discretization error caused by lumping the frictional heat flux, equation (3.A1), into a single node was minimized by running several simulations of the same problem, reducing the grid spacing until identical results were obtained for two successive runs. The minimum grid spacing required to insure numerical stability was 10^{-5} m and 10^{-4} m for slip velocities of 1 ms^{-1} and 10^{-1} ms^{-1}, respectively.

A solution procedure is employed where the heat-transfer and fluid-flow equations are solved sequentially for a given time step. An iterative technique is used to couple the heat-transfer and fluid-flow equations. The size of the time step is adjusted automatically following a procedure that limits the magnitude of changes in pressure and temperature to some specified value which will insure rapid convergence. Initial time steps were on the order of 10^{-6} s. The first step in the procedure is to solve for the temperature field using the fluid pressure, and material and fluid properties from the previous time step. The fluid-flow equation is then solved using the newly calculated temperature field to estimate the fluid-volume changes due to thermal expansion. Porosity is

updated by using the analytical solution of equation (3.16) over the time step

$$n_t = 1 - (1-n_{t-\Delta t})\exp[\ -(\overline{\beta}_{sf}-\overline{\xi\beta}_s)(p_t-p_{t-\Delta t}) - (\overline{\gamma}_{sf}-\overline{\gamma}_s)(\Theta_t-\Theta_{t-\Delta t})\ ] \qquad (3.A2)$$

where the porosity is assumed to be linearly independent of Θ and p, and the bar denotes the average value of the variable over the time step. The fluid and material properties are then updated using the new estimate of the temperature, fluid pressure and porosity fields, and equation (3.11) is integrated over the flow domain to obtain the displacement of the nodes from their position at the previous time step. An iterative sequence is then employed until the maximum pressure and temperature change between successive iterations is less than a specified tolerance (10^{-2} MPa and 10^{-2} °C, respectively). Once this criterion is met, the model proceeds to the next time step.

NOTATION

c_w	isobaric specific heat of water.
e	volumetric strain (dilatation) $e_{11}+e_{22}+e_{33}$.
e_{ij}	solid matrix strain.
f	as a subscript denotes fluid.
k	porous medium permeability.
k_s	bulk modulus of the solid grains.
k_{sf}	bulk modulus of the porous medium.
K_s	thermal conductivity of the solid grains.
K_w	thermal conductivity of water.
K_{sf}	thermal conductivity of the solid-fluid composite.
n	porosity.
p	fluid pressure increase above ambient conditions.
P	pore fluid pressure.
P_0	initial fluid pressure.
q_x	fluid specific discharge relative to the solid matrix.
s	as a subscript denotes solid.
t	time.
T	temperature.
T_0	initial temperature.
U_x	displacement of the solid matrix from its initial position.
$\mathbf{v}_s$	solid-matrix velocity with respect to a fixed coordinate system.
V_{sv}	relative slip velocity across the fault surface.
w	as a subscript denotes water.
a_h	hydraulic diffusivity.
a_t	thermal diffusivity.
Γ	thermal pressurization coefficient.
β_s	isothermal compressibility of the solid grains.
β_{sf}	porous medium compressibility.
β_w	isothermal compressibility of water.
δ_{ij}	Kronecker delta function.
η	characteristic diffusion length.

γ_s isobaric thermal expansivity of the soild grains.

γ_{sf} linear thermal expansion coefficient of the porous medium.

γ_w isobaric thermal expansivity of water.

μ shear modulus.

μ_d dynamic coefficient of friction on the fault surface

μ_w dynamic viscosity of water.

ν Poisson's ratio

ρ_s density of the solid grains.

ρ_w density of water.

$(\rho c)_{sf}$ heat capacity of the soild-fluid composite.

$\overline{\tau}$ average effective normal stress $(\tau_{11}+\tau_{22}+\tau_{33})/3$.

τ_{ij} components of the effective stress tensor.

τ'_{ij} components of the total stress tensor.

τ_n effective normal stress acting on the fault surface.

τ'_n total normal stress acting on the fault surface.

τ_r resistive shear strength of the fault surface.

τ_{r_o} initial resistive shear strength of the fault surface.

Θ temperature increase over ambient conditions.

ξ proportionality constant between pore and bulk volume changes.

REFERENCES

Biot, M. A., General theory of three dimensional consolidation, *J. Appl. Phys.*, 12, 155-164, 1941.

Biot, M. A. and D. G. Willis, The elastic coefficients of the theory of consolidation, *J. Appl. Mech.*, 24, 594-601, 1957.

Byerlee, J. D., Friction of rocks, *Pure and Appl. Geophys.*, 116, 615-626, 1978.

Cardwell, R. K., D. S. Chinn, G. F. Moore, and D. L. Turcotte, Frictional heating on a fault of finite thickness, *Geophys. J. Roy. Astron. Soc.*, 52, 525-530, 1978.

Carslaw, H.C., and J.C. Jaeger, **Conduction of Heat in Solids**, 386pp., Oxford University Press, New York, 1959.

Holcomb, D.J., A quantitative model of dilatancy in dry rock and its application to Westerly granite, *J. Geophys. Res.*, 83(B10), 4941-4950, 1978.

Holcomb, D.J., Memory, relaxation, and microfracturing in dilatant rock, *J. Geophys. Res.*, 86(B7), 6235-6248, 1981.

Jaegar, J.C., Moving sources of heat and temperature at sliding contacts, *J. Proc. R. Soc. N.S.W.*, 76, 203-224, 1942.

Jorgensen, D.G., Relationships between basic soils-engineering equations and basic ground-water flow equations, *U.S. Geol. Survey Water-Supply Paper*, 2064, 46pp., 1981.

Keenan, J.H., F.G. Keyes, P.G. Hill, and J.G. Moore, **Steam Tables**, 162pp., John Wiley, New York, 1978.

Kestin, J., Thermal conductivity of water and steam, *Mech. Eng.*, 100(8), 1255-1258, 1978.

Lachenbruch, A. H., Frictional heating, fluid pressure, and the resistance to fault motion, *J. Geophys. Res.*, 85(B11), 6097-6112, 1980.

Lachenbruch, A.H., J.H. Sass, R.J. Munroe, and T.H. Moses,Jr., Geothermal setting and simple heat conduction models for the Long Valley Caldera, *J. Geophys. Res.*, 81, 769-784, 1976.

Lockner, D.A., and P.G. Okubo, Measurements of frictional heating in granite, *J. Geophys. Res.*, 88(B5), 4313-4320, 1983.

Logan, J.M., Brittle phenomena, *Rev. Geophys. Space Phys.*, 17, 1121-1132, 1979.

McKenzie, D. P. and J. N. Brune, Melting of fault planes

during large earthquakes, *Geophys. J. Roy. Astron. Soc.*, 29, 65-78, 1972.

Morrow, C.A., L.Q. Shi, and J.D. Byerlee, Strain hardening and strength of clay-rich fault gouges, *J. Geophys. Res.*, 87, 6771-6780, 1982.

Nur, A. and J. D. Byerlee, An exact effective stress law for elastic deformation of rock with fluids, *J. Geophys. Res.*, 76, 6414-6419,1971.

Raleigh, B., and J. Everden, Case for low deviatoric stress in the lithosphere, in *The Mechanical Behavior of Crustal Rocks, Geophys. Monogr. Ser.*, vol. 24, edited by N.L. Carter, M. Friedman, J.M. Logan, and D.W. Stearns, pp. 173-186, AGU, Washington, D.C., 1981.

Rice, J.R. and J.W. Rudnicki, Earthquake precursory effects due to pore fluid stabilization of a weakening fault zone, *J. Geophys. Res.*, 84(B5), 2177-2193, 1979.

Rice, J.R. and D.A. Simons, The stabilization of spreading shear faults by coupled deformation-diffusion effects in fluid-infiltrated porous media, *J. Geophys. Res.*, 81, 5322-5334, 1976.

Richards, P.G., Dynamic motions near an earhquake fault: a three dimensional solution, *Bull. Seis. Soc. Am.*, 66, 1-32, 1976.

Scholz, C.H., Shear heating and the state of stress on faults, *J. Geophys. Res.*, 85(B11), 6174-6184, 1980.

Teufel, L.W., and J.M. Logan, Effect of displacement rate on the real area of contact and temperatures generated during frictional sliding of Tennessee sandstone, *Pure and Appl. Geophys.*, 116, 840-865, 1979.

Watson, J.T.R., R.S. Basu, and J.V. Sengers, An improved representative equation for the dynamic viscosity of water substance, *J. Phys. Chem. Ref. Data*, 9(3), 1255-1279, 1980.

Woodside, W. and J.H. Messmer, Thermal conductivity of porous media, *J. Appl. Phys.*, 32, 1688, 1961.

TABLE 3.1. Parameter Values for Porous Medium and Solid Properties Constant for All Simulations.

Property	Value
Porosity n	0.20
ξ	1.0
Thermal expansivity of the porous medium γ_{sf}	10^{-5} °C^{-1}
Compressibilty of the solid β_s	10^{-11} Pa^{-1}
Density of the solid ρ_s	2.6×10^3 kg m^{-3}
Specific heat of the solid c_s	10^3 J kg^{-1} °K^{-1}
Thermal conductivity of the solid K_s	2.5 W m^{-1} °K^{-1}
Compressibilty of the solid β_s	10^{-11} Pa^{-1}
Thermal expansivity of the solid γ_s	2.5×10^{-5} °C^{-1}

FIGURE CAPTIONS

Figure 3.1. Conceptual model of planar fault zone.

Figure 3.2. Temperature rise during displacement on a fault surface with a uniform coefficient of friction μ_d=0.6, constant-slip velocity V_{sv}=10^{-1} ms^{-1}, and initial effective stress τ_n=24 MPa acting on the fault surface. The k (m^2) and β_{sf} (Pa^{-1}) are the permeability and compressibility of the surrounding porous medium. The initial thermal pressurization coefficient is: (a) Γ=1.4x10^6 Pa °C^{-1}; (b) Γ=6.6x10^5 Pa °C^{-1}; (c) Γ=1.1x10^5 Pa °C^{-1}; (d) Γ=1.1x10^4 Pa °C^{-1}.

Figure 3.3. Change in the dynamic shear strength τ_r with displacement on a fault surface with a uniform coefficient of friction μ_d=0.6, constant-slip velocity V_{sv}=10^{-1} ms^{-1}, and initial effective stress τ_n=24 MPa acting on the fault surface. The k (m^2) and β_{sf} (Pa^{-1}) are the permeability and compressibility of the surrounding porous medium. The initial thermal pressurization coefficient is: (a) Γ=1.4x10^6 Pa °C^{-1}; (b) Γ=6.6x10^5 Pa °C^{-1}; (c) Γ=1.1x10^5 Pa °C^{-1}; (d) Γ=1.1x10^4 Pa °C^{-1}.

Figure 3.4. Summary of constraints on permeability and compressibility of the porous medium for a substantial reduction in shear strength to occur. Region where large

reductions will occur for earthquake events with a total displacement greater than 10^{-1} m, a slip velocity V_{sv} of 1 ms^{-1}, and a coefficient of friction, μ_d, of 0.6. For permeability and compressibility values lying outside the shaded region the thermal expansion of pore fluids is not effective in reducing the shear strength of the fault surface. For $V_{sv}=10^{-1}$ ms^{-1}, or $\mu_d=0.2$, the boundary of the shaded region moves inward to curve (*i*); for $V_{sv}=10^{-1}$ ms^{-1} and $\mu_d=0.2$ to (*ii*).

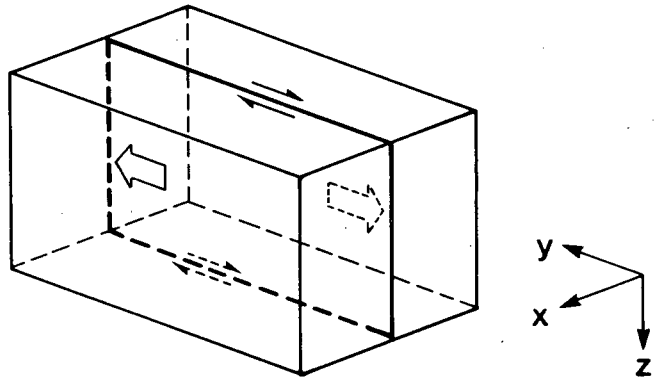

Figure 3.1

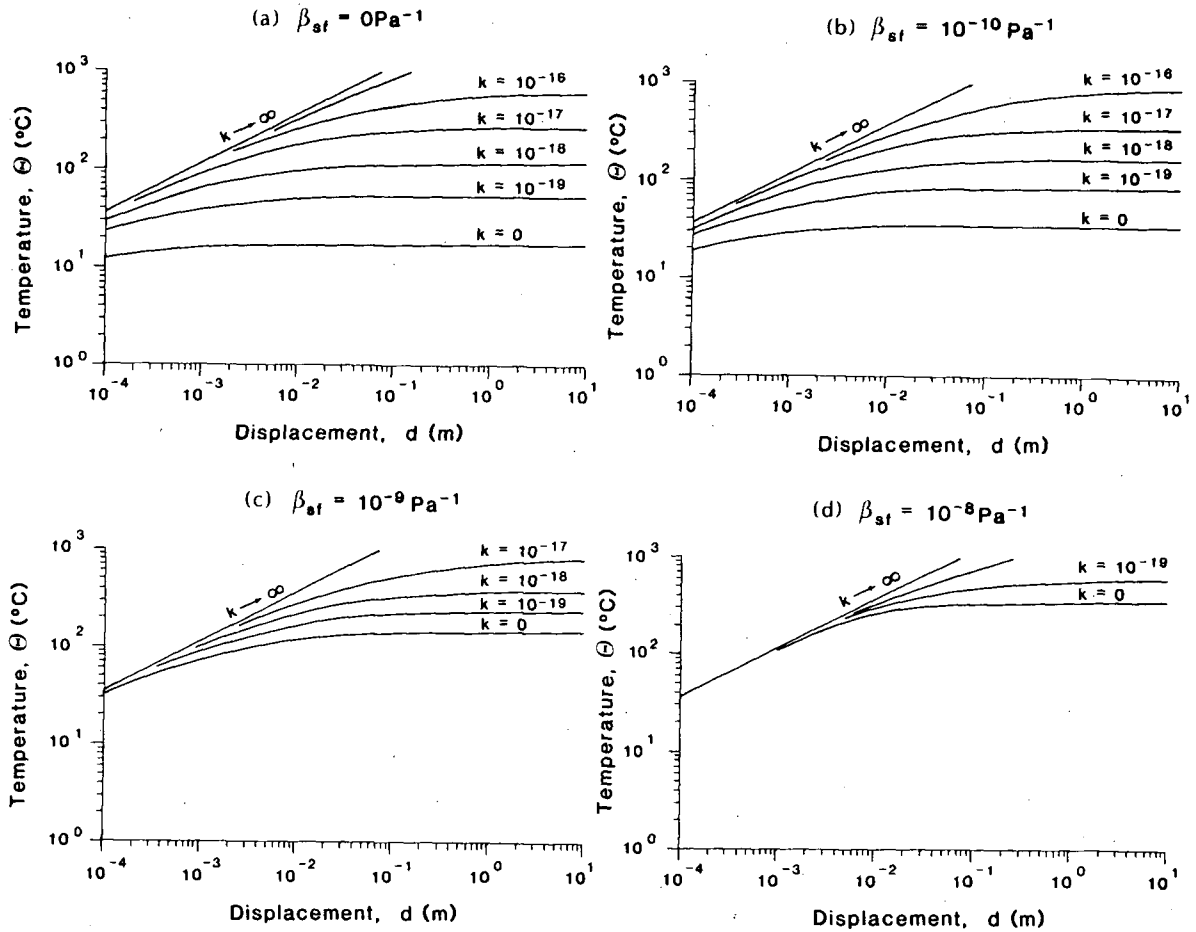
(a) β_{sf} = 0Pa^{-1}
(b) β_{sf} = 10^{-10}Pa^{-1}
(c) β_{sf} = 10^{-9}Pa^{-1}
(d) β_{sf} = 10^{-8}Pa^{-1}
Temperature, Θ (°C)
Displacement, d (m)
k → ∞
k = 10^{-16}
k = 10^{-17}
k = 10^{-18}
k = 10^{-19}
k = 0

Figure 3.2

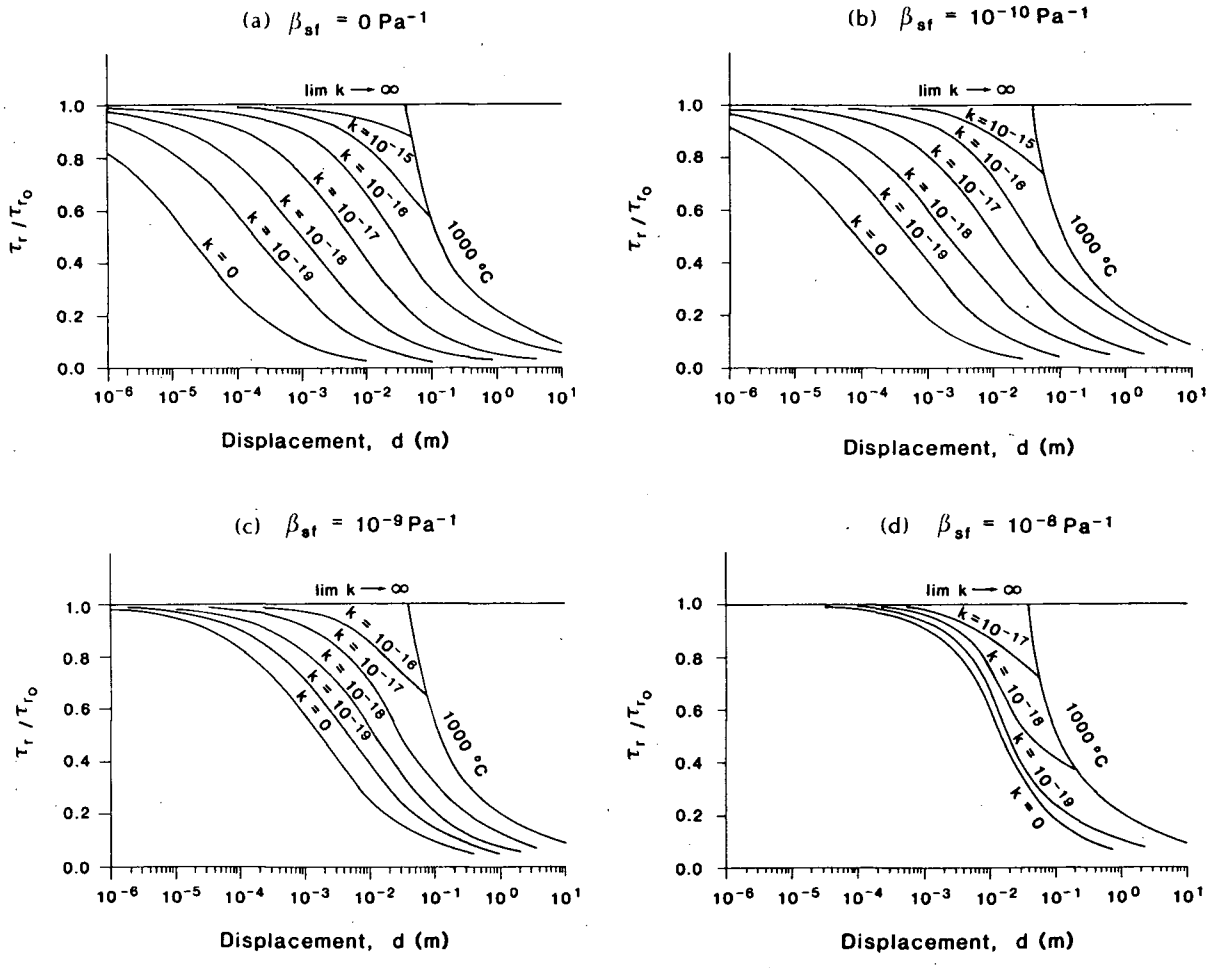
(a) β_{sf} = 0 Pa^{-1}
(b) β_{sf} = 10^{-10} Pa^{-1}
(c) β_{sf} = 10^{-9} Pa^{-1}
(d) β_{sf} = 10^{-8} Pa^{-1}
τ_r / τ_{ro}
Displacement, d (m)
lim k → ∞
k=10^{-15}
k = 10^{-16}
k = 10^{-17}
k = 10^{-18}
k = 10^{-19}
k = 0
1000 °C

Figure 3.3

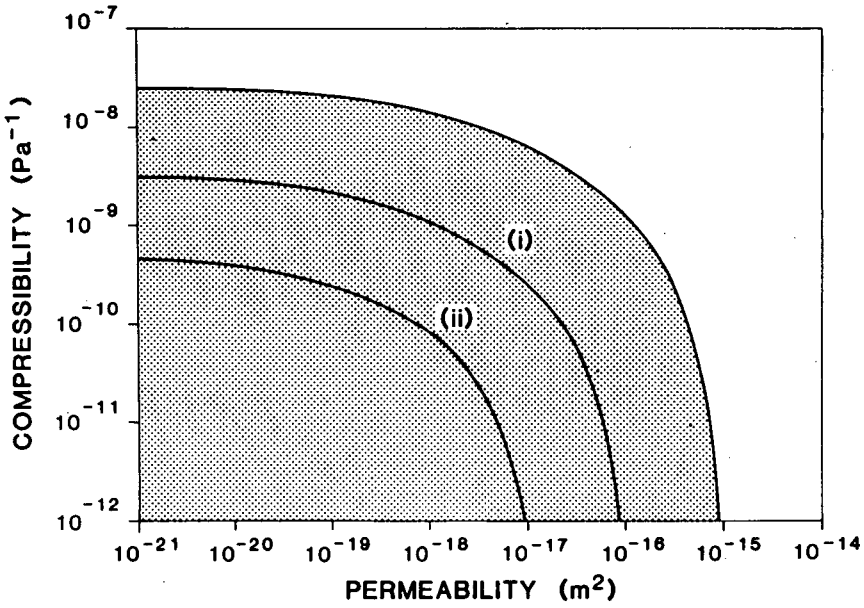
COMPRESSIBILITY (Pa^{-1})
10^{-7}
10^{-8}
10^{-9}
10^{-10}
10^{-11}
10^{-12}
(i)
(ii)
10^{-21} 10^{-20} 10^{-19} 10^{-18} 10^{-17} 10^{-16} 10^{-15} 10^{-14}
PERMEABILITY (m^2)

Figure 3.4

CHAPTER IV

THE EFFECTS OF FRICTIONAL HEATING ON THE THERMAL, HYDROLOGIC, AND MECHANICAL RESPONSE OF A FAULT DURING SLIP

Hubbert and Rubey (1959) were the first to suggest that the movement of a large thrust sheet requires a low frictional resistance to motion along its base. Given that the coefficient of friction is reasonably uniform for a variety of rock types and a wide range of normal stresses, if the resistive shear stress is small, then high fluid pressures are fundamental to the Hubbert-Rubey theory of thrust faulting. If thrusting and other forms of faulting are initiated and sustained by abnormally high fluid pressures, then mechanisms for generating and maintaining that pressure pose a fundamental problem in fault mechanics. One such mechanism, a transient increase in fluid pressure due to thermal expansion of pore fluids caused by frictional heating within a fault zone, is the subject of this paper.

Assuming the failure surface is established, many investigators have shown that frictional heating could play an important role in the dynamics of fault processes. Jaeger (1942), McKenzie and Brune (1972), Richards (1976), Cardwell *et al.* (1978), Scholz (1980), and Sibson (1980) suggested frictional heating could lead to partial melting on the fault surface with a subsequent reduction in dynamic shear strength. These studies have neglected the presence and possible effect

of pore water. If water is present, the dynamics are more complicated. Sibson (1973) showed that for an impermeable medium frictional heating could result in lithostatic fluid pressures causing the dynamic shear strength to approach near-zero values. Lachenbruch (1980) discussed the governing equations for heat and fluid flow, and analyzed for special cases the interaction of parameters controlling thermal pressurization and their critical range of values. The concepts discussed in this work form the basis for our analyses. Lachenbruch concluded that if permeability or pore-dilatation rate exceed 10^{-13} m^2 or 2%, respectively, then coupling of thermal, hydrologic, and mechanical effects could probably be neglected, with fluid pressure and dynamic shear strength remaining constant during slip. Raleigh and Everden (1981), assuming no transport of fluid or heat, calculated the maximum fluid pressure increase for various displacements, slip velocities, and fault widths. While these studies have illustrated the basic features of the response, they have considered only a fault zone of constant width and fixed strain rate, for the following two limiting cases: those cases where fluid transport is so large it nullifies thermal pressurization, and those cases where transport of heat or fluid, or both, are so small they can be neglected. For intermediate conditions, these studies do not provide an adequate description of the transient increase in temperature within a fault zone during slip, and its effect on the fluid pressure and stress fields.

In a previous paper (Mase and Smith, 1985), we examined these intermediate conditions using numerical modeling techniques, and discussed the temperature and fluid pressure rise on a fault surface for a simple kinematic model of slip. It was shown that the response of fluid pressures to frictional heating could be described by the following two limiting cases. If the permeability or compressibility of the porous medium are greater than 10^{-15} m^2 or 10^{-8} Pa^{-1}, then the thermal expansion of pore fluids is accomodated by fluid flow from or pore dilatation within the heated region adjacent to the fault surface. In this case the fluid pressure and dynamic shear strength remain unchanged during slip. Consequently, the fault is a large source of frictional heat and partial melting may occur. This upper limit for permeability is lower than the 10^{-13} m^2 limit of Lachenbruch because of coupled thermal and hydrologic effects, and our assumption of a planar fault. If the permeability and compressibility of the porous medium are less than 10^{-19} m^2 and 10^{-11} Pa^{-1}, then the heating process takes place at constant fluid mass and substantial increases in fluid pressure can occur. If fluid pressures approach lithostatic values, the sliding surfaces will lose cohesion and the rate of frictional heating and the dynamic shear strength will approach zero. In this case the maximum temperature attained on the fault surface is substantially less than that required for frictional melting.

In this study we expand this model to account for both fault zones of finite width and for the dynamics of a variable

resistive stress. We examine the physical parameters that control the thermal and hydrologic fields, and discuss an important parameter, the thermal pressurization coefficient. This parameter controls the rates of pore dilatation and fluid pressurization due to a temperature rise. We describe the thermal and hydrologic effects during fault motion, dimensionless measures of their importance, and characteristic time scales for thermal pressurization. The aim of this paper is to examine the full nonlinear behavior of fault motion, and to determine limits to fault behavior for various ranges of the controlling parameters. A list of mathematical symbols is given in the notation list at the end of the paper.

A MATHEMATICAL MODEL FOR SLIP ACROSS A FAULT ZONE

Most models concerning earthquakes are based on elastic rebound theory (e.g., Reid, 1910, 1911; Mavko, 1981). In this theory elastic strain energy arising from long-term tectonic movement is abruptly released during earthquakes. This process of strain buildup and release repeats itself in a roughly cyclic fashion, and is commonly referred to as *stick-slip* behavior (e.g., Brace and Byerlee, 1966; Walsh, 1968; Dietrich, 1974, 1979a, 1979b). Figure 4.1a shows a schematic model of this behavior for a strike-slip fault. The fault is represented by a vertical zone of finite width that is comprised of patches of relatively high strength rock (barriers) surrounded by weaker intervening areas. This zone accomodates the relative motion between the two fault blocks.

Long-term tectonic motion causes the adjacent elastic region to deform and the stress at the barriers to increase. At the instant of failure a barrier ruptures and slip spreads through the locked portion of the fault until fault motion is halted by a barrier (e.g., Das and Aki, 1977; Mikumo and Miyatake, 1978; Aki, 1979, 1984; McGarr, 1981; Das and Scholz, 1981; Papageorgiou and Aki, 1983a, 1983b; Rundle *et al.*, 1984; Stuart *et al.*, 1985). We do not propose to solve for the temperature, fluid pressure, slip distribution, and stress drop over the entire fault. Rather, we examine only the thermal, hydrologic and mechanical response of a small patch of the fault that is arbitarily located on the failure surface, and consider the physical parameters that control its response. We will assume the initial material properties within and adjacent to the patch are uniform. In a later section we return to the topic of spatial heterogeneities, and discuss their effects on the spatial variability of the stress drop, slip rate, and displacement over the fault.

Figure 4.1b shows a simplified geometry for such a patch. The patch consists of two elastic blocks which slide past each other on a narrow planar zone. The width of the elastic blocks is defined by the characteristic length between barriers. This length may be on the order of hundreds of meters to tens of kilometers, whereas the width of the fault zone is on the order of hundreths of meters to several meters. The fault zone deforms by simple shear in the presence of uniaxial compression normal to the fault, and undergoes strains that

are finite and irrecoverable. Prior to slip quasi-static stress conditions apply within the blocks, with the shear stress at the initiation of slip given by the static shear strength of the fault. We assume that fault rupture starts suddenly with a uniform stress drop and slip velocity over the entire patch. The failure surface may be a preexisting fault zone or a new fracture caused by failure. Energy consumed in breaking cohesive bonds or creating new fracture surfaces is assumed to be negligible (e.g., Richards, 1976; Lachenbruch and Sass, 1980). In addition, fluid-pressure changes that might arise from effects at the propagating ends of the failure surface (e.g.; Rice and Simons, 1976; Rice and Rudnicki, 1979) are assumed to be small in comparison to changes in fluid pressure arising from frictional heating. These assumptions are reasonable for earthquakes where the propagation velocities of the fault tips are several orders of magnitude greater than the relative slip velocity across the failure surface. During slip the width of the thermal and hydrologic fields caused by frictional heating is negligible in comparison to the width of the elastic blocks. Consequently, the effects of thermal pressurization can be regarded as a transient drop in stress on the boundaries of the elastic blocks. In this case the slip velocity of the blocks is determined by the decrease in the shear strength of the fault patch. Using this approach, it is possible to characterize how the decrease in shear strength during slip relieves the elastic strain energy that has risen slowly

because of long-term tectonic movement.

Any calculation of the thermal and hydrologic fields depends upon the rheological relation which links the shear strength to deformation rate, fluid pressure, and temperature. Currently, little is known about the rheological behavior of a fault zone at any depth. For disaggregated fault gouge it is probable the rheology would follow a friction law behavior; that is the shear strength approaches zero as the fluid pressures appoach lithostatic values (e.g., Handin *et al.*, 1963; Jaeger and Cook, 1969; Savage, 1977; Lachenbruch, 1980). We assume that the shear stress required for slip across the fault is given by the friction law

$$\tau_r = \mu_d(\tau_n - P) \qquad (4.1)$$

where τ_r is the resistive shear stress, μ_d is the dynamic coefficient of friction, τ_n is the total normal stress acting across the fault, and P is the pore-fluid pressure. A principal motivation for using this law is its wide-spread applicability in describing the results of laboratory experiments for a variety of rock types. For most rocks μ_d is insensitive to composition and hardness, and has values between 0.4 and 1.0 (Byerlee, 1978). For surfaces separated by a thin clay-rich layer of fault gouge, Morrow *et al.* (1982) reported values for μ_d that ranged from 0.2 to 0.6. In general, the coefficient of friction is dependent on the effective normal stress and deformation history of the fault

zone (e.g., Dietrich, 1979a, 1979b; Rice, 1983; Ruina, 1983, 1984). Because this law describes the gross resistance between two sliding blocks, the shear stress is influenced only by the effect that frictional heating has on the fluid pressure and slip rate. This approach decouples the equations describing motion within the fault zone from the equations describing fluid pressure and temperature. Thus it is not possible to examine the evolution of inelastic deformation, and *a priori* assumptions about the width of deformation and the strain rate across the zone must be made to calculate the fluid-pressure and temperature fields. Without a rheological law relating the shear strength to fluid pressure and deformation rates, we simply note when these calculations imply that deformation would expand or contract about the edges of the zone.

If we assume a width $2w$ for the fault zone, then the rate of shear heating within the zone is given by

$$\mu_d(\tau_n - P) \cdot \frac{V_y}{w} \tag{4.2}$$

where $2V_y$ is the relative slip velocity of the elastic blocks. This relationship assumes that deformation is not continuous across the zone, but is comprised of a number of slip planes with a spacing such that frictional heat generated on the planes acts as a distributed heat source for the time scale of interest. Measurements of frictional heating in granite and sandstone suggest that (4.2) gives a good representation of the average temperature generated on the fault surface, but

yields little information about local maxima at asperity contacts (Teufel and Logan, 1978; Logan, 1979; Lockner and Okubo, 1983). For the case where fluid pressures remain constant, equation (4.2) has been used to predict high temperatures during slip (McKenzie and Brune, 1972; Richards, 1976; Cardwell, 1978; Lachenbruch, 1980).

In this framework the transfer of fluid and heat occurs at right angles to the fault, and the mathematical problem involves finding solutions to the one-dimensional equations describing heat transfer, fluid flow, and stress. These equations are outlined below. All equations are expressed in a Lagrangian reference frame with respect to the solid matrix of the porous medium.

Heat Transfer Equation

The equation of heat transfer describing the temperature distribution in a saturated porous medium is given by

$$\frac{\partial}{\partial x}(K_{sf}\frac{\partial T}{\partial x}) - \rho_w c_w q_x(\frac{\partial T}{\partial x}) + n\gamma_w[\frac{\partial P}{\partial t} + \frac{q_x}{n}(\frac{\partial P}{\partial x})]T +$$

$$\mu_d(\tau_n - P)\frac{V_y}{w}[H(x+w)-H(x-w)] = (\rho c)_{sf}\frac{\partial T}{\partial t} \qquad (4.3)$$

where mathematical symbols are defined separately in the notation list. For mathematical convenience the centerline of the fault is fixed at $x=0$. The terms on the lefthand side are, in order, the rate of conductive heat transport, the rate of

advective heat transport, the rate of heat addition due to pressurization of the fluid, and the rate of frictional heating within the fault zone. The term on the righthand side represents the rate of internal heat storage. Local thermal equilibrium between the solid matrix and the fluid is assumed. The thermal conductivity of the solid-fluid composite is given by $K_{sf} = K_s^{(1-n)} K_w^n$ (Woodside and Messmer, 1961).

Fluid and Solid Mass Conservation Equations

Assuming the pores are saturated with water, and that the solid and fluid phases are mechanically distinct, the equation for conservation of fluid mass is

$$-\frac{\partial}{\partial x}(q_x) - q_x[\beta_w(\frac{\partial P}{\partial x}) - \gamma_w(\frac{\partial T}{\partial x})] + [n\gamma_w + (1-n)\gamma_s]\frac{\partial T}{\partial t} = \frac{\partial e}{\partial t} + [n\beta_w \frac{\partial P}{\partial t} + (1-n)\beta_s \frac{\partial \bar{T}}{\partial t}] \qquad (4.4a)$$

$$q_x = -\frac{k}{\mu_w}\frac{\partial P}{\partial x} \qquad (4.4b)$$

where q_x is the Darcy flux. The terms on the lefthand side of (4.4a) are, in order, the rate of fluid transport, the change in fluid mass due to pressure contraction or thermal expansion of fluids along the flow path, and the change in fluid mass due to the difference in thermal expansivities of the fluid and solid phases. The terms on the righthand side are the change in fluid mass due to volumetric dilatation of the

porous medium and the change in fluid mass due to the difference in the compressibility of the fluid and solid phases. In equation (4.4b) fluid flow due to gravitational forces is assumed to be negligible for the time scale of interest. For water the compressibility β_w and thermal expansivity γ_w coefficients are strongly temperature dependent. This dependence is shown in Figure 4.2.

The condition for conservation of the solid mass requires the following compatibility constraint for porosity:

$$\frac{\partial n}{\partial t} = (1-n)\left[\frac{\partial e}{\partial t} + \beta_s \frac{\partial \bar{\tau}}{\partial t} - \gamma_s \frac{\partial T}{\partial t}\right] \tag{4.5}$$

where e is the volumetric-dilatation. Equation (4.5) states that the pore-dilatation rate ($\partial n/\partial t$) is given by the rate at which solids are leaving a unit volume minus the rate at which they are expanding due to decreases in the average effective normal stress or increases in temperature within the volume.

Equations of Motion

Deformation of the porous medium is governed by the effective stress τ_{ij} which is defined as

$$\tau_{ij} = \tau'_{ij} - \xi P \delta_{ij} \tag{4.6}$$

where stresses are defined as positive when compressive, τ'_{ij} is the total stress, and ξ is the ratio of fluid volume

expelled to the volumetric dilatation for drained conditions. From stress-strain measurements Biot and Willis (1957), and Nur and Byerlee (1971) have suggested that

$$\xi = \frac{k_{sf} - k_s}{k_{sf}} \tag{4.7}$$

where k_s and k_{sf} are the bulk moduli of the solid grains and porous medium, respectively. For media with appreciable porosity, $k_s/k_{sf} \ll 1$, with $\xi \simeq 1$, and the fluid volume expelled is equal to the volumetric dilatation. With equation (4.6) the equations of motion for the block are

$$\frac{\partial}{\partial x}\tau_{xx} + \frac{\partial}{\partial x}(\xi P) + \rho_{sf}\frac{\partial}{\partial t}V_x = 0 \tag{4.8a}$$

$$\frac{\partial}{\partial x}\tau_{xy} + \rho_{sf}\frac{\partial}{\partial t}V_y = 0 \tag{4.8b}$$

For a linear-elastic porous medium the constitutive equations for stress and strain are (after Biot and Willis, 1957)

$$\tau_{ij} = -2\mu\left[\frac{\nu}{(1-2\nu)}e_{kk}\delta_{ij} + e_{ij}\right] + \frac{2\mu(1-\nu)}{(1-2\nu)}\gamma_{sf}(T-T_0)\delta_{ij} \tag{4.9}$$

where solid-matrix strains and displacements are positive in extension. Substitution of (4.9) into (4.8), and writing the strains and velocities in terms of solid-matrix displacements yields

$$\frac{\partial}{\partial x}\left[\frac{2\mu(1-\nu)}{(1-2\nu)}\left(\frac{\partial}{\partial x}U_x-\gamma_{sf}\Theta\right)-\xi p\right] = \rho_{sf}\frac{\partial^2}{\partial t^2}U_x \qquad (4.10a)$$

$$\frac{\partial}{\partial x}\left(\mu\frac{\partial}{\partial x}U_y\right) = \rho_{sf}\frac{\partial^2}{\partial t^2}U_y \qquad (4.10b)$$

where $p=(P-P_0)$ is the fluid pressure increase above the initial value P_0, and $\Theta=(T-T_0)$ is the temperature increase above the initial value T_0. Equation (4.10a) determines the volumetric-dilatation rate, and (4.10b) determines the relative displacement and slip velocity across the fault.

The tendency of the pore-volume to dilatate with increasing fluid pressure provides a mechanism to accomodate the thermal expansion of pore waters. As we are interested primarily in conditions that can arrest the rate of pressurization, we consider only extension within the thermal and fluid pressure fields caused by frictional heating. In this case, because the rate at which heat and fluid pressure diffuse is significantly less than the compressional wave velocity, we can neglect the inertial term of (4.10a). Integration of (4.10a) over the thermal and fluid pressure fields, with the centerline of the fault fixed at $x=0$, yields

$$U_x(x,t) = \int_0^x \left[\frac{(1-2\nu)\xi}{2\mu(1-\nu)}p(\eta,t)+\gamma_{sf}\Theta(\eta,t)\right]d\eta \qquad (4.11)$$

where U_x represents the solid matrix displacement from its initial position. The corresponding volumetric-strain and pore-volume-dilatation rates are, respectively,

$$\frac{\partial e}{\partial t} = \frac{\partial}{\partial t}\left[\frac{(1-2\nu)\xi}{2\mu(1-\nu)}\, p + \gamma_{sf}\,\Theta\right] \tag{4.12a}$$

$$\frac{\partial n}{\partial t} = (1-n)\,\frac{\partial}{\partial t}\left\{\left[\frac{(1-2\nu)\xi}{2\mu(1-\nu)} - \xi\beta_s\right]p + (\gamma_{sf}-\gamma_s)\Theta\right] \tag{4.12b}$$

The quantity in front of the pressure term in equation (4.12a) is the compressibility of the porous medium, β_{sf}, where:

$$\beta_{sf} = \frac{(1-2\nu)\xi}{2\mu(1-\nu)} \tag{4.13}$$

This parameter characterizes the volumetric dilatation that will take place for a unit change in effective stress. Table 4.1 summarizes the range of compressibilities that have been suggested for various rock types. Because p, Θ, β_{sf}, γ_{sf}, μ, ν, and ξ are nonlinear functions of U_x, e and n, equations (4.11) and (4.12) represent implicit equations for U_x, e and n.

For calculation of the thermal and fluid pressure fields we need to solve (4.10b) only for the relative slip velocity across the fault. The initial shear stress within the elastic blocks is given by the static shear strength of the fault

$$\tau_{xy} = \mu_s(\tau_n - P_0) \qquad \text{at } t=0 \tag{4.14}$$

where μ_s is the static coefficient of friction ($\mu_s > \mu_d$). Once slip is initiated, the frictional resistance drops to the dynamic value with the shear stress on the surface of the

elastic block described by the boundary condition

$$\mu \frac{\partial}{\partial x} U_y = \mu_d[(\tau_n - P_0) - p(x,t)] \qquad \text{at } x=0 \qquad (4.15)$$

where μ is the shear modulus of the elastic block. Solving equation (4.10b) for the slip velocity, given the initial condition (4.14), the boundary condition (4.15) and the position of the block fixed at $x=w_e$, yields

$$V_y(t) = \frac{1}{\sqrt{\rho_s f \mu}} \{ (\mu_s - \mu_d)(\tau_n - P_0)H(t_s - t) + \mu_d \frac{\partial}{\partial t} \int_0^t p(t-\tau)[H(\tau) - H(\tau - t_s)]d\tau \} \quad \text{at } x=0 \qquad (4.16a)$$

$$t_s = \frac{2w_e}{v} \qquad (4.16b)$$

where t_s is a characteristic slip duration, w_e is the width of the elastic region, and v is the shear wave velocity. For an instantaneous drop in shear strength across the fault, t_s is the characteristic (or relaxation) time for the release of strain energy within the elastic blocks. Equation (4.16) is referred to as the elastic-block (EB) model for slip velocity. We now modify this solution: first, to account for edge effects due to fault propagation; and, second, to consider only the average velocity of the elastic block.

If fluid pressure remains constant, equation (4.16) reduces to the slip model suggested by Brune (1970). His model

consisted of a tangential stress pulse applied uniformly and instantaneously over one fault block, with an equal pulse applied in the opposite direction to the other block. This model assumes that for distances less than the block width the shear stress is uniform and non-zero, whereas for distances greater than the block width the stress is zero. Thus, the slip velocity is constant for durations less than t_s, and abruptly falls to zero for greater durations. In actuality, the stress would peak at the fault and decline with distance. Consequently, the decay in slip velocity would reflect the decline in shear stress with distance. To account for this effect, and the effects of fault propagation, Brune suggested replacing the constant slip velocity with

$$V_y(t) = \frac{\sigma}{\sqrt{\rho_{sf}\mu}} \exp(-\frac{t}{t_r}) \qquad (4.17)$$

where σ is the initial drop in shear stress across the fault surface, and t_r is a relaxation time constant. To use this relationship, we assume the initial stress drop is given by the difference in the static and dynamic shear strengths of the fault surface. Because the stress drop and slip velocity are affected by changes in the resistive stress, equation (4.17) is modified to account for changes in fluid pressure:

$$V_y(t) = \frac{1}{\sqrt{\rho_{sf}\mu}} \{ (\mu_s-\mu_d)(\tau_n-P_o)\exp(-\frac{t}{t_r}) + \mu_d \frac{\partial}{\partial t} \int_o^t p(t-\tau)\exp(-\frac{\tau}{t_r})H(\tau)\, d\tau \} \quad \text{at } x=0 \qquad (4.18)$$

If fluid pressures remain constant and $t_r=t_s$, then both models yield the same displacement and maximum slip velocity. Equation (4.18) is referred to as the edge-effects (EE) model for slip velocity.

A third model for slip is the *spring-rider* model where only the average displacement and velocity of the elastic blocks are considered (e.g.; Burridge and Knopoff, 1967; Jaeger and Cook, 1969, p. 61; Nur, 1978; Israel and Nur, 1979). For this model equation (4.10b) is integrated with respect to x over the width of the elastic block and is rewritten as

$$\rho_{sf} \frac{\partial^2}{\partial t^2} \bar{U}_y + \frac{\mu}{w_e} \bar{U}_y = (\mu_s-\mu_d)(\tau_n-P_o) + \mu_d p(0,t) \qquad (4.19)$$

where $\bar{U}_y$ is the average displacement of the block from its initial position and the initial conditions are $\bar{U}_y(0)=\partial\bar{U}_y(0)/\partial t=0$. The terms on the lefthand side are, respectively, the inertial force of moving the block and the restoring force exerted by the block once motion begins. The term on the righthand side is the force available to accelerate the block due to a drop in the resistive stress across the fault. Solving equation (4.19) for the average

velocity of the block yields

$$\bar{V}_y(t) = \frac{1}{\sqrt{\rho_{sf}\mu}} \{ (\mu_s-\mu_d)(\tau_n-P_0)\sin(\frac{vt}{w_e})H(\frac{\pi}{2}t_s-t) + \mu_d \frac{\partial}{\partial t} \int_0^t p(t-\tau)\sin(\frac{v\tau}{w_e})[H(\tau)-H(\tau-\frac{\pi}{2}t_s)]d\tau \} \quad (4.20)$$

This model is referred to as the spring-rider (SR) model for slip velocity.

These three models are valid while the slip velocity is greater than zero. When the slip velocity equals zero, we assume that static friction is sufficient to prevent backsliding and slip ceases. Figure 4.3 shows the velocity as a function of time for each model. In this figure, the velocity is normalized by its initial value and the fluid pressure is constant. Both the amount and duration of slip are dependent on the coefficients and width of the elastic region, the difference between the dynamic and static coefficients of friction, and the fluid pressure on the fault surface. For each model the maximum velocity and final displacement are the same. If fluid pressures increase during slip, however, this may not be the case, and exact solutions for the displacement and slip velocity must be obtained by solution of the coupled equations.

Solution Technique

Substituting the Darcy flux and the volumetric strain rate into equations (4.3) and (4.4), and assuming that the total normal stresses remain constant during slip yields the final form of the equations governing the temperature increase,

$$\frac{\partial}{\partial x}(K_{sf}\frac{\partial\Theta}{\partial x}) + (\rho_w c_w \frac{k}{\mu_w})(\frac{\partial p}{\partial x})(\frac{\partial\Theta}{\partial x}) + n\gamma_w[\frac{\partial p}{\partial t} - \frac{k}{n\mu_w}(\frac{\partial p}{\partial x})^2](\Theta+T_0) +$$

$$\mu_d(\tau_n-P_0-p)\frac{V_y}{w}[H(x+w)-H(x-w)] = (\rho c)_{sf}\frac{\partial\Theta}{\partial t} \qquad (4.21)$$

and the pressure increase,

$$\frac{\partial}{\partial x}(\frac{k}{\mu_w}\frac{\partial p}{\partial x}) + \frac{k}{\mu_w}[\beta_w(\frac{\partial p}{\partial x})^2 - \gamma_w(\frac{\partial\Theta}{\partial x})(\frac{\partial p}{\partial x})] + [n\gamma_w+(1-n)\gamma_s-\gamma_{sf}]\frac{\partial\Theta}{\partial t} =$$

$$[n\beta_w-(1-n)\xi\beta_s+\beta_{sf}]\frac{\partial p}{\partial t} \qquad (4.22)$$

Equation (4.21) and (4.22) can be solved by a Galerkin finite-element technique to give an approximate solution to this coupled system of equations. In addition, porosity is determined by the compatibility equation (4.12) and slip velocity is given by equations (4.16), (4.18) or (4.20). Details of the approach are summarized in the Appendix.

For all simulations, we assume a uniform temperature T_0 and fluid pressure P_0 as initial conditions, and that the

solutions remain bounded as $|x|$ approaches infinity. The latter condition is satisfied by moving the boundaries of the finite element mesh far enough from the fault surface so that they experience no temperature or fluid pressure perturbations. Thus the width of the finite element grid is determined by the size of the thermal and hydrologic fields caused by frictional heating. The size of these fields are negligible in comparison to the width of the elastic blocks. Consequently, the effect of thermal pressurization is regarded as a transient stress drop on the boundary of the elastic block and motion of the elastic block is determine by numerical integration of the equations of motion. In addition, the permeability and porous medium compressibility are assumed to be independent of changes in fluid pressure and temperature, and to be uniform and equal on both sides of the fault. Although these assumptions may be relaxed easily, they are retained in order to clarify their separate effects in the thermal-pressurization process.

RESULTS

Controlling Parameters for Thermal Pressurization

From equation (4.22) it can be shown that thermal pressurization and flow of pore fluids are determined by the parameter

$$\Gamma = \frac{n\gamma_w + (1-n)\gamma_s - \gamma_{sf}}{n\beta_w - (1-n)\xi\beta_s + \beta_{sf}} \qquad (4.23a)$$

$$= \frac{\gamma}{\beta} \qquad (4.23b)$$

where Γ is defined as the thermal pressurization coefficient for the porous medium, and γ and β represent the fluid volume expansion due to a unit increase in temperature and a unit decrease in fluid pressure, respectively. The thermal pressurization coefficient characterizes the increase in fluid pressure per unit change in temperature for undrained conditions. Hence, it is a measure of the balance between pressurization and pore dilatation. Figure 4.4 shows that the thermal pressurization coefficient Γ is strongly dependent on temperature and porous medium compressibility. Values assigned to the solid properties are summarized in Table 4.2.

Whether pressurization or pore-dilatation are dominant in response to a temperature rise will depend on the relative magnitudes of the compressibilities for the pore water β_w and the porous medium β_{sf}. For porous medium compressibilities less than 10^{-11} Pa^{-1}, the thermal pressurization coefficient can be approximated by

$$\Gamma \simeq \frac{\gamma_w}{\beta_w} \qquad \beta_{sf} << \beta_w \qquad (4.24)$$

In this case the porous medium is stiff, and pressurization and fluid flow are the only mechanisms for accomodating the

heating of pore waters. Because the rate at which water pressurizes is large, a temperature rise of only a few degrees could cause fluid pressures to approach lithostatic values. For compressibilities greater than 10^{-9} Pa^{-1}, the porous medium is more compressible than the pore water and the thermal pressurization coefficient can be approximated by

$$\Gamma \simeq \frac{n\gamma_w}{\beta_{sf}} \qquad \beta_{sf} >> \beta_w \qquad (4.25)$$

In this case thermal expansion and pressurization of pore waters initiates a pore-volume expansion. Consequently, the heating of pore waters is accomodated primarily by pore-dilatation and fluid flow. If the porous medium compressibility exceeds 10^{-8} Pa^{-1}, then large temperature increases (>100 °C per MPa increase in fluid pressure) are required to pressurize the fluid.

The hydraulic diffusivity characterizes the rate at which the disturbance in fluid pressure propagates from the thermal source. From equation (4.22) the hydraulic diffusivity is given by

$$a_h = \frac{k}{\mu_w[n\beta_w - (1-n)\xi\beta_s + \beta_{sf}]} \qquad (4.26a)$$

For a stiff porous medium the hydraulic diffusivity can be approximated by

$$a_h \simeq \frac{k}{\mu_w n \beta_w} \qquad \beta_{sf} << \beta_w \qquad (4.26b)$$

In this case the hydraulic diffusivity characterizes the balance between pressurization and fluid flow. For a compressible medium

$$a_h \simeq \frac{k}{\mu_w \beta_{sf}} \qquad \beta_{sf} >> \beta_w \qquad (4.26c)$$

and the hydraulic diffusivity characterizes the balance between pressurization, pore-dilatation and fluid flow. The thermal diffusivity

$$a_t = \frac{K_{sf}}{(\rho c)_{sf}} \qquad (4.27)$$

characterizes the rate at which a temperature perturbation propagates from its heat source.

To compare the widths of the hydraulic and thermal fields it is convenient to define a characteristic length for each field (e.g., Lachenbruch, 1980; Delaney, 1982). The hydraulic diffusion length, defined as

$$l_h = \sqrt{4 a_h t} \qquad (4.28a)$$

reflects the distance a fluid pressure perturbation will propagate from its thermal source in time t. The thermal conduction length

$$l_t = \sqrt{4 a_t t} \qquad (4.28b)$$

reflects the distance a temperature perturbation will propagate by thermal conduction from its heat source in time t. If the hydraulic diffusivity is much greater than the thermal diffusivity, then the width of the hydraulic field is much greater than the width of the thermal field ($l_h >> l_t$). Consequently, the heating of pore waters is readily accomodated by fluid expansion and flow from the thermal field. In such a case the fluid pressure rise is distributed over a broad region and has a relatively small peak value.

The competing effects between thermal pressurization, pore dilatation and fluid flow make it necessary to specify explicitly the thermal pressurization coefficient and the hydraulic diffusivity to characterize fully the fluid-pressure response due to increases in temperature. However, both parameters are dependent on the the thermal expansivity, compressibility, and viscosity of the pore waters. This dependence means it is not possible to specify unique values for these parameters when there are large temperature variations. The porous medium compressibility and permeability, however, are not dependent on fluid properties. Hence, for numerical solutions the fluid pressure response will be expressed in terms of these two parameters. Because the range of values for solid properties is considerably smaller than that of variations in the hydraulic characteristics of porous media, a subset of solid properties

is not varied in subsequent examples (Table 4.2). Changes in these properties will not significantly alter the results to follow. To include the temperature-dependent properties of water for conditions where there are large temperature increases, we examine the influence of porous-medium properties for a set of initial conditions representative of a particular depth. For all numerical solutions, fluid pressures are initially hydrostatic and the fault surface is located at a depth of 2 km. Table 4.3 summarizes the initial conditions for this depth. Unless stated otherwise, we have chosen the dynamic coefficient of friction and relative slip velocity to be 0.6 and 10^{-1} ms^{-1} for all numerical computations.

Failure Surface

In this section we examine the undrained and drained response of a failure surface for a given average slip velocity. For a failure surface, the rate of frictional heating enters the equation for the temperature rise (4.21) by the boundary condition. Analytical solutions for temperature, fluid pressure, resistive stress, and porosity assume constant coefficients for the fluid properties and that all nonlinear effects are small. Numerical solutions are used to examine nonlinear effects, and to extend the analytical solutions.

1) Undrained conditions — Effects of pore dilatation.

If the hydraulic diffusivity is less than the thermal diffusivity, there is no appreciable transport of fluid mass from the heated region and the pore water responds under undrained conditions (i.e., negligible transport of fluid over the time scale of an earthquake). In this case pressurization and pore dilatation are the only mechanisms for accomodating the heating of pore waters. For undrained conditions, the fluid pressure rise is related to the temperature rise by

$$p(x,t) \simeq \Gamma\, \Theta(x,t) \tag{4.29}$$

and the rate of frictional heating is determined by the boundary condition

$$-K_{sf}\frac{\partial \Theta}{\partial x} = \bar{\mu}_d[(\tau_n - P_0) - \Gamma\Theta]\bar{V}_y \qquad \text{at } x=0 \tag{4.30}$$

where $\bar{V}_y$ and $\bar{\mu}_d$ represent the average slip velocity and coefficient of friction over the event. The solution for the temperature rise is given by (after Carslaw and Jaeger, 1959, p. 72)

$$\Theta(x,t) = \frac{(\tau_n - P_0)}{\Gamma}\left[\operatorname{erfc}\left(\frac{x}{\sqrt{4a_t t}}\right) - \exp\left(\frac{x}{\sqrt{\psi_0 a_t}} + \frac{t}{\psi_0}\right)\operatorname{erfc}\left(\frac{x}{\sqrt{4a_t t}} + \sqrt{t/\psi_0}\right)\right] \tag{4.31}$$

The parameter ψ_0, defined by

$$\psi_0 = \frac{1}{\bar{\mu}_d^2 \bar{V}_y^2} \cdot \frac{K_{sf}(\rho c)_{sf}}{\Gamma^2} \tag{4.32}$$

is the characteristic time for thermal pressurization of the fault surface. The resistive stress on the fault surface is given by

$$\tau_r(t) = \bar{\mu}_d(\tau_n - P_0) \exp(t/\psi_0) \operatorname{erfc}(\sqrt{t/\psi_0}) \tag{4.33}$$

For slip events with a duration equal to ψ_0, the resistive stress declines to approximately half its initial value.

Figure 4.5a shows the temperature and resistive stress given by equations (4.31) and (4.33) as a function of nondimensional slip duration t/ψ_0. For events with a slip duration much less than the characteristic time ψ_0, the effects of thermal pressurization are negligible and the drop in resistive stress is small. As the pore fluids start to pressurize, the resistive stress and frictional heat generation diminish, and the temperature on the fault surface stabilizes. If the slip duration is much greater than ψ_0, the resistive stress approaches zero and the temperature on the failure surface is approximated by

$$\Theta_{max} \simeq \frac{(\tau_n - P_0)}{\Gamma} \tag{4.34}$$

Thus the maximum temperature rise is dependent only on the initial effective stress and the pore-dilatational characteristics of the adjacent medium. This response occurs because frictional heating vanishes as the fluid pressure approaches the value of total normal stress acting on the failure surface. Consequently, the rise in fluid pressure and temperature is limited by the initial effective stress acting on the failure surface.

For slip durations greater than $10^2\psi_0$, the thermal and hydrologic fields are no longer dependent on the characteristic time ψ_0, and thereby these fields are no longer influenced by the slip velocity and friction coefficient. Thus the slip velocity and friction coefficient act to determine only the rate at which thermal pressurization proceeds. For decreases in $\bar{V}_y$ or $\bar{\mu}_d$, the displacement required for an equivalent reduction in resistive stress is increased. If either the slip velocity or friction coefficient deviates from its average value during slip and that deviation is small, then the characteristic time ψ_0 and the rate of thermal pressurization will not be altered significantly. In such a case the rate of thermal pressurization will depend primarily on variations in the initial effective stress and porous medium compressibility. For porous medium compressibilities less than that of water, pore dilatation is negligible and the

heating of pore waters causes rapid pressurization. If the compressibility is greater than that of water, thermal pressurization initiates a pore-volume expansion. This expansion must be accompanied by an increase in the thermal expansion rate of the pore waters before pressurization can occur. Consequently, the resistive stress remains at its initial value for a longer duration creating a larger temperature rise. Thus for slip events with the same displacement, the temperature rise is greater and the reduction in resistive stress is smaller for media with larger compressibilities.

These results can be used to estimate the minimum displacement required for a significant reduction in resistive stress. As an example, for a coefficient of friction of 0.6 and relative slip velocity $2\bar{V}_y$ of 10^{-1} ms^{-1}, Table 4.3 shows the value of ψ_0 for selected porous medium compressibilities. For a stiff medium, $\psi_0 \simeq 10^{-3}$ s, and events with a duration greater than 10^{-3} s (or, equivalently, displacements greater than 10^{-4} m) would cause the resistive stress to decrease to less than half its initial value. If the porous medium compressibility is 10^{-9} Pa^{-1}, the temperature rise increases more than tenfold. In this case, $\psi_0 \simeq 0.4$ s and displacements greater than 0.04 m are required for the same reduction in resistive stress. If the coefficient of friction and slip velocity are reduced to $\bar{\mu}_d = 0.2$ and $2\bar{V}_y = 10^{-2}$ ms^{-1}, then $\psi_0 \simeq 400$ s and displacements greater than 4 m are required.

For porous medium compressibilities greater than 10^{-10} Pa^{-1}, the increase in the thermal pressurization coefficient with temperature will limit the validity of the analytical solutions, equations (4.31) and (4.33). Figure 4.5b shows a comparison of analytical and numerical solutions for selected porous medium compressibilities, and the initial conditions of Table 4.3. Although the temperature rise increases with compressibility, the analytical solution increasingly overpredicts the magnitude of that temperature rise. The larger the temperature rise, the poorer the agreement between the analytical and numerical solutions. For compressibilities less than 10^{-9} Pa^{-1}, the temperature rise is small and the analytical solutions provide good approximations for the temperature rise and resistive stress. If the compressibility exceeds 10^{-9} Pa^{-1}, the temperature rise is large (>100°C). In this case the increase in the thermal pressurization coefficient is large, and the analytical solutions are poor approximations.

2) Drained conditions – Effects of fluid transport.

For most porous media, pore waters diffuse more readily than heat. In such cases the movement of pore fluids from the thermal field can restrict the applicability of the undrained model. To examine the effects of fluid transport, we first consider the thermal and hydrologic fields for large slip durations when the fluid pressure on the failure surface is approximately lithostatic. As the fluid pressures approach

lithostatic values, frictional heating vanishes and the temperature on the failure surface stabilizes. Thus for large slip durations the thermal field can be approximated by the diffusion of heat from a constant temperature surface (e.g., Carslaw and Jaeger, 1959):

$$\Theta_l(x,t) \simeq \Theta_{max}\ \mathrm{erfc}\left(\frac{x}{\sqrt{4a_t t}}\right) \tag{4.35}$$

where Θ_{max} represents the temperature rise on the failure surface needed to sustain fluid pressures at lithostatic values. Because the advection of heat is generally small, equation (4.35) provides a good approximation of the temperature distribution for large times. The corresponding fluid pressure rise is (see also Delaney, 1980)

$$p_l(x,t) \simeq \frac{a\Gamma\Theta_{max}}{(1-a^2)}\left[\mathrm{erfc}\left(\frac{x}{\sqrt{4a_h t}}\right) - a\cdot\mathrm{erfc}\left(\frac{x}{\sqrt{4a_t t}}\right)\right] \tag{4.36a}$$

where

$$a = \left(\frac{a_t}{a_h}\right)^{1/2} \tag{4.36b}$$

Because the fluid pressure rise is limited to the initial effective stress, equation (4.36) can be used to estimate the maximum temperature rise. Setting x=0 and equating the fluid pressure rise to the initial effective stress yields

$$\Theta_{max} \simeq \frac{\tau_n - P_o}{\Gamma_f} \tag{4.37}$$

where

$$\Gamma_f = \frac{a\Gamma}{(1+a)} \tag{4.38}$$

is the rise in fluid pressure per unit rise in temperature on the failure surface. Note that Γ_f is valid only for the failure surface. Substitution of equation (4.37) into (4.36) yields the fluid pressure distribution for large slip durations

$$p_l(x,t) \simeq \frac{\tau_n - P_o}{1-a} \left[\operatorname{erfc}\left(\frac{x}{\sqrt{4a_h t}}\right) - a \cdot \operatorname{erfc}\left(\frac{x}{\sqrt{4a_t t}}\right) \right] \tag{4.39}$$

For $a_h >> a_t$ most of the hydraulic region is isothermal and equation (4.39) provides an excellent approximation of the fluid pressure distribution for large times.

The coefficient Γ_f can be used to estimate the temperature and resistive stress as a function of slip duration. For drained conditions the rate of frictional heating on the failure surface is determined by the boundary condition (4.30), where the thermal pressurization coefficient Γ is replaced by Γ_f. The temperature rise is obtained from equation (4.31) by replacing Γ with Γ_f, and the characteristic time with

$$\psi_0 = \frac{1}{\bar{\mu}_d^2 \bar{V}_y^2} \cdot \frac{(1+a)^2 K_{sf} (\rho c)_{sf}}{(a\Gamma)^2} \qquad (4.40)$$

where ψ_0 now represents the characteristic time of thermal pressurization for drained conditions. With these changes equations (4.31) and (4.33), and Figure 4.5a describe the temperature rise and resistive stress on a failure surface for drained conditions. For slip durations much greater than ψ_0, the temperature and fluid pressure fields are approximated by the large time solutions. The temperature rise necessary to sustain fluid pressures at lithostatic values depends primarily on the initial effective stress on the fault surface, and the fluid and thermal transport properties and pore-dilatation characteristics of the adjacent medium. If the temperature rise is large (>100°C), these solutions overestimate the temperature rise and resistive stress. This effect is due primarily to the increase in the thermal pressurization coefficient with temperature and, to a lesser extent, the contraction of pore fluids as they flow from the thermal field. Equations (4.31) and (4.33), however, provide upper limits for the temperature rise and resistive stress.

Numerical solutions for the temperature and resistive stress on the failure surface are shown in Figure 4.6 to illustrate the variety of fault behaviors possible for variations in the porous medium compressibility and permeability. An average slip velocity of $2\bar{V}_y = 10^{-1}$ ms^{-1} is assumed, and the initial conditions are summarized in Table

4.3. The 1000 °C isotherm is shown to delineate the conditions where partial melting may occur. When the permeability is less than 10^{-19} m^2 the response is the same as in the limit for zero permeability and the pore waters respond under undrained conditions. For permeabilities greater than 10^{-15} m^2, thermal pressurization is nullified by the transport of pore fluids, and the fluid pressure and resistive stress remain unchanged during slip. This problem has been discussed by McKenzie and Brune (1972). The temperature rise is given by (Carslaw and Jaeger, 1959, p. 262)

$$\Theta(x,t) = \frac{\bar{\mu}_d(\tau_n - P_0)\bar{V}_y}{K_{sf}} \left[\frac{\sqrt{4a_t t}}{\sqrt{\pi}} \exp\left(\frac{-x^2}{4a_t t}\right) - |x| \operatorname{erfc}\left(\frac{|x|}{\sqrt{4a_t t}}\right) \right] \qquad (4.41)$$

In this case the temperature on the fault surface continues to rise with displacement and partial melting may occur before the effects of thermal pressurization become significant.

The lower figures in Figure 4.6 show the resistive stress as a function of displacement. As the resistive stress decreases the rate of temperature rise diminishes. Large reductions in resistive stress coincide with large reductions in frictional heating and, consequently, stabilization of the temperature rise on the fault. For stiff porous media with permeabilities less than 10^{-19} m^2, fluid flow from the thermal

field is negligible. In such a case the initial resistive stress is maintained only for a short displacement ($<10^{-3}$ m) before frictional heating causes the fluids to pressurize within the thermal field. Consequently, the temperature rise is small. For media with larger permeabilities, heating of pore waters can be accomodated by the thermal expansion and flow of fluids from the thermal field. Because of this fluid volume loss, the resistive stress remains at its initial value and the temperature continues to rise until the thermal expansion of fluids exceeds the loss of fluids due to transport. Once this condition is established, the pore fluids within the thermal field start to pressurize causing frictional heat generation to diminish rapidly, and the temperature on the fault surface to stabilize. Hence, for a given displacement, the magnitude of the temperature rise increases with permeability. Similiarly, if the medium is also compressible, thermal pressurization will initiate a pore-volume expansion providing a third mechanism for accomodating the heating of pore waters. In this case the initial resistive stress is maintained over an even greater displacement before the thermal expansion of pore waters exceeds the pore dilatation and flow rates, and pressurizes the fluids. Thus the temperature rise increases with compressibility. In addition, the rate of reduction in resistive stress is enhanced by the increase in the thermal pressurization coefficient with temperature.

Figure 4.6 can be scaled for other values of initial effective stress, average slip velocity, and friction coefficient. For changes in the initial effective stress, the temperature in Figure 4.6 is multiplied by the ratio of the new value for initial effective stress to the reference value (24 MPa). For changes in the slip velocity and friction coefficient the displacement scales are multiplied by

$$\frac{\bar{\mu}_d^2}{\bar{\mu}_d'^2} \cdot \frac{\bar{V}_y}{\bar{V}_y'} \tag{4.42}$$

where the primed values denote the new values, and the unprimed values represent the reference values $\bar{\mu}_d$=0.6 and $2\bar{V}_y$=10^{-1} ms^{-1}. These scaling factors hold provided the change in effective stress does not yield a temperature rise considerably larger than that of the unscaled temperature rise. If this is not the case, then the larger temperature rise would lead to a large increase in the thermal pressurization coefficient, and thereby a decrease in the maximum temperature and an increase in the rate of stress reduction. Results would have to be obtained by numerical solution. These scaling factors, however, provide upper limits for the temperature rise and stress reduction.

3) Thermal and hydrologic fields.

To illustrate how the diffusion of frictional heat stabilizes the temperature rise on the failure surface,

selected results for the thermal and hydrologic fields within the adjacent porous medium are shown in Figures 4.7 and 4.8. These results correspond to the equivalent curves shown in Figure 4.6 for the temperature and resistive stress on the failure surface. For a stiff medium ($\beta_{sf}<\beta_w$) with a permeability of 10^{-17} m^2, Figure 4.7 shows the thermal and hydraulic fields as a function of distance from the failure surface for selected times. The distance from the fault is non-dimensionalized by the thermal conduction length. For a slip duration of 10 s (d=1 m), the width of the thermal and fluid-pressure fields are 0.02 m and 0.5 m ($2l_t$ and $2l_t/a$, respectively). Figure 4.7a shows the temperature and fluid-pressure fields. The large-time solutions apply for times greater than 10 s. During slip the fluid pressure front extends well beyond the thermal front, with the fluid pressures rising uniformly within the thermal field. Note that in this figure, the temperature is normalized by the maximum temperature predicted by equation (4.37), and not by the maximum value calculated in the numerical model. The maximum temperature rise (260 °C) is less than the temperature (370 °C) predicted by equation (4.37) due to the increase in the thermal expansivity of water with temperature.

Figure 4.7b shows the thermal expansion and pressure contraction rates of the fluid volume. Note that the vertical scales are normalized by time so that the large time solutions plot as fixed curves. Both the thermal expansion and pressure contraction rates are strongly dependent on the slip duration,

initial effective stress, and the hydraulic characteristics of the adjacent medium. The peaked profiles arise because of the tandem operation of three processes. First, frictional heating causes pressurization within the thermal field. Second, because the porous medium is permeable, pressurization within the thermal field causes pressurization and contraction of the fluids within the adjacent region. Third, the contraction of fluids within the adjacent region causes thermal expansion and flow of fluids from the leading edge of the thermal field. For small durations (<1 s) the thermal expansion and pressure contraction rates are greatest on the fault surface where the rate of the temperature and fluid pressure rise is greatest. The large increase in the pressure contraction rate within the thermal field occurs because the increase in water compressibility with temperature is faster than the decline in the rate of fluid pressure rise. Once the fluid pressure and temperature on the fault stabilizes, the thermal expansion and fluid contraction rates approach zero near the fault. For large slip durations (>10 s), a dynamic balance is established between the fluid pressure and temperature fields where the decrease in resistive stress is just sufficient for frictional heating to maintain the temperature at the level required for thermal pressurization of the pore waters at near-lithostatic values. At this stage fluid expansion within the thermal field is accomodated by pressurization, flow and contraction within the adjacent region, and the thermal front drives a fluid pressure front that extends increasingly beyond it.

Consequently, for large slip durations, the maximum thermal expansion and pressure contraction rates occur along the leading edges of the fronts where the rates of temperature and fluid pressure rise are the greatest. Figure 4.7c shows the fluid flux. The flow field is characterized by the redistribution of fluid mass from the heated region to the adjacent cooler region. Hence the maximum fluid flux occurs midway between the thermal and fluid pressure fronts.

Figure 4.8 shows the hydraulic and thermal fields for a porous medium with a compressibility of 10^{-9} Pa^{-1} and a permeability of 10^{-17} m^2. For this case pore dilatation and fluid flow are the primary means for accomodating the heating of pore waters. Compared to the previous example, the increase in compressibility results in a decrease in the hydraulic diffusivity and, consequently, the hydrologic field is considerably smaller than the field for a stiff medium. For a slip duration of 10 s, the width of the pressure field is now 0.12 m ($\alpha^{-1} \simeq 6$). Figure 4.8a shows the temperature and fluid pressure rise. With a higher compressibility, larger temperature rises and greater displacements are required for an equivalent rise in fluid pressure. Hence, the large-time solutions now apply for slip durations greater than 10^2 s. The maximum temperature (700 °C) is approximately half the value predicted by the analytical solution, equation (4.37). Figure 4.8b shows the thermal expansion and pore dilatation rates. The thermal expansion rate of the fluid volume shows a peaked value whose location coincides with the temperature for the

peaked value of the thermal pressurization coefficient in Figure 4.4b. The negative pore-dilatation rate corresponds to expansion of the solid grains along the leading edge of the thermal front. As in the case for a stiff medium, the spatial configuration of these rates depends upon the tandem operation of three processes; the generation of frictional heat, pressurization and pore-volume expansion within the thermal field and adjacent region, and the thermal expansion and flow of fluids from the edge of the thermal front. Since the porous medium compressibility is greater than the compressibility of water, the thermal expansion of the pore waters is accomodated by pore dilatation within a narrower region adjacent to the thermal front. Because the pressure front is narrower, the fluid flux shown in Figure 8c is greater than the flux for a stiff medium.

The final strain of the pore volume can be estimated from the solution to the compatibility constraint for porosity (4.12b). For an arbitrary rise in fluid pressure and temperature, the solution for porosity is approximated by

$$n(x,t) \simeq 1 - (1-n_0)\exp[-(\beta_{sf}-\xi\beta_s)p(x,t) - (\gamma_{sf}-\gamma_s)\Theta(x,t)] \qquad (4.43)$$

The final strain of the pore volume is given by

$$\frac{\Delta n}{n_0} = \frac{(1-n_0)}{n_0}\{1-\exp[-\lambda(\tau_n - P_0)]\} \qquad (4.44)$$

where

$$\lambda = (\beta_{sf} - \xi\beta_s) + (\gamma_{sf} - \gamma_s)\frac{(1+a)}{a\Gamma} \qquad (4.45a)$$

$$\simeq \beta_{sf} \qquad \beta_{sf} \geq 10^{-9}\ \mathrm{Pa}^{-1} \qquad (4.45b)$$

reflects the change in solid volume per unit volume of porous media per unit increase in fluid pressure. Because the decrease in porosity due to thermal expansion of the solid matrix is generally small, equations (4.43) and (4.44) provide good approximations for the change in porosity. For porous medium compressibilities greater than 10^{-9} Pa^{-1}, the rate of pore-volume expansion is large. In this case it is unlikely that deformation would remain confined to the failure surface. For example, the increase in porosity is almost twofold for a medium with a compressibility of 10^{-8} Pa^{-1} and the initial conditions of Table 4.3. This increase would suggest a loss of cohesion and shear strength within the medium adjacent to the fault, and thereby a widening of the zone of deformation.

Effects of Fault Zone Width

In the previous section, deformation was confined to a failure surface. We now examine the effects of fault width. If the fault width is less than the thermal conduction length

($w<l_t$), then the width of the fault zone is negligible in comparison to the size of the thermal field. In this case the fault zone can be approximated by a failure surface and the previous results would apply. If, however, deformation occurs over a fault zone a few centimeters in width, then the rate of the temperature rise would be lower and, consequently, the thermal and fluid pressure effects may differ considerably from that of a failure surface.

1) Undrained conditions - no transport of heat.

To examine the effects of fault width, we first consider the response of a fault zone for undrained conditions and negligible transport of heat. For these conditions, Lachenbruch (1980) discussed the temperature rise and reduction in resistive stress for a constant dilatational strain-rate of the pore volume ($n^{-1}\partial n/\partial t$=const. and $\Gamma=\gamma_w/\beta_w$). When changes in porosity occur due to fluid pressure and temperature increases within a compressible porous medium, the temperature rise within the fault zone is given by

$$\Theta(t) = \frac{(\tau_n - P_o)}{\Gamma} [\ 1 - \exp(-t/\psi)\ ] \qquad (4.46)$$

The parameter ψ, defined by

$$\psi = \frac{(\rho c)_{sf}}{\overline{\mu}_d\ \Gamma} \cdot \frac{w}{V_y} \qquad (4.47)$$

is the characteristic time for thermal pressurization of the fault zone. The resistive stress of the fault zone is given by

$$\tau_r(t) = \bar{\mu}_d(\tau_n - P_0)\exp(-t/\psi) \tag{4.48}$$

For these solutions, the conditions for negligible fluid and heat loss are satisfied if the hydraulic diffusion and thermal conduction lengths calculated for the characteristic time of thermal pressurization are less than the fault width ($a_h\psi<w^2$ and $a_t\psi<w^2$). For slip events with a duration much greater than the characteristic time ψ, the resistive stress approaches zero and the temperature within the zone stabilizes.

For negligible loss of heat and fluid from the zone, we can write the equations for temperature and resistive stress in terms of the shear strain across the fault (see also Lachenbruch, 1980):

$$\Theta(d) = \frac{(\tau_n - P_0)}{\Gamma}\left[\, 1 - \exp(-\psi_e^{-1}\,\frac{d}{2w})\,\right] \tag{4.49}$$

$$\tau_r(d) = \bar{\mu}_d(\tau_n - P_0)\exp(-\psi_e^{-1}\,\frac{d}{2w}) \tag{4.50}$$

where $d/2w$ is the shear strain across the zone. The parameter ψ_e, defined by

$$\psi_e = \frac{(\rho c)_{sf}}{\bar{\mu}_d\,\Gamma} \tag{4.51}$$

controls the rate of increase in temperature and decrease in resistive stress per unit strain across the fault. In this case the slip rate may vary with displacement, and equation (4.51) can be used to calculate the shear strain required for a significant drop in resistive stress. As an example, from equation (4.50) the resistive stress decreases by a factor of e^{-1} for shear strains that exceed ψ_e. For a stiff medium, $\psi_e \simeq 3.0$ and the resistive stress would decrease to approximately one third of its initial value when the displacement exceeded the fault width by a factor of three. If the compressibility of the porous medium is 10^{-8} Pa^{-1}, however, $\psi_e \simeq 40$ and the displacement would have to exceed the fault width by a factor of forty for an equivalent reduction.

The curves labeled *A* in Figure 4.9 show the temperature and resistive stress given by equations (4.46) through (4.51) as a function of slip duration t/ψ or shear strain $d/2w\psi_e$. In addition, numerical solutions are shown for selected porous medium compressibilities, and the initial conditions of Table 4.3. For porous medium compressibilities greater than 10^{-9} Pa^{-1}, the increase in the thermal pressurization coefficient with temperature enhances the rate of decrease in resistive stress. Consequently, the analytical solutions overestimate the temperature rise and resistive stress. As with the fault surface model for undrained conditions (Figure 4.5), the maximum temperature rise is dependent solely on the initial value of the effective stress and thermal pressurization coefficient. The fault zone width, along with the slip rate

and friction coefficient determine only the rate at which thermal pressurization proceeds. If the width is increased, then the displacement required for an equivalent increase in temperature and pore pressure also increases. Once pressurization begins the relative rate of stress reduction would be greater for a broad zone ($w>l_t$) than for a narrow zone ($w<l_t$).

The change in porosity within the fault zone is given by equation (4.43), where the temperature and fluid pressure are given by (4.46) and (4.29), respectively. Figure 4.10 shows the dilatational strain rate of the pore volume. The analytical solution is indicated by the dashed line. Numerical solutions (solid lines) are shown for the porous medium compressibilities of Figure 4.9, and the initial conditions of Table 4.3. For slip durations less than the characteristic time ψ, the temperature rises linearly with displacement and the pore-dilatation rate is approximated by

$$\frac{1}{n}\frac{\partial n}{\partial t} \simeq \frac{\lambda(\tau_n - P_0)(1-n_0)}{n_0 \psi_e} \cdot \frac{\bar{V}_y}{w} \qquad (4.52a)$$

$$\simeq \gamma_w (1-n_0) \cdot \frac{\bar{\mu}_d (\tau_n - P_0)}{(\rho c)_{sf}} \frac{\bar{V}_y}{w} \qquad \beta_{sf} > 10^{-9}\ \mathrm{Pa}^{-1} \qquad (4.52b)$$

Thus the pore-dilatation rate is most strongly affected by the shear strain rate, the influence of the porous medium compressibility on the coefficients ψ_e and λ, and the initial

effective stress. Once the pore fluid starts to pressurize, the pore-dilatation rate approaches zero and the final strain of the pore volume is given by equation (4.44). For compressibilities greater than 10^{-9} Pa^{-1}, the pore-dilatation rate is proportional to the thermal expansivity of water and relatively insensitive to changes in the compressibility. Thus large increases in the pore dilatation rate reflect the large increase in the thermal expansivity of water with temperature. In such cases the thermal expansion of fluid volume is matched by pore dilatation, and the pore volume undergoes a large volume increase as the temperature rises. This behavior could lead to extensive microfracturing of the fault zone and adjacent medium. The improved interconnectivity of pore spaces caused by these fractures could lead to substantial increases in permeability and enhanced fluid flow, which may arrest the thermal pressurization process and cause a restoration of the shear strength. For compressibilities greater than 10^{-8} Pa^{-1}, pressurization is nullified by pore dilatation and the resistive stress would remain unchanged for earthquakes with realistic displacements. In this case, however, extensive microfracturing could cause strain softening through nonlinear material properities (e.g., Rudnicki, 1977).

2) Drained conditions - Fluid and heat transport.

If the hydraulic diffusion length calculated for the characteristic time ψ is greater than the fault width

($a_h\psi > w^2$), the thermal expansion and flow of fluids from the fault zone can restrict the applicability of the undrained model. For example, Figure 4.11 shows the temperature rise and resistive stress at the center of a fault zone whose width $2w$ and average slip rate $2\bar{V}_y$ are 10^{-1} m and 10^{-1} ms^{-1}, respectively. The curves are plotted as a function of shear strain for the initial conditions of Table 4.3. For permeabilities less than 10^{-17} m^2, fluid flow from the zone is negligible and the fault responds under undrained conditions. If the permeability exceeds 10^{-14} m^2, the thermal expansion and flow of fluids from the fault zone nullifies thermal pressurization. In this case the shear strength remains constant and the temperature continues to rise with displacement. This problem has been discussed by Cardwell *et al.* (1978) and Lachenbruch (1980), and the rise in central temperature is given by (Carslaw and Jaeger, 1959, p.80)

$$\Theta(t) = \frac{\bar{\mu}_d(\tau_n - P_o)\bar{V}_y}{(\rho c)_{sf}\, w}\left[t - 4i^2\mathrm{erfc}\left(\frac{w}{\sqrt{4a_t t}}\right)\right] \qquad \text{at } x=0 \qquad (4.53)$$

If conductive heat loss from the zone is negligible, the temperature rises linearly with displacement and shear strains greater than 10^2 could cause melting. For permeabilities between these two limits, the rate of the temperature rise decreases with increasing displacement and the temperature starts to stabilize at the maximum value for the drained response of a failure surface. The increase in shear strength

for strains greater than 10^2 reflects the decrease in the thermal pressurization coefficient for temperatures greater than the critical temperature of water. For porous medium compressibilities greater than 10^{-9} Pa^{-1}, it is doubtful that thermal pressurization could reduce the shear strength except for large events. Regardless of the hydraulic characteristics, however, thermal pressurization is negligible if the displacement is less than the fault width.

The results of Figure 4.11 are valid for a fault width and slip velocity of 10^{-1} m and 10^{-1} ms^{-1}. If either the fault width and slip velocity are varied, and if the combined variations are less than a factor of ten, then Figure 4.11 would still provide a good approximation of the temperature rise and shear strength versus shear strain. For greater variations in $\bar{\mu}_d$ and $\bar{V}_y$, limits to fault behavior can be estimated from the controlling parameters. If the hydraulic diffusion length is less than or equal to the fault width ($a_h \psi \lesssim w^2$), then the temperature and resistive stress are approximated by the undrained response. If, however, the hydraulic diffusion length is greater than the fault width and the slip duration exceeds ψ , then the temperature rise and resistive stress are approximately the same as that for a failure surface. This similiarity occurs because the maximum temperature rise is determined by the initial effective stress and hydraulic characteristics of the porous medium, whereas the fault width determines only the initial rate of the temperature rise within the zone. Once the slip duration

exceeds ψ, thermal pressurization becomes significant and the decline in the resistive stress and rate of the temperature rise is determined by the diffusion of excess pore pressures into the adjacent medium. Hence the effects of thermal pressurization can be regarded as a fluid pressure pulse at the midpoint of the zone, and the temperature and resistive stress are given to a first approximation by the solutions for a failure surface. In either case solutions would have to be obtained by numerical methods. The above approximations, however, provide limits to fault behavior for various ranges of the controlling parameters.

3) Nonuniform hydraulic properties.

Thus far we have considered a fault zone with hydraulic properties equal to those of the adjacent wall rock. With a contrast in hydraulic properties, the fault behavior can be approximated by examining relative ratios of the fault width to the thermal conduction and hydraulic diffusion lengths. If the fault width is small in comparison to the thermal field ($w<l_t$ or $w^2<a_t\psi$), then regardless of the fault zone properties, the response is determined by the properties of the adjacent rock and the fault zone can be approximated as a failure surface. For negligible heat loss from the zone ($w>l_t$ or $w^2>a_t\psi$), the ratio of the fault width to the hydraulic diffusion length of the fault zone material will determine whether the hydraulic characteristics of the zone, or the wall rock, will control the response of the fault.

If the fault width is less than the hydraulic diffusion length calculated for the fault zone material and characteristic time of thermal pressurization ($w^2 < a_h \psi$), the diffusion of excess fluid pressure into the wall rock controls the response of the fault. In such a case the response can be approximated by assuming a uniform medium whose compressibility and permeability are given by those of the adjacent wall rock. Figure 4.12a shows the temperature and fluid pressure fields for permeabilities of 10^{-13} and 10^{-18} m^2 for the fault zone and adjacent rock, respectively. For this figure the fault width and relative slip velocity are 10^{-1} m and 10^{-1} ms^{-1}. Both the fault zone and adjacent wall rock are stiff, and the initial conditions of Table 4.3 are assumed. As shown in Figure 4.12a, the adjacent wall rock acts to confine the excess fluid pressures within the fault zone. Consequently, the rise in fluid pressure is uniform across the zone and the fault response is controlled by the diffusion of excess fluid pressure into the wall rock. The rise in central temperature and decline in shear strength are given to a good approximation by the equivalent curves for a stiff medium with a uniform permeability of 10^{-18} m^2 (see Figure 4.11). The diffusion of excess fluid pressures from the fault could cause a progressive weakening of the adjacent wall rock. For these conditions it is not unreasonable to expect the zone of deformation to increase as slip progresses. Whether or not the zone will widen sufficiently to halt thermal pressurization, or stabilize at a certain width and shear strength, depends

upon the rheological relation between shear strength and effective stress for the wall rock.

The opposite situation occurs when the fault width is greater than the hydraulic diffusion length ($w^2 > a_h \psi$). For this condition fluid loss from the zone is negligible and the response is determined primarily by the compressibility of the fault zone material. In such a case, however, the diffusion of excess fluid pressure into the adjacent rock causes the shear strength and, consequently, the temperature rise to be greater along the edges of the zone than at the center. This in turn could cause fluid pressures within the central region to exceed lithostatic values. If the hydraulic diffusivity of the wall rock is less than that of the fault zone material, the increase in temperature is minimal and the shear strength declines uniformly across the zone. Conversely, if the diffusivity of the wall rock is greater, the shear strength along the edges will remain close to its initial value and the temperature rise will be large. For example, Figure 4.12b shows the temperature and fluid pressure fields for permeabilities of 10^{-18} and 10^{-13} m^2 for the fault zone and wall rock, respectively. This is the opposite permeability configuration to that used in Figure 4.12a. As shown in Figure 4.12b, the fluid pressure within the wall rock remains near its initial value. Consequently, there is little loss of shear strength along the edges of the zone and the temperature rise there is large. The shear strength at the center of the fault, however, is given to a good approximation by the undrained

response (equation (4.50) and Figure 4.9). For these conditions one would expect deformation to contract about the central region where the initial fluid pressure rise and, consequently, the decline in shear strength is greatest. Thus for large shear strains it would not be unreasonable to expect the development of a very narrow deformation zone within the central region of the fault zone. The width of this zone would depend on the rheological relation between shear strength, effective stress, and deformation rate for the fault material. For disaggregated fault gouge it is likely such a relation would follow a friction law behavior. If that were so, the decline in shear strength at the center of the zone would be approximated by the undrained response (Figure 4.9), and the temperature rise along the edges of the deformation zone would stabilize at the maximum temperature (4.37) for the permeability and compressibility of the fault material.

Dynamic Models - Effects of Variable Resistive Stress

The primary mechanical effect of thermal pressurization is to induce a loss of shear strength during slip and thereby increase the stress available to accelerate the fault blocks. For fault zones comprised of stiff media with low permeability loss of shear strength can occur rapidly. In such cases events where shear strains exceed ψ_e would cause substantial strain-weakening of the fault and, consequently, large stress drops, accelerations, slip velocities, and displacements. In addition the resultant increase in slip velocity would further

enhance the rate of thermal pressurization and thereby the decrease in shear strength.

1) Failure surface - Narrow zones.

For a narrow zone with significant heat loss ($w<l_t$ or $w^2<a_t\psi$), we can express the condition required for a rapid loss in shear strength by comparing the temperature rise for a failure surface with constant shear strength (4.41) to the temperature rise required for pressurization of pore waters at lithostatic values (4.37). Thus large decreases in shear strength occur when

$$\frac{\bar{\mu}_d(\tau_n-P_0)\bar{V}_y}{K_{sf}}\frac{\sqrt{4a_t t}}{\sqrt{\pi}} \gtrsim \frac{(\tau_n-P_0)}{\Gamma}\frac{(1+a)}{a} \qquad (4.54)$$

where $\bar{V}_y$ represents the average slip velocity for the initial drop from the static to the dynamic friction coefficients at constant fluid pressure (see Figure 4.3). Expressing this condition in terms of displacement we obtain

$$d \gtrsim \frac{K_{sf}^2}{a_t}\cdot\frac{(1+a)^2}{(a\Gamma)^2}\cdot\frac{1}{\bar{\mu}_d^2\,\bar{V}_y} \qquad (4.55)$$

From this expression, the displacement required for a large reduction in shear strength is dependent primarily on the hydraulic characteristics of the medium, the dynamic coefficient of friction, and the average slip velocity for

constant fluid pressure. If the porous medium compressibility or permeability are increased, or if the average slip rate and friction coefficient are decreased, then a greater displacement will be needed for large reductions in shear strength. For example, for a stiff medium with undrained conditions, equation (4.55) is approximated by

$$d \gtrsim \frac{10^{-6}}{\bar{\mu}_d^2 \bar{V}_y} \tag{4.56}$$

In such a case a few millimeters of displacement would cause a complete loss of shear strength for earthquake events. Consequently, we could approximate the effects of thermal pressurization on the slip velocity by assuming that the shear strength during slip is zero (or, equivalently, that the dynamic friction coefficient is zero). If the compressibility and permeability are 10^{-9} Pa^{-1} and 10^{-16} m^2, however, then (4.55) is approximated by

$$d \gtrsim \frac{10^{-1}}{\bar{\mu}_d^2 \bar{V}_y} \tag{4.57}$$

and displacements greater than 2 m are required for large reductions in shear strength for $\bar{\mu}_d$=0.6 and $2\bar{V}_y$=10^{-1} ms^{-1}. Hence thermal pressurization may be negligible and the dynamic slip velocity could be calculated by assuming a constant dynamic shear strength during slip.

For the latter case, however, frictional melting may occur on the failure surface. The onset of frictional melting

can be estimated by

$$d \gtrsim \frac{K_s f^2}{a_t} \cdot \left(\frac{T_s}{\tau_n - P_0}\right)^2 \cdot \frac{1}{\bar{\mu}_d^2 \bar{V}_y} \qquad (4.58)$$

where T_s is the solidus temperature for the fault zone material. For a solidus temperature of 10^3 and the initial conditions of Table 4.3, equation (4.58) is approximated by

$$d \gtrsim \frac{10^{-2}}{\bar{\mu}_d^2 \bar{V}_y} \qquad (4.59)$$

Hence for the previous example, frictional melting would occur before the effects of thermal pressurization become significant. In this case the presence of a partial melt distributed along grain boundaries might act as a fluid phase under pressure and thereby reduce the shear strength of the fault (McKenzie and Brune, 1972; Cardwell *et al.*, 1978; Sibson, 1980). Thus for an earthquake event with moderate displacement ($\gtrsim$1 m) occurring across a narrow zone ($\lesssim$1 cm) with friction coefficients greater than 0.2 and slip velocities in the range 0.1 to 1 ms^{-1} (Brune, 1970), a large reduction in shear strength should occur either by thermal pressurization or frictional melting. In this case there would be a complete release of elastic strain energy within the blocks, and the slip velocity could be approximated by assuming the shear strength at the initiation of slip is zero. If, however, the coefficient of friction and slip velocity are less than 10^{-1} and 10^{-1} ms^{-1}, then it is doubtful whether

thermal pressurization or frictional melting could reduce the dynamic shear strength during an earthquake. In these conditions frictional heating is small and the temperature rise would be minimal.

2) Fault zone - Effects of fault width.

For deformation occurring over a fault zone a few centimeters in width, the rate of the temperature rise is lower and, consequently, the displacement required for large reductions in shear strength is greater. This behavior could limit the stress available to accelerate the blocks and change the dynamic characteristics of the slip velocity. To illustrate the effects of thermal pressurization on the slip rate, we first consider an approximate solution to the fully-coupled equations. For this approximation we assume negligible fluid loss from the zone, and that the shear strength is given by equation (4.48) where the characteristic time for thermal pressurization ψ is determined by the maximum slip velocity for the initial drop in shear strength at constant fluid pressure. With these assumptions the slip velocity is readily calculated for each velocity model. For example, for an initial drop of 3% in the shear strength, Figure 4.13 shows the slip velocity for each of the three velocity models. In this figure time is normalized by the characteristic slip duration t_s (4.16b) for the release of strain energy within the elastic blocks due to a instantaneous drop in shear strength across the fault. The slip velocity is

normalized by the maximum velocity for a complete loss of shear strength at the initiation of slip. The curves are labeled in values of t_s/ψ, which is the ratio of the characteristic slip duration to the characteristic time for thermal pressurization. As seen from Figure 4.13, both the slip rate and duration are strongly dependent on the characteristic time for pressurization. Because the value of ψ is proportional to the fault width and compressibility, the slip rate and displacement decrease with increasing width and compressibility.

Since the characteristic slip duration t_s depends primarily on the geometry of the fault blocks, the ratio t_s/ψ is a measure of the importance of thermal pressurization during slip. If the characteristic slip duration is much greater than the characteristic time for thermal pressurization ($t_s>10\psi$), then thermal pressurization dominates the character of fault motion and a rapid loss of shear strength accompanies slip motion. In such a case the shear strength decreases with slip faster than the release of strain energy from the adjacent blocks, and the excess stress accelerates the block to higher slip rates. Thus the slip rate could be readily approximated by assuming a complete loss of shear strength at the initiation of slip, and changes in the friction coefficient have little affect on the character of fault motion once that motion begins. Fault motion is arrested when the block dynamically overshoots the equilibrium position, defined as the state of zero stress within the

block. At this point there is a buildup of shear stress that resists the continued motion of the block and deceleration occurs. Such behavior would lead to earthquakes of relatively short duration with large stress drops, accelerations and displacements. Conversely, if the characteristic time for thermal pressurization is much greater than the characteristic slip duration ($\psi > 10t_s$), then the effects of thermal pressurization are negligible and the slip velocity is determined by the initial drop in the static shear strength. In this case the constitutive relation that links the friction coefficient to slip rate and slip rate history will dominate the character of fault motion (e.g., Dietrich, 1979a, 1979b; Rice and Ruina, 1983; Ruina, 1983; Okubo and Dietrich, 1984; Weeks and Tullis, 1985; Rice and Tse, 1986). For such behavior the slip duration is approximately the same as that for a complete drop in shear strength, however, displacements and particle velocities are relatively small. For $\psi \simeq 10t_s$, the rate of decline in shear strength approximately equals the rate of release in elastic strain energy. Consequently, quasi-static stress conditions exist and the fault continues to slip under nearly steady state conditions until the shear stress within the blocks is zero. This behavior would lead to earthquakes with relatively large slip durations and displacements, but low particle velocities and accelerations.

The analytical solutions shown in Figure 4.13 underestimate the slip rate for two reasons. First, the analysis fails to incorporate the enhancement in the rate of

decline in shear strength due to increases in the slip rate. Second, as slip progesses the temperature rise causes an increase in the thermal pressurization coefficient and thereby a decrease in the characteristic time for thermal pressurization. In either case, the characteristic time for thermal pressurization ψ will decrease and the ratio t_s/ψ will increase once slip begins. Figure 4.13, however, provides a good approximation of the fault response for conditions where $t_s >> \psi$ or $t_s << \psi$. For $t_s >> \psi$, the characteristic time for thermal pressurization is large and, consequently, any increase in the ratio t_s/ψ caused by increases in the slip rate or temperature results in only a small shift of the curve. For $t_s << \psi$, the slip rate remains near its initial value and the change in the ratio t_s/ψ with slip rate is small. If, however, $\psi \simeq t_s$, Figure 4.13 provides only a qualitative description of the slip rate and exact results would have to be obtained by numerical solution of the coupled equations.

The restriction of negligible fluid loss from the fault zone imposes a more severe constraint on the results of Figure 4.13. This constraint is satisfied if the fault width is greater than the hydraulic diffusion length calculated for the fault material and characteristic slip duration ($w^2 \gtrsim a_h t_s$). For a hydraulic diffusion length that is much greater than the fault width ($a_h t_s >> w^2$ or $a_h \psi >> w^2$), the fluid pressure rise is minimal and the slip velocity is given by initial drop in static shear strength (see Figure 4.3). For intermediate conditions the diffusion of excess fluid pressures causes a

lower rate of shear strength decline than the rate predicted by (4.48) and Figure 4.13 will overestimate the increase in the slip rate. For an initial 3% drop in the shear strength, Figure 4.14 shows the slip rate and shear strength across a fault zone as a function of time. The curves are labeled in terms of permeability, and all calculations are for a fault width of 10^{-1} m, a porous medium compressibility of 10^{-9} Pa^{-1}, and the initial conditions of Table 4.3. For these conditions initial and maximum slip rates ($2V_y$) are 0.1 and 3.5 ms^{-1}, the initial characteristic time for thermal pressurization ψ is approximately 20 s, and the initial ratio of the characteristic slip duration to thermal pressurization time t_s/ψ is approximately 0.3. As shown in Figure 4.14 the constraint for negligible fluid loss is satisfied for permeabilities less than 10^{-16} m^2. If the permeability is greater than or equal to 10^{-14} m^2, then thermal pressurization is negligible and the slip rate is determine by the initial drop in the static shear strength. For intermediate values of permeability, the shear strength continues to decline while the slip rate is increasing. Once the slip rate starts to decrease, the diffusion of excess fluid pressures from the fault causes a restoration of shear strength, and thereby a further reduction in the slip rate. For the spring-rider model with a permeability of $10^{-14.5}$ m^2, the slip rate stabilizes and then starts to rapidly increase due to the increase in the thermal pressurization coefficient with temperature. The dashed segments of the curve show the restoration of shear

strength after the cessation of slip. Because the shear strength is low at this stage, the shear stress built up within the blocks during deceleration may exceed the static shear strength of the fault. If this were the case, the block would begin backsliding and experience a damped oscillation about the equilibrium position. However, dynamic overshoot and potential backsliding are expected to be less pronounced in a continuous system.

As shown in Figures 4.13 and 4.14, the fault exhibits a complex rheology that is characterized by strain-weakening during acceleration and strain-hardening during deceleration of the fault blocks. The exact nature of the relation between shear strength and deformation rate is strongly dependent on the width and hydraulic characteristics of the fault zone. In addition, if the friction coefficient varies due to the breaking and formation of new barriers along the slip planes, then the acceleration and slip rates would be very erratic. In such a case Figures 4.13 and 4.14 would exhibit a high frequency oscillation superimposed on the slip rate profiles (e.g., Nur, 1978). The magnitude and frequency of these oscillations would depend on the constitutive relation linking the friction coefficient to the slip rate and displacement history. These oscillations, however, would be greatest during the early stages of slip, and gradually decline as the temperature rises and the fault zone pressurizes. Once the fluid pressures approach near-lithostatic values, subsequent changes in the friction coefficient will have little effect on

the shear strength, acceleration and slip rate. We do not suggest that the simple fault block models of Figures 4.13 and 4.14 can be made to correspond closely to an actual fault. Rather the analysis is intended to provide an understanding of how thermal pressurization influences the character of fault motion when variable resistive stress and inertial forces are dominant.

DISCUSSION

Our results suggest that the nature of fault motion depends critically upon the characteristic time scales for thermal pressurization and slip duration. In turn, these parameters depend upon the fault geometry, and the hydraulic characteristics of the fault zone and the adjacent medium. Because of the wide variations possible in these parameters, a wide variety of fault behavior is possible. Knowledge of these parameters appears essential in understanding the dynamics of fault motion.

The width of a fault zone is probably the least-well known parameter. Field evidence from exhumed faults suggests that within the brittle regime of the crust, fault slip may be confined to zones a few centimeters or less in width (e.g., Wilson, 1970; Flinn, 1977, 1979; Sibson, 1977, 1979; Sieh, 1978; Bustin, 1983). If the fault width is less than a few centimeters, then for large earthquakes a substantial reduction in shear strength should occur either by thermal

pressurization or frictional melting. If the fault width exceeds a few centimeters, then the rate of the frictional heating is too small to cause melting within the zone during an earthquake. However, thermal pressurization could still act to reduce the shear strength. In this case, if the displacement exceeds the fault width, then the response of the fault zone will depend primarily upon the hydraulic characteristics of the fault zone and adjacent wall rock.

Extensive fracturing of the wall rock could lead to relatively high permeabilities adjacent to a fault zone. Within the fault zone, however, the presence of a fine cataclastic gouge with a possible high clay content would suggest low permeabilities. Morrow *et al.* (1981, 1984) measured the permeability of both non-clay and clay-rich fault gouges at various confining pressures and shear strains. Permeabilities ranged from 10^{-22} to 10^{-18} m^2. The low permeability of these fault gouges indicates that fluid loss from a fault zone may be negligible over the time scale of an earthquake. In this case the compressibility of fault zone material is probably the most important parameter controlling fault motion. Little is known about the compressibility of fault gouge at depth. The fine grain size and low permeability of fault gouge suggest compressibilities similiar to compacted argillaceous sediments. Such compressibilities typically range from 10^{-10} to $5x10^{-8}$ Pa^{-1} (Domenico and Mifflin, 1965; Smith, 1973; Rieke and Chilingarian, 1974; Touloukin, 1981). This range is not unreasonable for fault gouge derived from low

compressibility rocks at the confining pressures expected at depths in excess of one kilometer. Nor is this range unreasonable for fault gouge where repeated thermal pressurization and fluid explusion over successive earthquakes would tend to compact the gouge material. Raleigh (1977) showed that a transient rise in temperature could cause dehydration of clays, and thereby compaction of the fault gouge. If narrow zones with gouge of low permeability and compressibility are typical, then thermal pressurization is probably an important process in the dynamics of fault motion.

Various lines of evidence support the argument that shear strength and frictional heat generation could be greatly reduced by thermal pressurization. Lachenbruch and Sass (1980), and Lachenbruch (1980) suggested that the lack of an anomaly in surface heat flow across the San Andreas fault could result from a low dynamic friction caused by thermal pressurization. Measurements of the levels of organic maturation within and adjacent to thrust zones by Bustin (1983) revealed no detectable thermal metamorphism attributable to frictionally generated heat, with the exception of narrow films of high vitrinite reflectance immediately adjacent to and within the zones. These films suggest that temperatures on the order of 300-650°C were generated during thrusting and indicated that the elevated temperatures were very short lived. Such high temperatures along the edges of thrust zones could be generated readily if slip was primarily confined to the boundary between the zone

and wall rock, or if the permeability of the adjacent rock exceeds that of the thrust zone. Wilson (1970), and Brock and Engelder (1977) have described a number of large fractures adjacent to thrust zones that have been intruded by shale dikes. If thermal pressurization causes fluid pressures to approach lithostatic values, fluidization of the fault gouge could occur. Such behavior could lead to hydrofracturing and the injection of gouge dikes into the adjacent wall rock. The subsequent reduction in fluid pressure within the zone would cause a restoration of shear strength, and thereby inhibit further fault motion. Hydrofracturing during the latter stages of slip, however, would not alter the conditions required for thermal pressurization to reduce the dynamic shear strength. In addition, dilatancy recovery accompanying the release of shear strain during faulting could cause a negative pore dilatation and thereby a further enhancement in the rate of thermal pressurization (e.g., Nur 1972; Scholz *et al.*, 1973; Sibson, 1973; Lachenbruch, 1980; Holcomb,1981). If that were the case, then the calculations of the fluid pressure rise for a stiff medium would be on the conservative side.

The emphasis in this study has been on a fault block model with uniform stress and material properties over the rupture surface. It is important, however, to consider the role that heterogeneities could play in the dynamics of fault motion. Fault models with uniform properties are useful for understanding slip when the length scales over which there are significant changes in material properties are much greater

than the fault rupture length. Such models characterize the low-frequency response of a fault. To explain high frequency seismic radiation and the strong ground motions observed for large earthquakes, a heterogeneous stress drop and an irregular rupture propagation and slip rate are required. This in turn requires that heterogeneities in material properties have length scales much smaller than the rupture length. In addition, a mechanism is required to maintain that heterogeneity between successive earthquake cycles. Many models proposing how heterogeneities affect the earthquake cycle have been discussed (e.g., Das and Aki, 1977; Kanamori and Stewart, 1978; Mikumo and Miyatake, 1978; Aki, 1979, 1984; Mahrer and Nur, 1979; Madariaga, 1979; Das and Scholz, 1981; Lindh and Boore, 1981; McGarr, 1981; Rudnicki and Kanamori, 1981; Papageorgiou and Aki, 1983a, 1983b; Rundle *et al.*, 1984; Stuart *et al.*, 1985). These models are of two primary types. The first consists of a fault with uniform properties but an irregular geometry, whereas the second assumes a simple geometry but a rupture process that proceeds in the presence of obstacles, or barriers of various strengths. Both models yield a heterogeneous stress drop, and thereby an irregular rupture propagation and fault slip. We shall examine only barrier models here, and consider the material properties that may form them.

The term barrier applies to strong patches of the fault that are resistive to slip (e.g., Das and Aki, 1977; Aki, 1979, 1984). Hence a barrier is characterized by the material

properties that control its strength, and its areal extent. Barriers can initiate failure when the tectonic stress exceeds the strength of the barrier, or slow down and halt the rupture front as it propagates through the barrier. It can also contribute to an irregular fault motion by remaining unbroken at the initial passage of the rupture front, but then break subsequently because of increased stress around its boundaries. While much consideration has been given to the mechanics of barriers, little work has been done to characterize the conditions and material properties that form a barrier. Models of barriers fall into two main types. The first type are described by the spatial variability in the friction coefficient (e.g., Burridge and Knopoff, 1968; Mikumo and Miyatake, 1978; Israel and Nur, 1978). A limitation of these models is that long-term slip would tend to smooth out variations in the friction coefficient. Consequently, the resistive stress would tend to become uniform with successive earthquakes until all events rupture the entire fault length and heterogeneous processes cease to become important (Nur, 1978). The second type of model employs a peak-stress constitutive law to describe barrier strength versus fault slip (eg., Rudnicki, 1977; Stuart 1979; Stuart and Mavko, 1979; Li and Rice, 1983; Stuart *et al.*, 1985). Here the shear strength is assumed to initially increase with fault slip (strain hardening) up to a peak stress, and then to decrease with continued slip (strain weakening). While such a law predicts earthquakes, its form and the spatial variability of

coefficient values are poorly known.

The results presented in this study suggest that the spatial variations in the width of the fault zone, and in the hydraulic characteristics of the fault zone and adjacent medium could readily explain both the presence of barriers along faults and the strong motion observed in seismic records. Patches of the fault that act as barriers may be characterized by relatively broad zones of deformation with high porous medium compressibility and permeability. Because thermal pressurization would be negligible for such patches, they would retain their initial shear strength and resist fault motion. Conversely, patches characterized by narrow zones of deformation and stiff material with low permeability would experience a rapid decrease in shear strength. In this case the resistive stress of the patch decreases more rapidly than the shear stress applied by the elastic region, and the slip velocity rapidly accelerates. Because the stress drop and accelerations would be high across such patches, it is possible for an earthquake with a low average stress drop to generate high frequency waves. This behavior provides an explanation of the strong motions observed near the epicenter of earthquakes. Of course, a wide variety of transition behaviors exist between these two limits. For small earthquakes thermal pressurization may be negligible and the patch may act as a barrier, whereas for large earthquakes the shear strength may be reduced to near-zero values. This response would depend on the relative magnitudes of the

characteristic time scale for thermal pressurization of the patch and the slip duration of the earthquake.

The fault patch may also exhibit a complex rheology that could be characterized by strain weakening during the early stages of slip when fluid loss from the zone is negligible, and strain hardening during the latter stages when fluid loss may be substantial. This behavior depends not only on the characteristic time scales, but also on the relative magnitudes of the hydraulic diffusion length and the fault width throughout the duration of slip. A fault patch might also exhibit a bimodal behavior over an earthquake cycle. For example, prior to an earthquake a patch comprised of a wide zone of inelastically deforming rock may be driven past a peak strength and into a strain-softening regime by far field tectonic strains. When the shear strength of the patch decreases more rapidly than the tectonic shear stress, static equlibrium cannot be maintained and an earthquake occurs (e.g., Rudnicki, 1977; Rice and Rudnicki, 1979; Stuart *et al.*, 1985). Once failure begins, adjacent stronger patches with narrow zones of deformation may experience a rapid decline in shear strength due to thermal pressurization. The wide patch, however, may tend to remain near its initial failure strength because heating is distributed over a broad region and is insufficient to cause thermal pressurization. Thus a patch with a broad zone of deformation may initiate fault slip, but then act to resist slip once fault motion begins.

These results suggest that spatial variations in fault width and hydraulic characteristics play an important role in the dynamics and statistical characteristics of earthquake processes. Because the spatial distribution of these parameters can endure through many earthquakes cycles, earthquakes recurrent on a given fault may have the same set of characteristic displacements and magnitudes. Variations within the set would depend on the relative magnitudes of the fault length, and the characteristic length scales for the fault width and hydraulic characteristics. If the characteristic length scales for these parameters are much less than the fault length, then variations in the displacements and magnitudes would be large. If, however, the characteristic length for these parameters is on the order of the fault length, then the fault block model would apply and the variations would be small. This scale dependency would conform to the frequency-magnitude relations observed for many faults (e.g., Nur, 1978; Aki 1984; Stuart *et al.*, 1985). Thus it may be possible to determine characteristic length scales for these parameters from the statistics of frequency-magnitude relations, and open the possibility of quantitative prediction of earthquake behavior.

SUMMARY AND CONCLUSIONS

We have formulated a simple model for an earthquake which incorporates the effects of frictional heating on the thermal, hydrologic, and mechanical response of a fault. This model has

been used to examine the parameters that control the fault response, and to determine their critical range of values where thermal pressurization is significant. The main conclusions of this analysis are:

1. Motion of the fault blocks can be characterized by two time scales, a characteristic slip duration for the release of elastic strain energy and a characteristic time for thermal pressurization due to frictional heating. These time scales depend primarily on the fault geometry, and the hydraulic characteristics of the fault zone and adjacent medium. Because of the wide variations in these parameters, a wide variety of fault behavior is possible.

2. For earthquakes occurring across narrow zones comprised of stiff material with low permeability ($<10^{-18}$ m^2), the characteristic time for thermal pressurization is much less than the characteristic slip duration. Consequently, during slip the resistive stress decreases more rapidly than the shear stress applied by the elastic region, and the fault blocks rapidly accelerate. This behavior would lead to earthquakes of relatively short durations with large stress drops, accelerations and displacements, and provide an explanation for strong motions.

3. For earthquakes occurring across zones where shear strains are less than one, or the porous medium compressibility and permeability exceeds 10^{-8} Pa^{-1} and 10^{-14} m^2, the characteristic time for thermal pressurization is much greater than the slip duration. Because thermal pressurization

would be negligible, the fault would retain its initial shear strength and resist further motion. This behavior would lead to earthquakes with relatively small stress drops, accelerations and displacements, and provide an explanation for the presence of barriers along faults.

4. The style of deformation across a fault zone may be controlled by the hydraulic characteristics of the zone and adjacent wall rock. If the hydraulic diffusivity of the wall rock is greater than that of the fault zone, deformation would tend to contract about the central region where the fluid pressure rise and, consequently, the decline in shear strength is greatest. In this case it is not unreasonable to expect very narrow deformation zones for large earthquakes. Conversely, if the hydraulic diffusivity of the wall rock is less than that of the zone, the wall rock acts to confine the excess fluid pressure within the zone. In this case the diffusion of excess pore pressures from the fault could cause a progressive weakening of the adjacent wall rock, and thereby a widening of the deformation zone.

5. The spatial variations in fault width and hydraulic characteristics could readily explain a heterogenous stress drop, and thereby an irregular rupture propagation and slip rate over the fault. Because these parameters can endure through many earthquake cycles, earthquakes recurrent on a given fault may have the same set of characteristic displacements and magnitudes. Thus the spatial distribution of these parameters may play an important role in the dynamics

and statistical characteristics of earthquakes.

APPENDIX: NUMERICAL SOLUTION OF EQUATIONS

Equations (4.21) and (4.22) are solved numerically using a Galerkin finite-element technique with linear basis functions and deforming coordinates. Temperature, fluid pressure, and material and fluid properties vary linearly across each element. Time derivatives are approximated by a fully implicit backward difference scheme. The thermodynamic properties of water are incorporated as state functions of fluid pressure and temperature using relations given by Keenan *et al.* (1978) for density and specific heat, Watson *et al.* (1981) for dynamic viscosity, and Kestin (1978) for thermal conductivity. For all simulations the grid spacing increases with distance from the fault surface, with the smallest grid spacing adjacent to the fault. For problems that are symmetric about the fault, the equivalent half-space problem is modeled. Discretization error was minimized by running several simulations of the same problem, reducing the grid spacing until identical results were obtained for two successive runs.

A solution procedure is employed where the heat-transfer and fluid-flow equations are solved sequentially for a given time step. The size of the time step is adjusted automatically following a procedure that limits the magnitude of changes in pressure and temperature to some specified value which will insure rapid convergence. Initial time steps were on the order of 10^{-5} s. An iterative technique is used to couple the heat-transfer and fluid-flow equations. The first step in the

procedure is to solve for the temperature field using the fluid pressure, slip velocity, and material and fluid properties from the previous time step. The fluid-flow equation is then solved using the newly calculated temperature field to estimate the fluid-volume changes due to thermal expansion. Porosity is updated by using the analytical solution of equation (4.12b) over the time step

$$n_t = 1 - (1-n_{t-\Delta t})\exp[\,-(\overline{\beta}_{sf}-\overline{\xi\beta}_s)(p_t-p_{t-\Delta t}) - (\overline{\gamma}_{sf}-\overline{\gamma}_s)(\Theta_t-\Theta_{t-\Delta t})\,] \qquad (4.A1)$$

where the porosity is assumed to be linearly independent of Θ and p, and the bar denotes the average value of the variable over the time step. The fluid and material properties are then updated using the new estimate of the temperature, fluid pressure and porosity fields, and equation (4.9) is integrated over the flow domain to obtain the displacement of the nodes from their position at the previous time step. The slip velocity is computed by numerically integrating equation (4.16), (4.18), or (4.20), respectively,

$$V_y(t_n) = \frac{1}{\sqrt{\rho_{sf}\mu}}\,[\,(\mu_s-\mu_d)(\tau_n-P_0)H(t_s-t_n) + \mu_d \sum_{i=1}^{n} \Delta p_i H(t_i+t_s-t_n\,] \qquad (4.A2a)$$

$$V_y(t_n) = \frac{1}{\sqrt{\rho_s f \mu}} \{ (\mu_s - \mu_d)(\tau_n - P_0)\exp(-\frac{t_n}{t_r}) + \mu_d \sum_{i=1}^{n} \Delta p_i \exp[-\frac{(t_n - t_i)}{t_r}] \} \qquad (4.A2b)$$

$$\bar{V}_y(t_n) = \frac{1}{\sqrt{\rho_s f \mu}} \{ (\mu_s - \mu_d)(\tau_n - P_0)\sin(\frac{vt}{w_e})H(\frac{\pi}{2}t_s - t_n) + \mu_d \sum_{i=1}^{n} \Delta p_i \sin[\frac{v(t_n - t_i)}{w_e}]H(t_i + \frac{\pi}{2}t_s - t_n) \} \qquad (4.A2c)$$

where

$$\Delta p_i = p(x,t_i) - p(x,t_{i-1}) \qquad \text{at } x=0 \qquad (4.A3)$$

is the fluid pressure increase on the fault surface between successive time steps, t_i is the time for the ith time step, and t_n is the time for the current time step. An iterative sequence is then employed until the maximum pressure and temperature change between successive iterations is less than a specified tolerance (10^2 Pa and 10^{-3} °C, respectively). Once this criterion is met, the model proceeds to the next time step.

NOTATION

c_w	isobaric specific heat of water.
e	volumetric strain (dilatation) $e_{11}+e_{22}+e_{33}$.
e_{ij}	solid matrix strain.
f	as a subscript denotes fluid.
$H(t)$	Heaviside unit step function
k	porous medium permeability.
k_s	bulk modulus of the solid grains.
k_{sf}	bulk modulus of the porous medium.
K_s	thermal conductivity of the solid grains.
K_w	thermal conductivity of water.
K_{sf}	thermal conductivity of the solid-fluid composite.
n	porosity.
n_o	initial porosity
p	fluid pressure increase above ambient conditions.
P	pore fluid pressure.
P_o	initial fluid pressure.
q_x	fluid specific discharge relative to the solid matrix.
s	as a subscript denotes solid.
sf	as a subscript denotes solid-fluid composite.
t	time.
T	temperature.
T_o	initial temperature.
$U_x U_y$	solid matrix displacements.
$2\underline{V}_y$	relative slip velocity across the fault.
$2V_y$	average slip velocity of the event.
$2w$	fault zone width.
w	as a subscript denotes water.
α	square root of the ratio of the thermal to the hydraulic diffusivities.
α_h	hydraulic diffusivity.
α_t	thermal diffusivity.
β	fluid volume expansion due to a unit decrease in fluid pressure.

β_s isothermal compressibility of the solid grains.

β_{sf} porous medium compressibility.

β_w isothermal compressibility of water.

Δn maximum change in porosity.

δ_{ij} Kronecker delta function.

Γ thermal pressurization coefficient.

γ fluid volume expansion due to a unit increase temperature.

γ_s isobaric thermal expansivity of the soild grains.

γ_{sf} volumetric thermal expansion coefficient of the porous medium.

γ_w isobaric thermal expansivity of water.

λ maximum change in solid volume per unit volume of porous media per unit increase in temperature for drained conditions.

ψ_o time constant for thermal pressurization of a fault surface for drained conditions.

ψ time constant for thermal pressurization of a fault zone for undrained conditions.

μ shear modulus.

μ_d dynamic coefficient of friction.

$\overline{\mu}_d$ average dynamic coefficient of friction over the slip event.

μ_s static coefficient of friction.

μ_w dynamic viscosity of water.

ν Poisson's ratio

ρ_s density of the solid grains.

ρ_w density of water.

$(\rho c)_{sf}$ heat capacity of the soild-fluid composite.

$\overline{\tau}$ average effective normal stress $(\tau_{11}+\tau_{22}+\tau_{33})/3$.

τ_{ij} components of the effective stress tensor.

τ'_{ij} components of the total stress tensor.

τ_n total normal stress acting on the fault surface.

τ_r resistive shear strength of the fault.

τ_{r_o} initial resistive shear strength of the fault.

Θ temperature increase over ambient conditions.

Θ_{max} temperature rise needed to sustain pore-fluid pressures at lithostatic values.

ξ proportionality constant between pore and bulk volume changes.

REFERENCES

Aki, K., Characterization of barriers on an earthquakes, *J. Geophys. Res.*, 84, 6140-6148, 1979.

Aki, K., Asperities, barriers, characteristic earthquakes and strong motion prediction, *J. Geophys. Res.*, 89, 5867-5872, 1984.

Biot, M. A. and D. G. Willis, The elastic coefficients of the theory of consolidation, *J. Appl. Mech.*, 24, 594-601, 1957.

Brace, W.F., and J.D. Byerlee, Stick-slip as a mechanism for earthquakes, *Science*, 153(3739), 990, 1966.

Brock, W.G., and T. Engelder, Deformation associated with the movement of the Muddy Mountain Overthrust in the Buffington window, southeastern Nevada, *Bull. Geol. Soc. Am.*, 88, 1667-1677, 1977.

Brune, J.N., Tectonic stress and the spectra of seismic shear waves from earthquakes, *J. Geophys. Res.*, 75, 4995-5009, 1970.

Burridge, R., and L. Knopoff, Model and theoretical seismicity, *Bull. Seis. Soc. Am.*, 57, 341-371, 1967.

Bustin, R.M., Heating during thrust faulting in the Rocky Mountains: friction or fiction?, *Tectonophysics*, 95, 309-328, 1983.

Byerlee, J. D., Friction of rocks, *Pure and Appl. Geophys.*, 116, 615-626, 1978.

Byerlee, J.D., The mechanics of stick-slip, *Tectonophysics*, 9 475, 1970.

Cardwell, R. K., D. S. Chinn, G. F. Moore, and D. L. Turcotte, Frictional heating on a fault of finite thickness, *Geophys. J. Roy. Astron. Soc.*, 52, 525-530, 1978.

Carslaw, H.C., and J.C. Jaeger, **Conduction of Heat in Solids**, 386pp., Oxford University Press, New York, 1959.

Das, S., and K. Aki, Fault plane with barriers: A versatile earthquake model, *J. Geophys. Res.*, 5658-5670, 1977.

Das, S., and C.H. Scholz, Theory of time-dependent rupture in the earth, *J. Geophys. Res.*, 6039-6051, 1981.

Delaney, P.T., Rapid intrusion of magma into wet rock: Groundwater flow due to pore pressure increases, *J. Geophys. Res.*, 87, 7739-7756, 1982.

Dietrich, J.H., Earthquake mechanisms and modeling, *Ann. Rev. Earth Planet. Sci.*, 2, 275-302, 1974.

Dietrich, J.H., Modeling of rock friction: 1. Experimental results and constitutive equations, *J. Geophys. Res.*, 84, 2161-2168, 1979a.

Dietrich, J.H., Modeling of rock friction: 2. Simulation of preseismic slip, *J. Geophys. Res.*, 84, 2161-2168, 1979b.

Domenico, P.A. and M.D. Mifflin, Water from low-permeability sediments and and land subsidence, *Water Resour. Res.*, 1, 563-576, 1965.

Flinn, D., Transcurrent faults and associated cataclasis in Shetland, *J. Geol. Soc. London,* 133, 231-248, 1977.

Flinn, D., The Walls Boundary Fault, Shetland, British Isles, Analysis of Actual faults in Bedrock, *U.S. Geol. Surv. Open File Rep.*, 79-1239, 181-200, 1979.

Handin, J., R.V. Hager Jr., M. Friedman, and J.N. Feather, Experimental deformation of sedimentary rocks under confining pressure: pore pressure tests, *Bull. Am. Assoc. Petrol. Geol.*, 47, 717-755, 1963.

Holcomb, D.J., Memory, relaxation, and microfracturing in dilatant rock, *J. Geophys. Res.*, 86(B7), 6235-6248, 1981.

Hubbert, M.K. and W.W. King, Role of fluid pressure in mechanics of overthrust faulting. I. Mechanics of fluid-filled porous solids and its application to overthrust faulting, *Bull. Geol. Soc. Am.*, 70, 115-166, 1959.

Israel, M., and A. Nur, A complete solution of a one-dimensional propagating fault with nonuniform stress and strength, *J. Geophys. Res.*, 84(B5), 2223-2234, 1979.

Jaegar, J.C., Moving sources of heat and temperature at sliding contacts, *J. Proc. R. Soc. N.S.W.*, 76, 203-224, 1942.

Jaeger, K.C., and N.G.W. Cook, **Fundamentals of Rock Mechanics.**, Methuen and Co., Ltd., London, 513p., 1979.

Johnson, A.I., R.P. Moston, and D.A. Morris, Physical and hydrologic properties of water-bearing deposits in subsiding areas in central California, *U.S. Geol. Surv. Prof. Paper 497A,* 1968.

Jorgensen, D.G., Relationships between basic soils-engineering equations and basic ground-water flow equations, *U.S. Geol. Survey Water-Supply Paper*, 2064, 46pp., 1981.

Kanamori, H., and G.S. Stewart, Seismological aspects of the

Guatemala earthquake of February, 4, 1976, *J. Geophys. Res.*, 83, 3427-3434, 1978.

Keenan, J.H., F.G. Keyes, P.G. Hill, and J.G. Moore, **Steam Tables**, 162pp., John Wiley, New York, 1978.

Kestin, J., Thermal conductivity of water and steam, *Mech. Eng.*, 100(8), 1255-1258, 1978.

Knopoff, L., J.O. Mouton, and R. Burridge, The dynamics of a one-dimensional fault in the presence of friction, *Geophys. J. R. Astr. Soc.*, 35, 168-184, 1973.

Lachenbruch, A.H., Frictional heating, fluid pressure, and the resistance to fault motion, *J. Geophys. Res.*, 85(B11), 6097-6112, 1980.

Lachenbruch, A.H., and J.H. Sass, Heat flow and energetics of the San Andreas Fault zone, *J. Geophys. Res.*, 85, 6185-6207, 1980.

Li, V.C., and J.R. Rice, Preseismic rupture progression and great earthquake instabilities at plate boundaries, *J. Geophys. Res.*, 88, 4231-4246, 1983.

Lindh, A.G., and D.M. Boore, Control of rupture by fault geometry during the 1966 Parkfield earthquake, *Bull. Seis. Soc. Am.*, 71, 95-116, 1981.

Lockner, D.A., and P.G. Okubo, Measurements of frictional heating in granite, *J. Geophys. Res.*, 88(B5), 4313-4320, 1983.

Logan, J.M., Brittle phenomena, *Rev. Geophys. Space Phys.*, 17, 1121-1132, 1979.

McGarr, A., Analysis of peak ground motion in terms of a model of inhomogeneous faulting, *J. Geophys. Res.*, 3901-3912, 1981.

McKenzie, D. P. and J. N. Brune, Melting of fault planes during large earthquakes, *Geophys. J. R. Astr. Soc.*, 29, 65-78, 1972.

Madariaga, R., On the relation between seismic moment and stress drop in the presence of stress and strength hetrogeneity, *J. Geophys. Res.*, 84, 2243-2250, 1979.

Mahrer, K.D., and A. Nur, Strike slip faulting in a downward varying crust, *J. Geophys. Res.*, 84, 2296-2302, 1979.

Mase, C.W. and L. Smith, Pore-fluid pressures and frictional heating on a fault surface, *Pure and Appl. Geophys.*, 122, 583-607, 1985.

Mavko, G.M., Mechanics of motion on major faults, *Ann. Rev.*

Earth Planet. Sci., 9, 81-111, 1981.

Mikumo, T., and T. Miyatake, Dynamical rupture process on a three-dimensional fault with non-uniform friction and near-field seismic waves, *Geophys. J. R. Astr. Soc.*, 54, 417-438, 1978.

Morrow, C.A., L.Q. Shi, and J.D. Byerlee, Permeability and strength of San Andreas fault gouge under high pressure, *Gephys. Res. Let.*, 8, 325-328, 1981.

Morrow, C.A., L.Q. Shi, and J.D. Byerlee, Strain hardening and strength of clay-rich fault gouges, *J. Geophys. Res.*, 87, 6771-6780, 1982.

Morrow, C.A., L.Q. Shi, and J.D. Byerlee, Permeability of fault gouge under confining pressure and shear stress, *J. Geophys. Res.*, 89, 3193-3200, 1984.

Nur, A., Dilatancy, pore fluids, and premonitory variations of t_s/t_p travel times, *Bull. Seis. Soc. Am.*, 62, 1217-1222, 1972.

Nur, A., Nonuniform friction as a physical basis for earthquake mechanics, *Pure and Appl. Geophys.*, 116, 964-988, 1978.

Nur, A., and J. D. Byerlee, An exact effective stress law for elastic deformation of rock with fluids, *J. Geophys. Res.*, 76, 6414-6419,1971.

Okubo, P.G., and J.H. Dietrich, Effects of physical fault properties on frictional instabilities produced on simulated faults, *J. Geophys. Res.*, 89, 5817-5827, 1984.

Papageorgiou, A.S., and K. Aki, A specific barrier model for the quantitative description on inhomogeneous faulting and prediction of strong ground motion. Part I. Description of the model, *Bull. Seis. Soc. Am.*, 73, 693-723, 1983a.

Papageorgiou, A.S., and K. Aki, A specific barrier model for the quantitative description on inhomogeneous faulting and prediction of strong ground motion. Part I. Applications of the model, *Bull. Seis. Soc. Am.*, 73, 953-987, 1983b.

Raleigh, C.B., Frictional heating, dehydration and earthquake stress drops, in *Proceedings of Conference II Experimental Studies of Rock Friction with Application to Earthquake Prediction*, pp 291-304, U.S. Geological Survey, Menlo Park, CA, 1977.

Raleigh, C.B., and J. Everden, Case for low deviatoric stress in the lithosphere, in *The Mechanical Behavior of Crustal Rocks, Geophys. Monogr. Ser.*, vol. 24, edited by N.L. Carter, M. Friedman, J.M. Logan, and D.W. Stearns, pp. 173-186, AGU,

Washington, D.C., 1981.

Reid, H.F., The mechanisms of the earthquake, in *The California Earthquake of April 18, 1906*, Rep. State Earthquake Investigation Comm., Carneige Inst., Washington, D.C., 1910.

Reid, H.F., The elastic rebound theory of earthquakes, *Univ. Calif. Publ. Geol.*, 6 413-444, 1911.

Rice, J.R., Constitutive relations for fault slip and earthquake instabilities, *Pure and Appl. Geophys.*, 121, 443-475, 1983.

Rice, J.R. and J.W. Rudnicki, Earthquake precursory effects due to pore fluid stabilization of a weakening fault zone, *J. Geophys. Res.*, 84(B5), 2177-2193, 1979.

Rice, J.R. and D.A. Simons, The stabilization of spreading shear faults by coupled deformation-diffusion effects in fluid-infiltrated porous media, *J. Geophys. Res.*, 81, 5322-5334, 1976.

Rice, J.R., and A.L. Ruina, Stability of steady frictional slipping, *J. Appl. Mech.*, 50, 343-349, 1983.

Rice, J.R., and S.T. Tse, Dynamic motion of a single degree of freedom system following a rate and state dependent friction law, *J. Geophys. Res.*, 91,521-530,1986.

Richards, P.G., Dynamic motions near an earthquake fault: a three dimensional solution, *Bull. Seis. Soc. Am.*, 66, 1-32, 1976.

Rieke, H.H., and G.V. Chilingarian, *Compaction of argillaceous sediments*, 424 pp., Elsevier, New York, 1974.

Rudnicki, J.W., The inception of faulting in a rock mass with a weakened zone, *J. Geophys. Res.*, 82, 844-854, 1977.

Rudnicki, J.W., and H. Kanamori, Effects of fault interaction on moment, stress drop, and strain energy release, *J. Geophys. Res.*, 86, 1785-1793, 1981.

Ruina, A.L., Slip instabilities and state friction laws, *J. Geophys. Res.*, 88, 10359-10370, 1983.

Ruina, A.L., Constitutive relations for frictional slip, in *Mechanics of Geomaterials*, edited by Z.P. Brant, John Wiley, New York, 1984.

Rundle, J.B., H. Kanamori, and K.C. McNally, An inhomogeneous fault model for gaps, asperities, barriers and seismicity migration, *J. Geophys. Res.*, 89, 10219-10231, 1984.

Savage, S.B., Gravity flow of cohesionless granular materials in chutes and channels, *J. Fluid. Mech.*, 92, 53-96, 1979.

Scholz, C.H., Shear heating and the state of stress on faults, *J. Geophys. Res.*, 85(B11), 6174-6184, 1980.

Scholz, C.H., L.R. Sykes, and Y.P. Aggarwal, Earthquake prediction - a physical basis, *Science*, 181, 803-810, 1973.

Sibson, R.H., Interactions between temperature and fluid pressure during earthquake faulting - A mechanism for partial or total stress relief, *Nature*, 243, 66-68, 1973.

Sibson, R.H., Kinetic shear resistance, fluid pressures, and radiation efficiency during seismic faulting, *Pure and Appl. Geophys.*, 115, 387-400, 1977.

Sibson, R.H., Power dissipation and stress levels on faults in the upper crust, *J. Geophys. Res.*, 85, 6239-6247, 1980.

Sieh, K.E., Prehistoric large earthquakes produced by slip on the San Andreas fault at Pallet Creek, California, *J. Geophys. Res.*, 83, 3907-3939, 1978.

Smith, J.E., Shale compaction, *Soc. Pet. Eng. J.*, 13, 12-22, 1973.

Stuart, W.D., Strain-softening instability model for the San Fernando earthquake, *Science*, 203, 907-910, 1979.

Stuart, W.D., R.J. Archuleta, and A.G. Lindh, Forecast model for moderate earthquakes near Parkfield, California, *J. Geophys. Res.*, 592-604, 1985.

Stuart, W.D., and G.M. Mavko, Earthquake instability on a strike-slip fault, *J. Geophys. Res.*, 84, 2153-2160, 1979.

Teufel, L.W., and J.M. Logan, Effect of displacement rate on the real area of contact and temperatures generated during frictional sliding of Tennessee sandstone, *Pure and Appl. Geophys.*, 116, 840-865, 1979.

Touloukian, Y.S., W.R. Judd, and R.F. Roy, *Physical Properties of Rocks and Minerals*, vol. II-2, McGraw-Hill, New York, 1981.

Walash, J.B., Mechanics of strike-slip faulting with friction, *J. Geophys. Res.*, 73, 761-776, 1968.

Watson, J.T.R., R.S. Basu, and J.V. Sengers, An improved representative equation for the dynamic viscosity of water substance, *J. Phys. Chem. Ref. Data*, 9(3), 1255-1279, 1980.

Weeks, J.D., and T.E. Tullis, Frictional sliding on dolomite: A variation in constitutive behavior, *J. Geophys. Res.*, 90,

7821-7826, 1985.

Wilson, C.R., Jr., *The mechanical properties of the shear zone of the Lewis overthrust, Glacier National Park, Montana*, Ph.D. Dissertion, Texas A&M University, Texas, 1970.

Woodside, W. and J.H. Messmer, Thermal conductivity of porous media, *J. Appl. Phys.*, 32, 1688, 1961.

TABLE 4.1. Porous Medium Compressibilities for various rock types (Domenico and Mifflin, 1965; Johnson, 1968; Smith, 1973; Reike and Chilingarian, 1974; Touloukin, 1981).

Rock Type	β_{sf} (Pa^{-1})
Unconsolidated clays	10^{-6}-10^{-8}
Unconsolidated sands	10^{-7}-10^{-9}
Unconsolidated gravel	10^{-8}-10^{-10}
Compacted sediments	10^{-9}-10^{-11}
Igneous and metamorphics rocks	10^{-9}-10^{-11}
Water (at 80 °C and 19 MPa)	4.2×10^{-10}

TABLE 4.2. Parameter Values for Porous Medium and Solid Properties Held Constant for All Simulations.

Property	Value
Initial porosity n_0	0.1
ξ	1.0
Solid density ρ_s	2.6×10^3 kg m^{-3}
Solid specific heat c_s	10^3 J kg^{-1} $°K^{-1}$
Solid thermal conductivity K_s	2.5 W m^{-1} $°K^{-1}$
Solid compressibilty β_s	10^{-11} Pa^{-1}
Solid thermal expansivity γ_s	2.0×10^{-5} $°C^{-1}$
Porous medium thermal expansivity γ_{sf}	10^{-5} $°C^{-1}$
Porous medium thermal conductivity K_{sf_0}	2.5 W m^{-1} $°K^{-1}$
Porous medium thermal diffusivity a_{t_0}	6.65×10^{-7} $m^2 s^{-1}$
Water compressibility β_{w_0}	4.2×10^{-10} Pa^{-1}
Water thermal expansivity γ_{w_0}	6.24×10^{-4} $°C^{-1}$

TABLE 4.3. Summary of initial parameter values for a fault surface at a depth of 2 km.*

β_{sf}	Γ	$\frac{\tau_n - P_o}{\Gamma}$	ψ_o	$\lambda(\tau_n - P_o)$	$\frac{\Delta n}{n_o}$
(Pa^{-1})	($MPa°C^{-1}$)	(°C)	(s)		
10^{-11}	1.687	15	0.002	0.000	0.00
10^{-10}	0.747	35	0.011	0.002	0.01
10^{-9}	0.125	208	0.400	0.023	0.20
10^{-8}	0.013	1945	35.00	0.231	1.90

*Parameters held constant

$2\bar{V}_y = 10^{-1}$ ms^{-1}	$\mu_d = 0.6$	$\mu_s = 0.6175$
$P_o = 19$ MPa	$T_o = 80$ °C	$n_o = 0.10$
$\tau_n = 45$ MPa	$\tau_n - P_o = 26$ MPa	$\tau_r = 15.6$ MPa
$w_e = 10$ km	$v = 3.3$ km s^{-1}	$t_s = 6.0$ s

FIGURE CAPTIONS

Figure 4.1. (a) Conceptual model for fault slip. The fault is represented by a vertical zone that is comprised of patches of relatively high strength rock (shaded) surrounded by weaker intervening areas. At the instant of failure a barrier ruptures and slip (stippled area) spreads through the locked portion until it is halted by another barrier. (b) Uniform strain rate model for a small patch of the failure surface. The arrows denote the displacement field.

Figure 4.2. Isothermal volumetric compressibility β_w and isobaric thermal expansivity γ_w of pure water as a function of temperature T for selected fluid pressures P. Curves are based on the analytic expression by Keenan *et al.* (p.128, 1978). The fluid pressure increment between curves is 5 MPa for 5-20 MPa, 10 MPa for 20-40 MPa, and 20 MPa for 40-100 MPa. The liquid-steam transition is indicated by dashed lines.

Figure 4.3. Slip velocity models for constant fluid pressure: EB, elastic-block model; EE, edge-effects model; and SR, spring-rider model.

Figure 4.4. The thermal pressurization coefficient Γ calculated as a function of temperature T for selected fluid pressures P and porous medium compressibilities β_{sf} using the solid properties summarized in Table 2. The fluid pressure

increment between curves is 5 MPa for 5-20 MPa, 10 MPa for 20-40 MPa, and 20 MPa for 40-100 MPa. The liquid-steam transition is indicated by dashed lines.

Figure 4.5. Temperature rise (solid) and resistive stress (dashed) on a failure surface as a function of slip duration. An average slip velocity and friction coefficient are assumed. (*a*) Temperature and resistive stress as given by the analytical solutions. (*b*) Comparison of the analytical and numerical solutions for selected porous medium compressibilities, undrained conditions, and the initial conditions of Table 4.3.

Figure 4.6. Temperature rise and resistive stress during displacement across a fault surface with an average slip velocity $2\bar{V}_y=10^{-1}$ ms^{-1}, friction coefficient $\bar{\mu}_d=0.6$, and initial effective stress $\tau_n=24$ MPa. The initial conditions are summarized in Table 4.3. The β_{sf} (Pa^{-1}) and k (m^2) are the compressibility and permeability of the adjacent porous medium. Numbers on curves represent values of permeability. Scales are adjustable for other value of $\bar{\mu}_d$, τ_n, and $2\bar{V}_y$ (see text).

Figure 4.7. The hydrologic and thermal fields as a function of distance from the fault surface for selected displacements. Calculations are for a stiff medium with a permeability of 10^{-17} m^2, and the initial conditions of Table 4.3. Diagram (a)

shows the temperature (solid) and pore pressure rise (dashed); (b) the thermal expansion (solid) and pressure contraction (dashed) rates of the fluid volume; and (c) the Darcy flux.

Figure 4.8. The hydrologic and thermal fields as a function of distance from the fault surface for selected displacements. Calculations are for a porous medium with a compressibility of 10^{-9} Pa^{-1}, a permeability of 10^{-17} m^2, and the initial conditions on Table 4.3. Diagram (a) shows the temperature (solid) and pore pressure rise (dashed); (b) thermal expansion rate of the fluid volume (solid) and dilatational strain rate of the pore volume (dashed); and (c) the Darcy flux. The parameter λ^* is given by $\lambda(\tau_n - P_0)$.

Figure 4.9. Temperature (solid) and resistive stress (dashed) within a fault zone as a function of slip duration t/ψ or shear strain $d/2w\psi_e$ for selected porous medium compressibilities. Undrained conditions and negligible loss of heat from the zone are assumed. Analytical solutions are labeled by *A*.

Figure 4.10. The dilatational strain rate of the pore volume within a fault zone as a function of slip duration t/ψ or shear strain $d/2w\psi$ for selected porous medium compressibilities. Undrained conditions and negligible loss of heat from the zone are assumed. Analytical solution is indicated by the dashed line.

Figure 4.11. Temperature rise and resistive stress at the center of a fault zone whose width $2w$ and average slip velocity are 10^{-1} m and 10^{-1} ms^{-1}, respectively. The initial conditions are summarized in Table 4.3. The β_{sf} (Pa^{-1}) and k (m^2) are the compressibility and permeability of the porous medium. Number on curves represent values of permeability.

Figure 4.12. Temperature (solid) and pore-fluid pressure rise (dashed) as a function of distance for slip across a fault zone with a width of 10^{-1} m and a relative slip rate of $2\bar{V}_y$ $=10^{-1}$ ms^{-1}. Calculations are for a stiff medium and the initial conditions of Table 4.3. The permeability of the fault and adjacent wall rock are: (a) 10^{-13} and 10^{-18} m^2; and (b) 10^{-18} and 10^{-13} m^2. Numbers on curves represent values of displacement.

Figure 4.13. Analytical solutions for the slip rate as a function of time for selected ratios of the characteristic slip duration t_s to the characteristic time for thermal pressurization ψ. Fault motion is initiated by a 3% drop in the static shear strength. The slip rate is normalized by the maximum rate for a complete loss of shear strength at the initiation of slip. Undrained conditions and negligible loss of heat from the zone are assumed.

Figure 4.14. Numerical solutions for the slip rate and

resistive stress as a function of time for slip across a fault zone with a width of 10^{-1} m. Fault slip is initiated by a 3% drop in the static shear strength. Numbers on curves represent values of permeability. Calculations are for a porous medium compressibility of 10^{-9} Pa^{-1}, and the initial conditions of Table 4.3. Dashed lines show the restoration of shear strength after the cessation of slip.

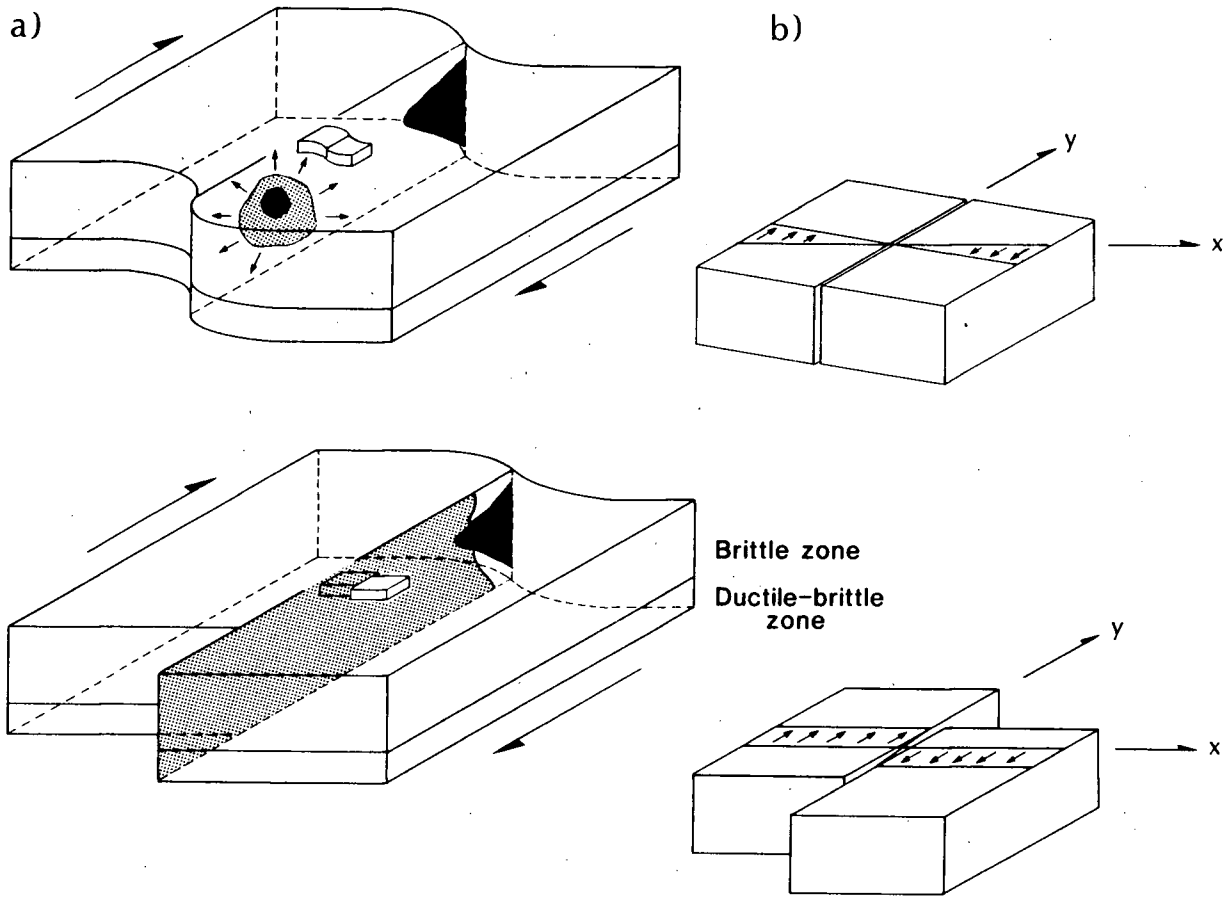

Figure 4.1

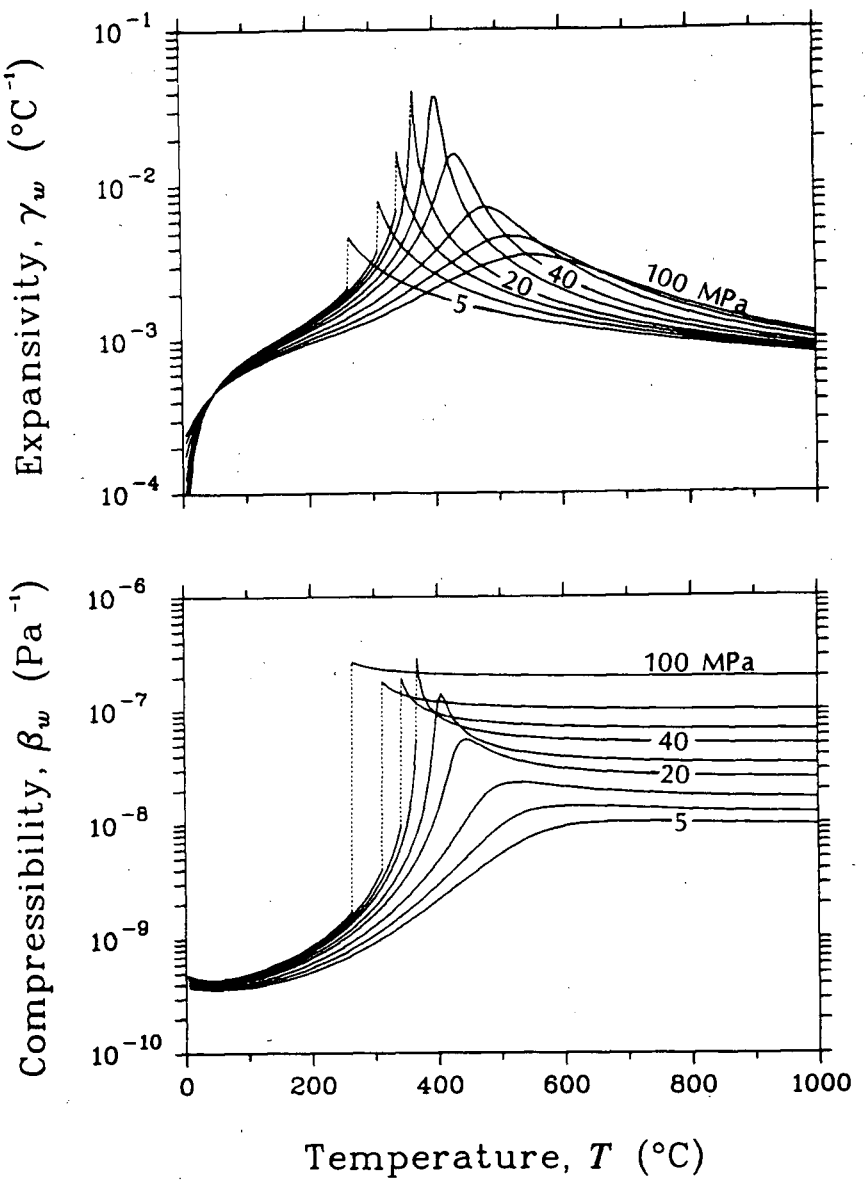
Expansivity, γ_w (°C^{-1})
10^{-1}
10^{-2}
10^{-3}
10^{-4}
100 MPa
40
20
5
Compressibility, β_w (Pa^{-1})
10^{-6}
10^{-7}
10^{-8}
10^{-9}
10^{-10}
100 MPa
40
20
5
0
200
400
600
800
1000
Temperature, T (°C)

Figure 4.2

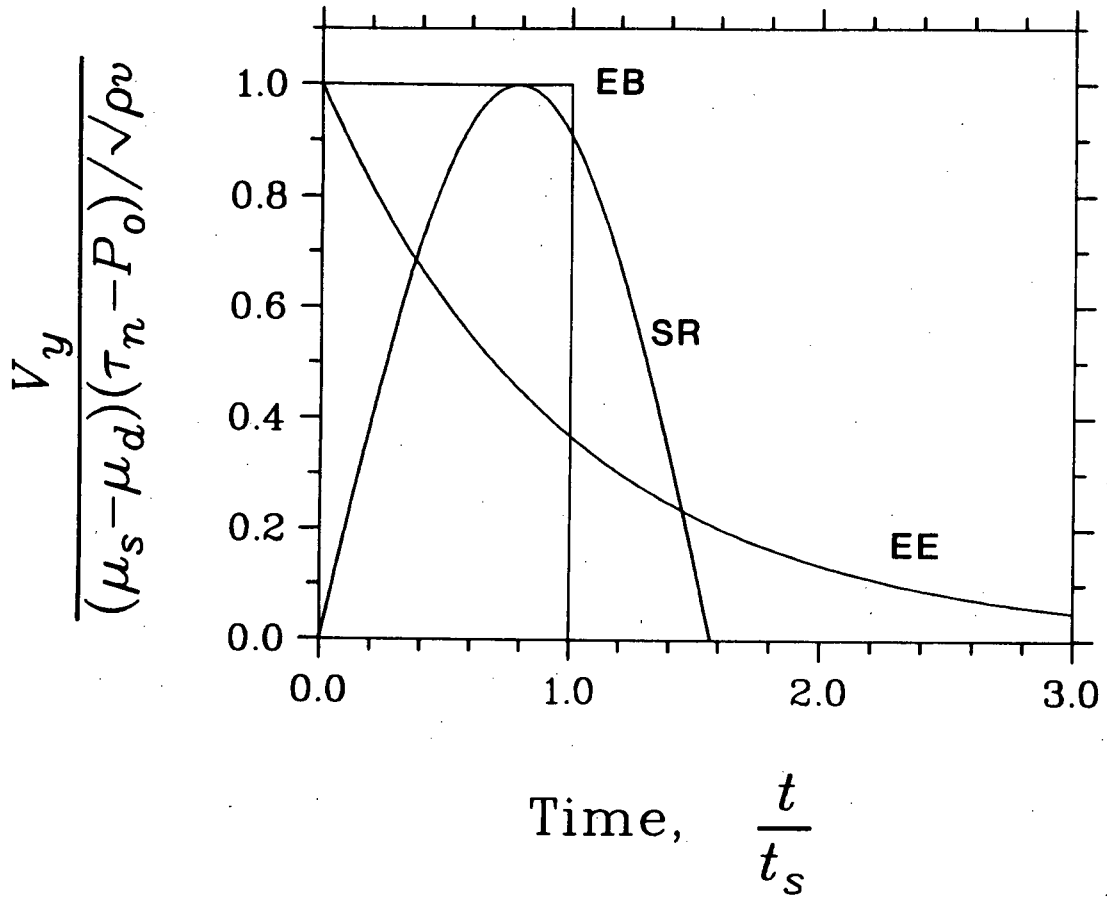
$\frac{V_y}{(\mu_s-\mu_d)(\tau_n-P_o)/\sqrt{\rho v}}$
1.0
0.8
0.6
0.4
0.2
0.0
EB
SR
EE
0.0
1.0
2.0
3.0
Time, $\frac{t}{t_s}$

Figure 4.3

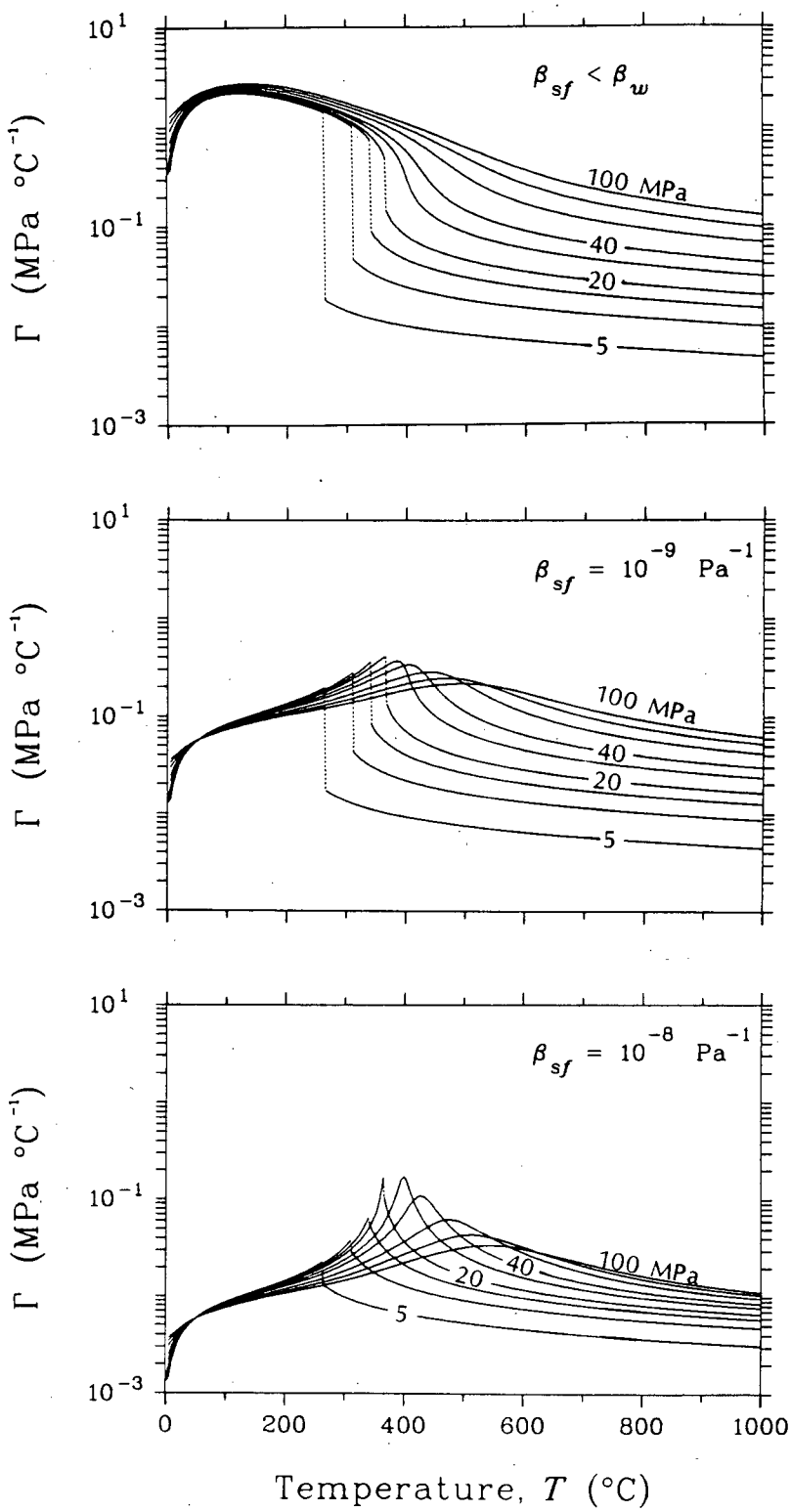
10^1
10^{-1}
10^{-3}
Γ (MPa °C^{-1})
$\beta_{sf} < \beta_w$
100 MPa
40
20
5
$\beta_{sf} = 10^{-9}$ Pa^{-1}
$\beta_{sf} = 10^{-8}$ Pa^{-1}
0
200
400
600
800
1000
Temperature, T (°C)

Figure 4.4

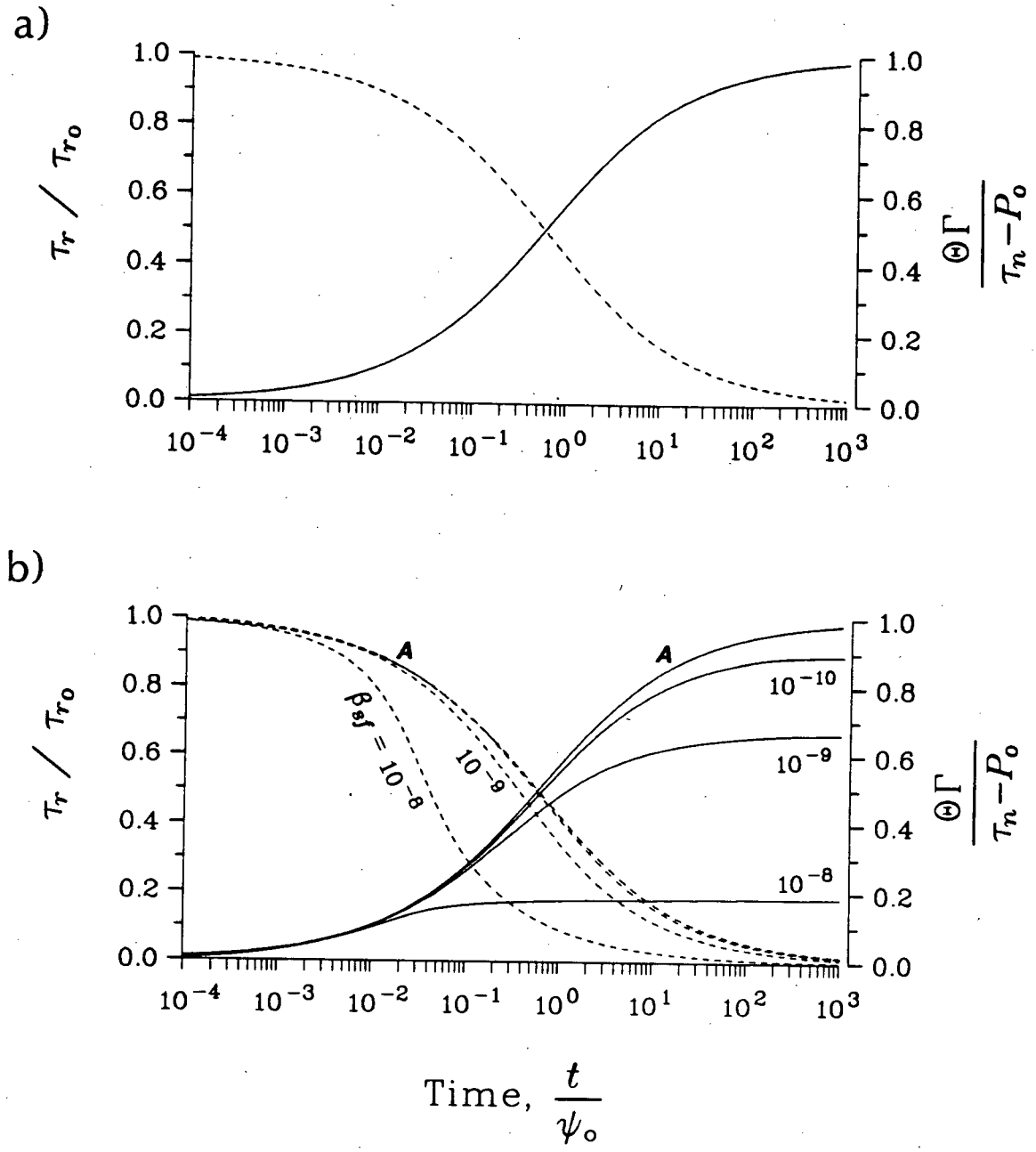
a)
b)
τ_r / τ_{ro}
$\frac{\Theta\Gamma}{\tau_n - P_o}$
1.0
0.8
0.6
0.4
0.2
0.0
10^{-4} 10^{-3} 10^{-2} 10^{-1} 10^{0} 10^{1} 10^{2} 10^{3}
A
A
$\beta_{sf} = 10^{-8}$
10^{-9}
10^{-10}
10^{-9}
10^{-8}
Time, $\frac{t}{\psi_o}$

Figure 4.5

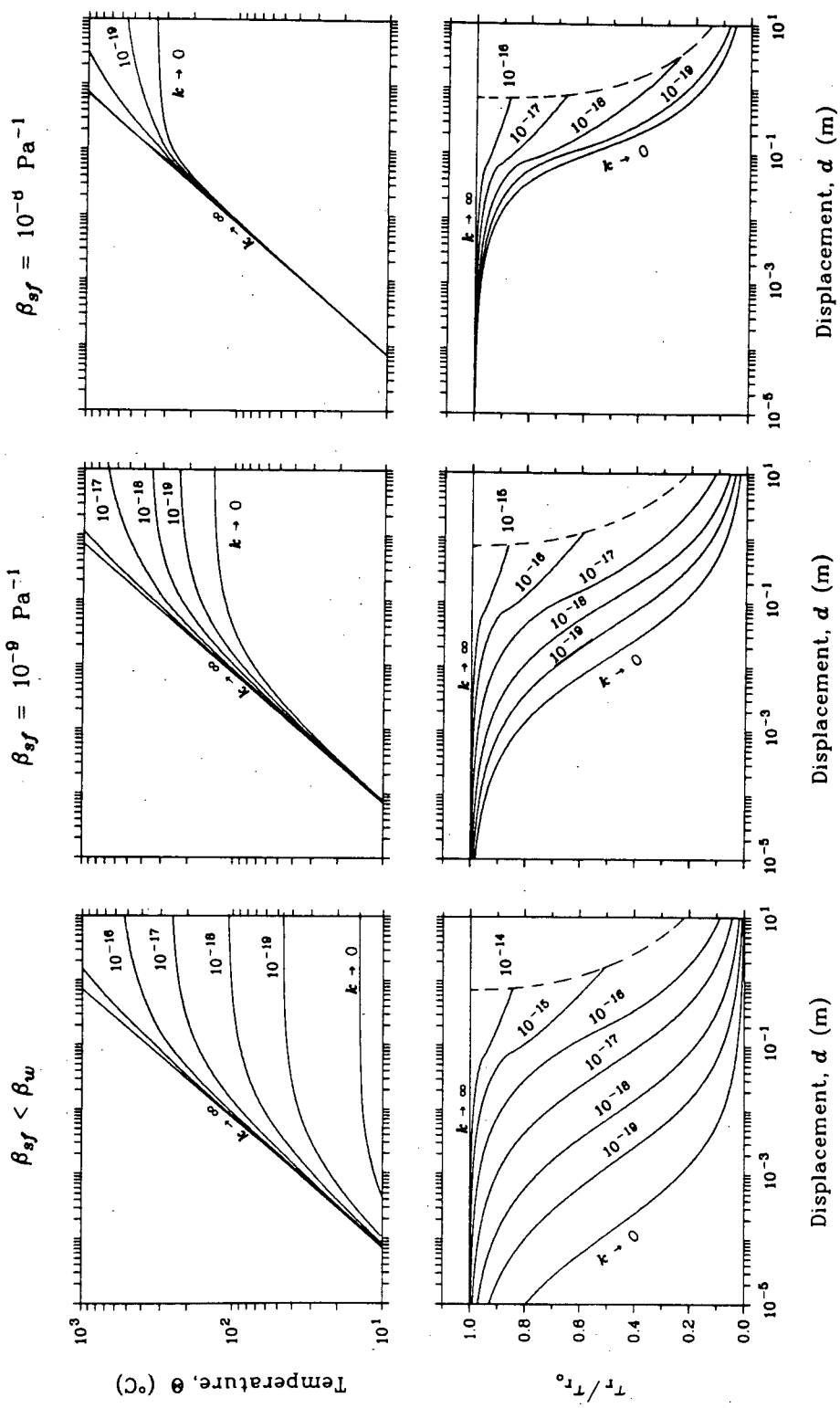
$\beta_{sf} < \beta_w$
$\beta_{sf} = 10^{-9}$ Pa^{-1}
$\beta_{sf} = 10^{-8}$ Pa^{-1}
Temperature, θ (°C)
T_r/T_{r_o}
Displacement, d (m)
Displacement, d (m)
Displacement, d (m)
k → ∞
k → 0
10^{-14}
10^{-15}
10^{-16}
10^{-17}
10^{-18}
10^{-19}

Figure 4.6

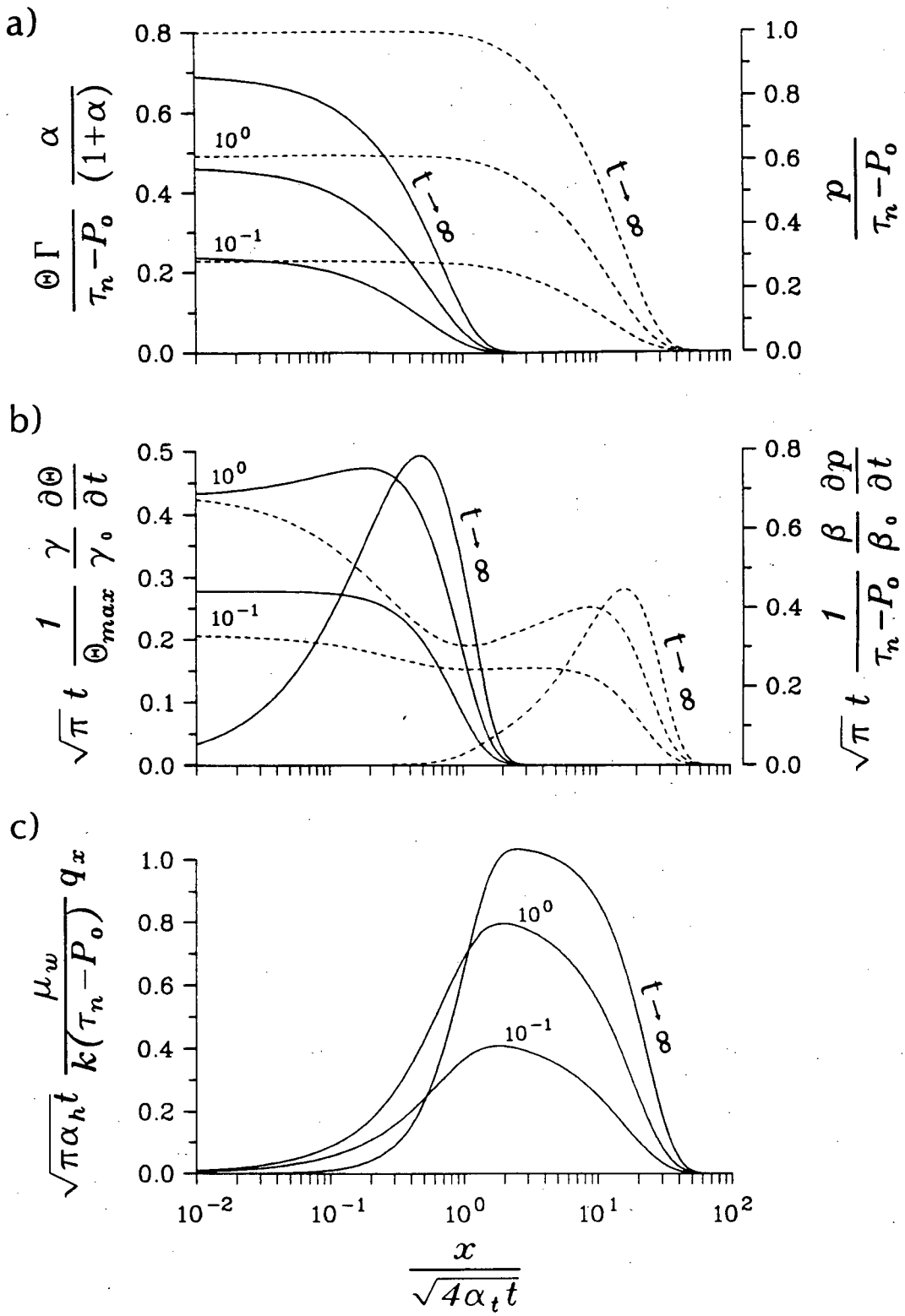
a)
b)
c)
10^0
10^{-1}
$t \to \infty$
$\frac{\Theta\,\Gamma}{\tau_n - P_o}\,\frac{\alpha}{(1+\alpha)}$
$\frac{p}{\tau_n - P_o}$
$\sqrt{\pi\, t}\,\frac{1}{\Theta_{max}}\,\frac{\gamma}{\gamma_o}\,\frac{\partial \Theta}{\partial t}$
$\sqrt{\pi\, t}\,\frac{1}{\tau_n - P_o}\,\frac{\beta}{\beta_o}\,\frac{\partial p}{\partial t}$
$\sqrt{\pi \alpha_h t}\,\frac{\mu_w}{k(\tau_n - P_o)}\,q_x$
$\frac{x}{\sqrt{4\alpha_t t}}$

Figure 4.8

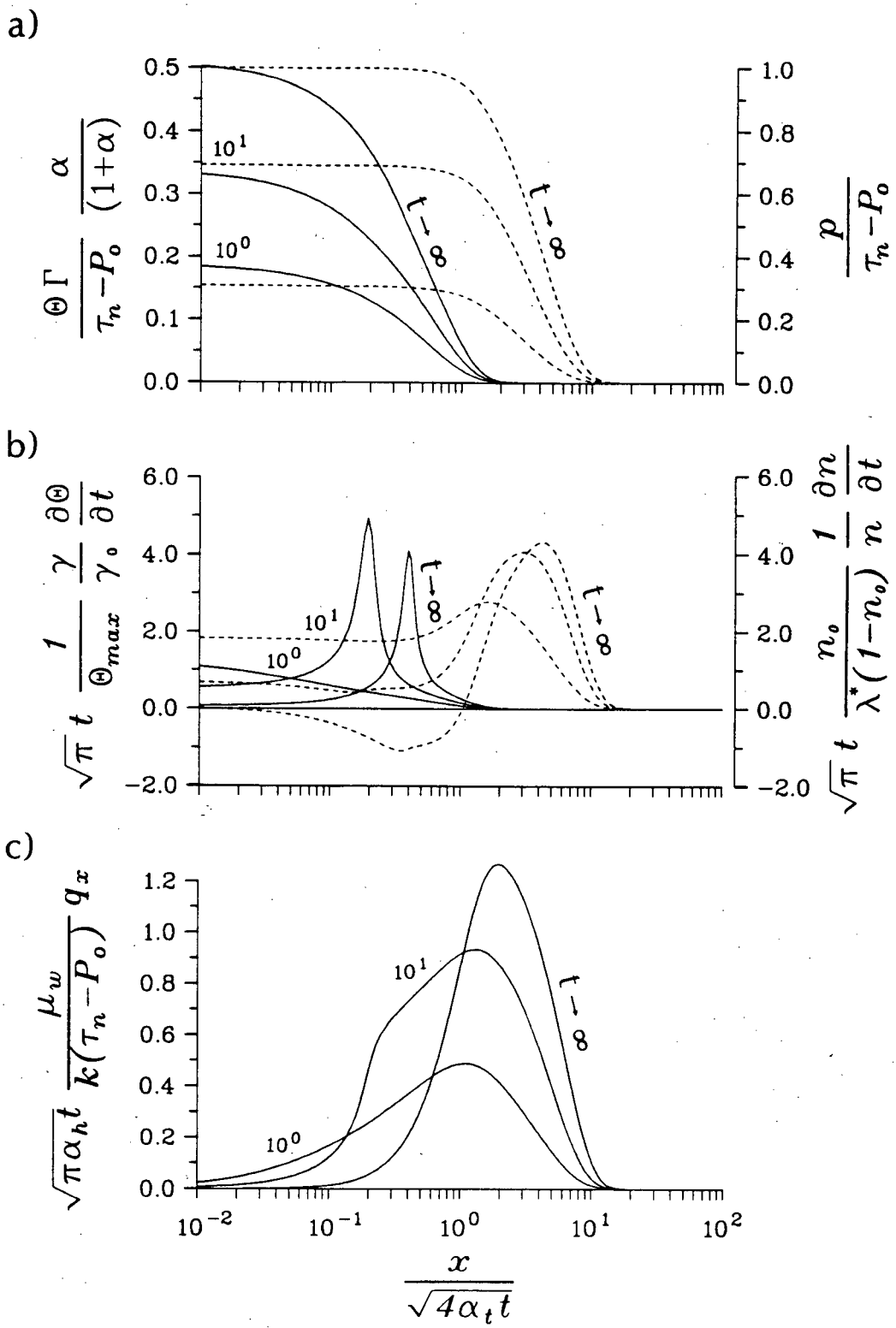
a)
b)
c)
10^1
10^0
$t \to \infty$
$\frac{\Theta\,\Gamma}{\tau_n - P_o}\,\frac{\alpha}{(1+\alpha)}$
$\frac{p}{\tau_n - P_o}$
$\sqrt{\pi\, t}\,\frac{1}{\Theta_{max}}\,\frac{\gamma}{\gamma_o}\,\frac{\partial\Theta}{\partial t}$
$\sqrt{\pi\, t}\,\frac{n_o}{\lambda^*(1-n_o)}\,\frac{1}{n}\,\frac{\partial n}{\partial t}$
$\sqrt{\pi\alpha_h t}\,\frac{\mu_w}{k(\tau_n - P_o)}\,q_x$
$\frac{x}{\sqrt{4\alpha_t t}}$

Figure 4.8

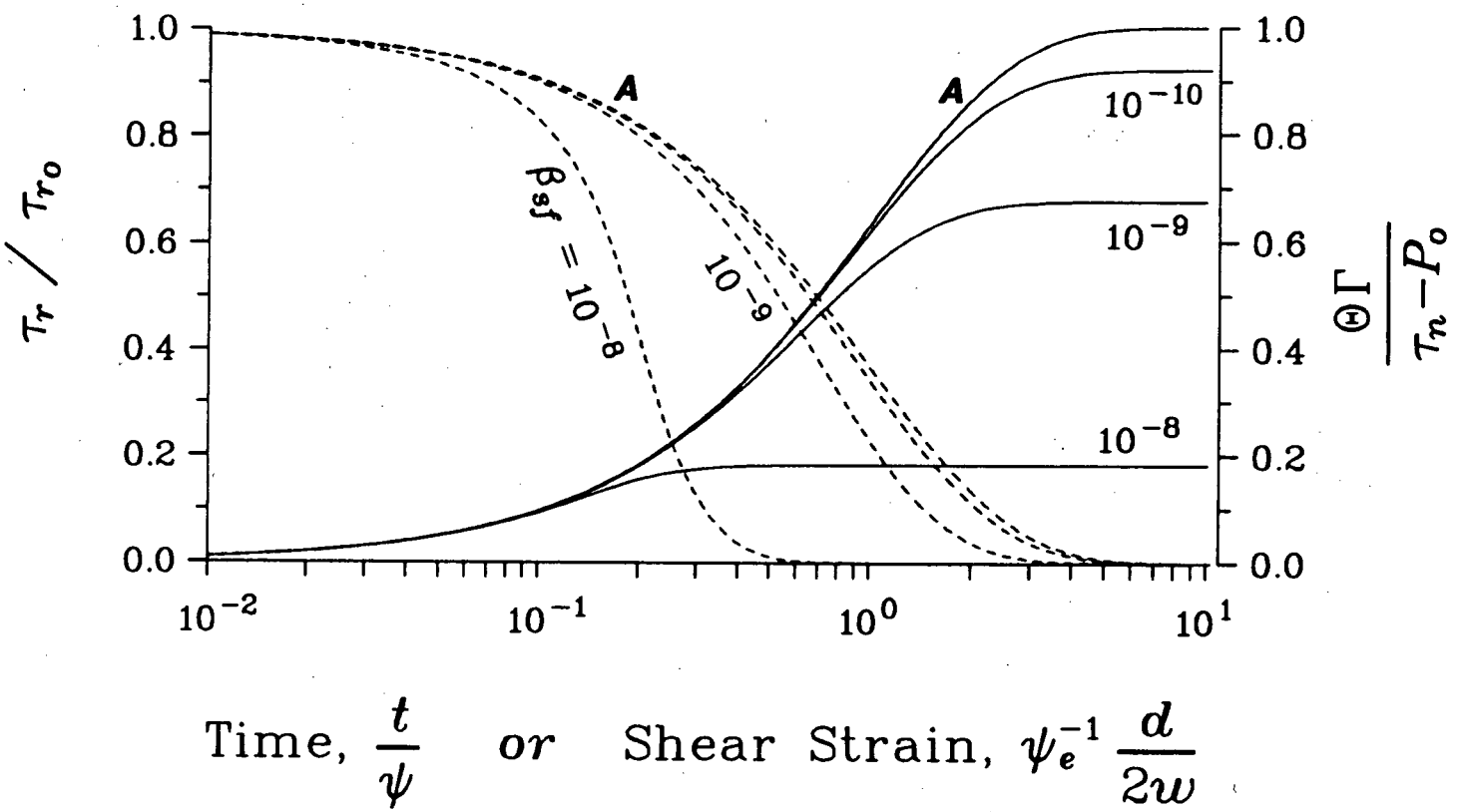
1.0
0.8
0.6
0.4
0.2
0.0
τ_r / τ_{ro}
A
A
$\beta_{sf} = 10^{-8}$
10^{-9}
10^{-10}
10^{-9}
10^{-8}
10^{-2}
10^{-1}
10^{0}
10^{1}
$\frac{\Theta\Gamma}{\tau_n - P_o}$
Time, $\frac{t}{\psi}$ or Shear Strain, $\psi_e^{-1} \frac{d}{2w}$

Figure 4.9

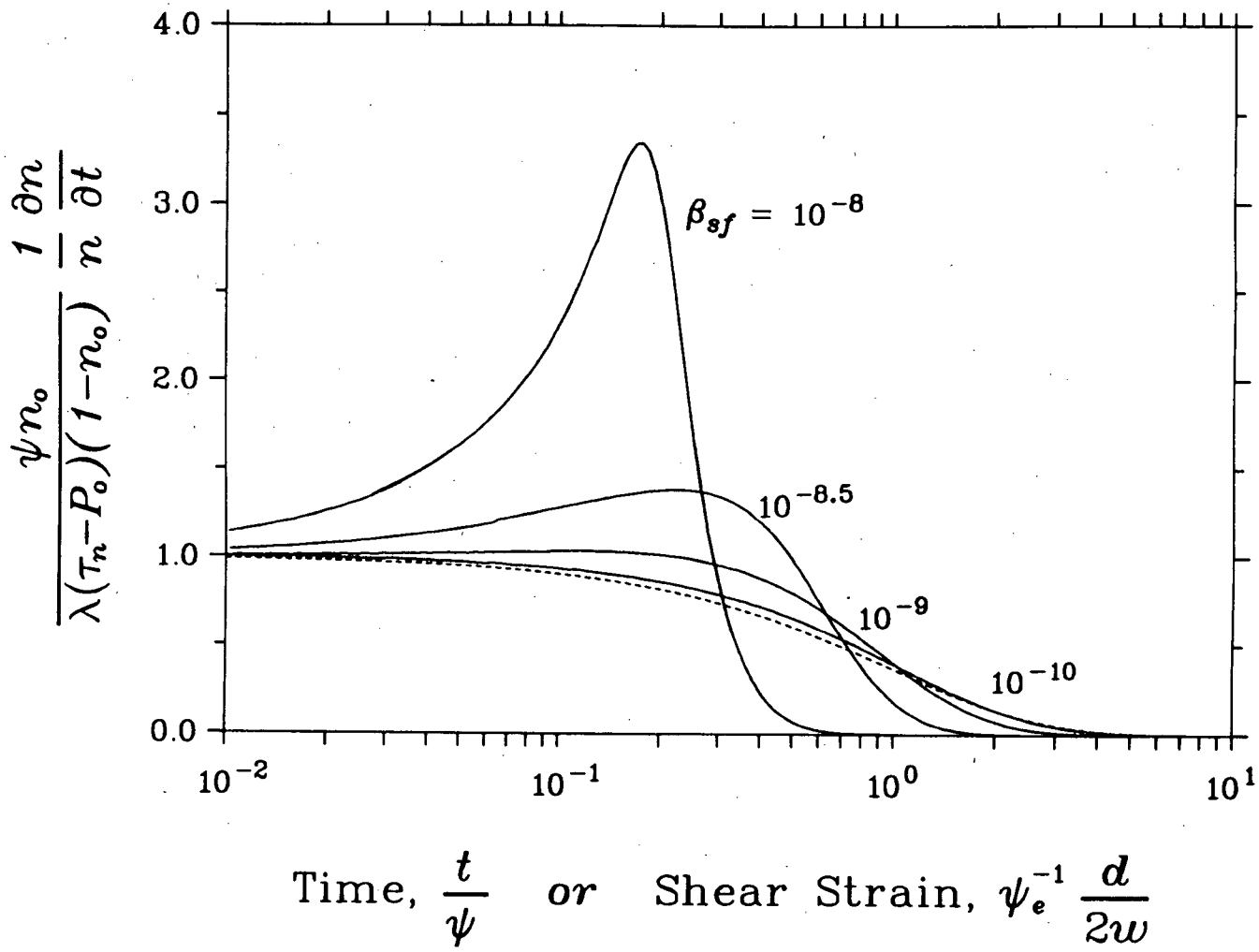
4.0
3.0
2.0
1.0
0.0
10^{-2}
10^{-1}
10^{0}
10^{1}
$\beta_{sf} = 10^{-8}$
$10^{-8.5}$
10^{-9}
10^{-10}
$\frac{\psi n_o}{\lambda(\tau_n - P_o)(1-n_o)} \frac{1}{n} \frac{\partial n}{\partial t}$
Time, $\frac{t}{\psi}$ or Shear Strain, $\psi_e^{-1} \frac{d}{2w}$

Figure 4.10

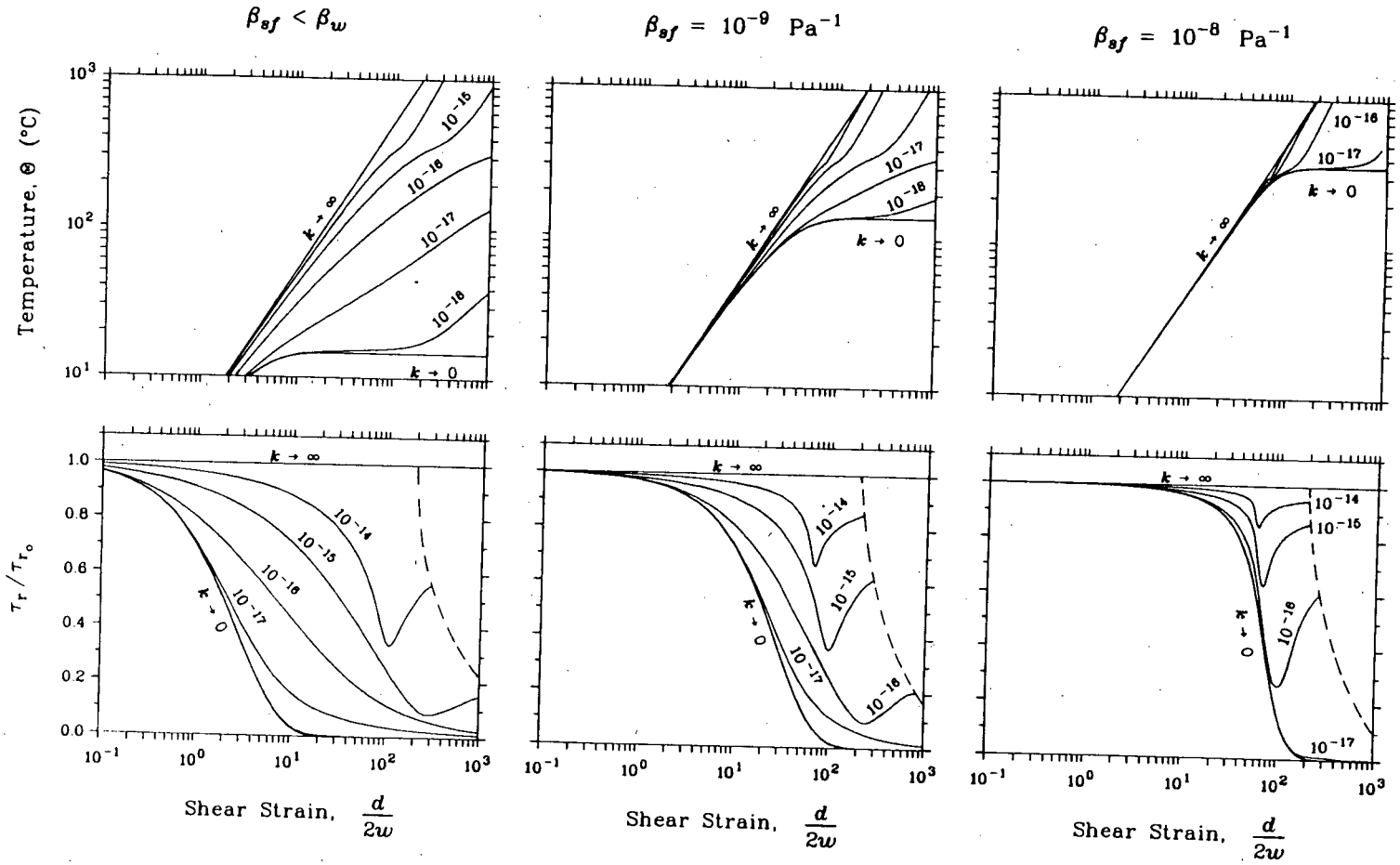
$\beta_{sf} < \beta_w$
$\beta_{sf} = 10^{-9}$ Pa^{-1}
$\beta_{sf} = 10^{-8}$ Pa^{-1}
Temperature, Θ (°C)
10^3
10^2
10^1
$k \to \infty$
10^{-15}
10^{-16}
10^{-17}
10^{-18}
$k \to 0$
10^{-16}
10^{-17}
10^{-18}
$k \to 0$
$k \to \infty$
10^{-16}
10^{-17}
$k \to 0$
τ_r / τ_{r_o}
1.0
0.8
0.6
0.4
0.2
0.0
$k \to \infty$
10^{-14}
10^{-15}
10^{-16}
10^{-17}
$k \to 0$
$k \to \infty$
10^{-14}
10^{-15}
10^{-16}
10^{-17}
$k \to 0$
$k \to \infty$
10^{-14}
10^{-15}
10^{-16}
10^{-17}
$k \to 0$
10^{-1}
10^0
10^1
10^2
10^3
Shear Strain, $\frac{d}{2w}$
Shear Strain, $\frac{d}{2w}$
Shear Strain, $\frac{d}{2w}$

Figure 4.11

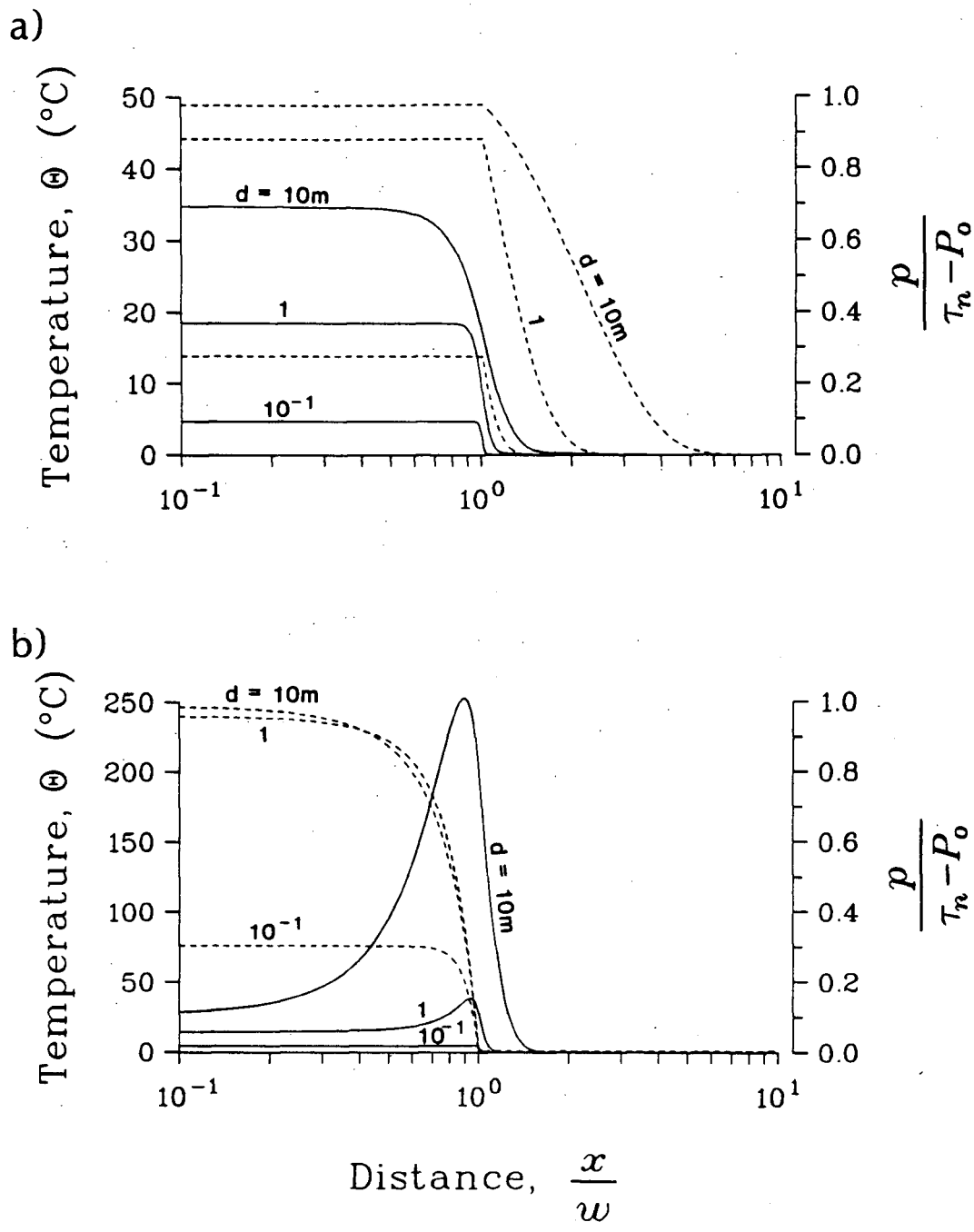
a)
Temperature, Θ (°C)
50
40
30
20
10
0
d = 10m
1
10⁻¹
d = 10m
1
1.0
0.8
0.6
0.4
0.2
0.0
p / τn − Po
10⁻¹
10⁰
10¹
b)
Temperature, Θ (°C)
250
200
150
100
50
0
d = 10m
1
10⁻¹
d = 10m
1
10⁻¹
1.0
0.8
0.6
0.4
0.2
0.0
p / τn − Po
10⁻¹
10⁰
10¹
Distance, x / w

Figure 4.12

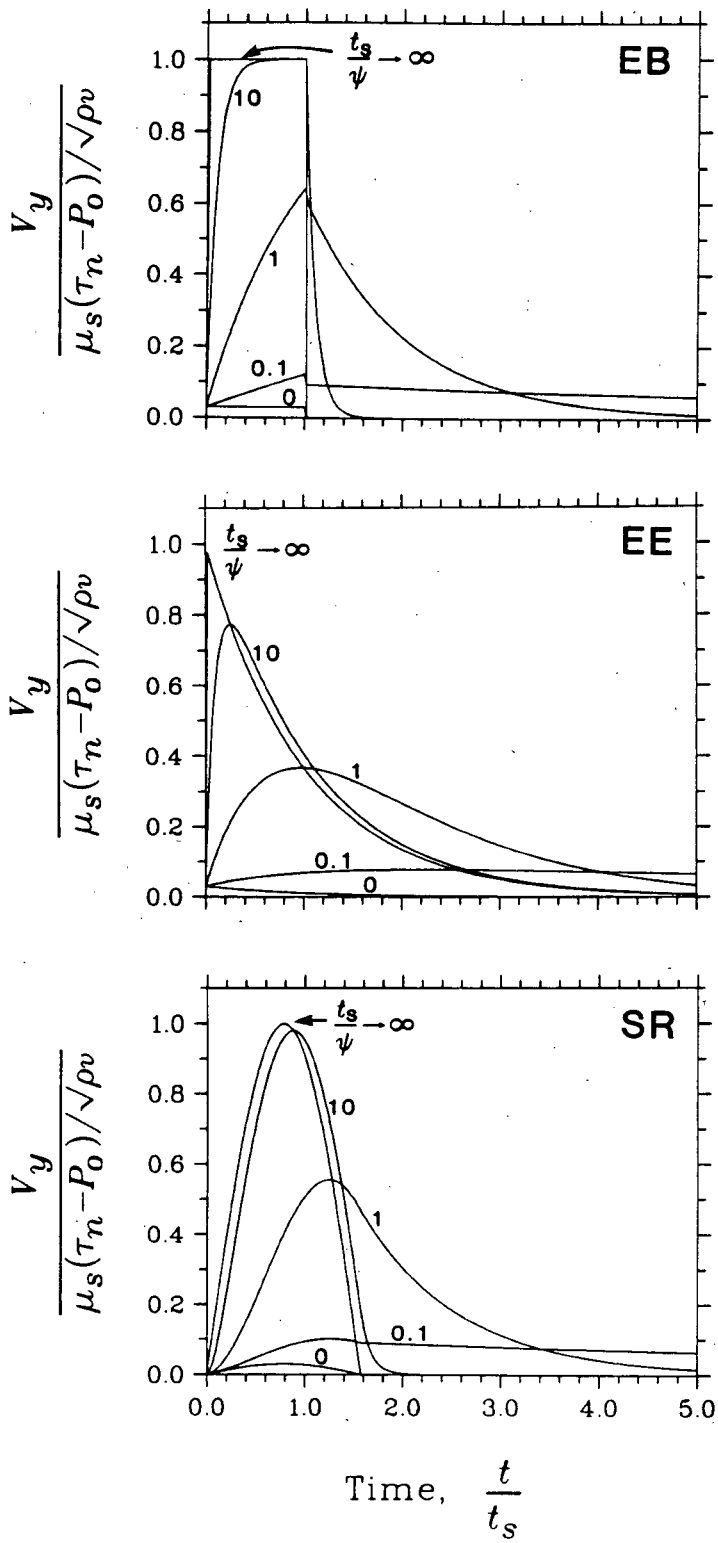
EB
EE
SR
$\frac{t_s}{\psi} \to \infty$
10
1
0.1
0
$\frac{V_y}{\mu_s(\tau_n - P_0)/\sqrt{\rho v}}$
1.0
0.8
0.6
0.4
0.2
0.0
0.0
1.0
2.0
3.0
4.0
5.0
Time, $\frac{t}{t_s}$

Figure 4.13

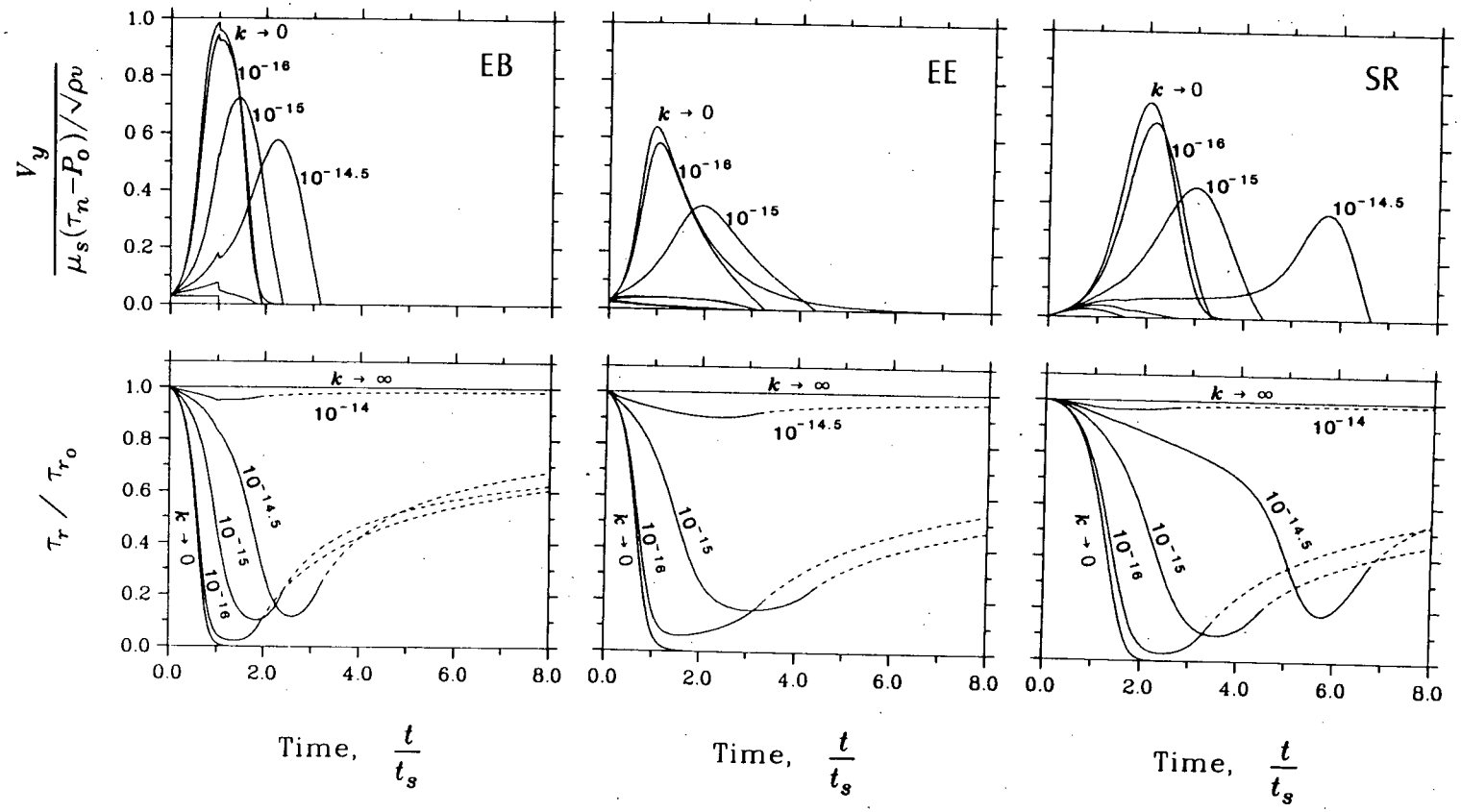
EB
EE
SR
$k \to 0$
10^{-16}
10^{-15}
$10^{-14.5}$
$k \to \infty$
10^{-14}
$\frac{V_y}{\mu_s(\tau_n - P_o)/\sqrt{\rho v}}$
τ_r / τ_{r_o}
Time, $\frac{t}{t_s}$
0.0
0.2
0.4
0.6
0.8
1.0
2.0
4.0
6.0
8.0

Figure 4.14

COMPILATION OF REFERENCES

Aki, K., Characterization of barriers on an earthquakes, *J. Geophys. Res.*, 84, 6140-6148, 1979.

Aki, K., Asperities, barriers, characteristic earthquakes and strong motion prediction, *J. Geophys. Res.*, 89, 5867-5872, 1984.

Anderson, D.L., An earthquake induced heat mechanism to explain the loss of strength of large rock or earth slides, Int'l. Conference on Engineering for Protection from Natural Disasters, Bangkok, 1980.

Barker, C., Aquathermal pressuring: role of temperature in development of abnormal pressure zones, *Am. Assoc. Pet. Geol. Bull.*, 56, 2068-2071, 1972.

Barker, C., and B. Horsfield, Mechanical versus thermal cause of abnormal high pore pressures in shales: discussion, *Am. Assoc. Pet. Geol. Bull.*, 66, 99-100, 1982.

Bear, J., *Hydraulics of Groundwater*, McGraw-Hill Inc., New York, 1979.

Bear, J., *Dynamics of Fluids in Porous Media*, 764 pp., American Elsevier, New York, 1972.

Bear, J., and M.Y. Corapcioglu, A mathematical model for consolidation in a thermoelastic aquifer due to the hot water injection, *Water Resour. Res.*, 17(3), 723-736, 1981.

Bell, M.L. and A. Nur, Strength changes due to reservoir-induced pore pressure and stresses and application to Lake Orville, *J. Geophys. Res.*, 83, 4469-4483, 1978.

Bernabe, Y., B. Evans, and W.F. Brace, Permeability, porosity, and pore geometry of hot pressed clacite, *Mech. Mater.*, 1, 173-183, 1982.

Biot, M. A., General theory of three dimensional consolidation, *J. Appl. Phys.*, 12, 155-164, 1941.

Biot, M. A. and D. G. Willis, The elastic coefficients of the theory of consolidation, *J. Appl. Mech.*, 24, 594-601, 1957.

Brace, W.F., Permeability from resistivity and pore shape, *J. Geophys. Res.*, 82, 3343-3349, 1977.

Brace, W.F., and J.D. Byerlee, Stick-slip as a mechanism for earthquakes, *Science*, 153(3739), 990, 1966.

Bradley, J.S., Abnormal formation pressure, *Am. Assoc. Pet. Geol. Bull.*, 59, 957-973, 1975.

Brock, W.G., and T. Engelder, Deformation associated with the

movement of the Muddy Mountain Overthrust in the Buffington window, southeastern Nevada, *Bull. Geol. Soc. Am.*, 88, 1667-1677, 1977.

Brownell, Jr., D.H., S.K. Garg, and J.W. Pritchett, Governing equations for geothermal reservoirs, *J. Geophys. Res.*, 6, 929-934, 1977.

Brun, J.P. and P.R. Cobbold, Strain heating and thermal softening in continental shear zones: a review, *J. Struct. Geol.*, 2, 149-158, 1980.

Brune, J.N., Tectonic stress and the spectra of seismic shear waves from earthquakes, *J. Geophys. Res.*, 75, 4995-5009, 1970.

Burridge, R., and L. Knopoff, Model and theoretical seismicity, *Bull. Seis. Soc. Am.*, 57, 341-371, 1967.

Bustin, R.M., Heating during thrust faulting in the Rocky Mountains: friction or fiction?, *Tectonophysics*, 95, 309-328, 1983.

Byerlee, J.D., The mechanics of stick-slip, *Tectonophysics*, 9 475, 1970.

Byerlee, J. D., Friction of rocks, *Pure and Appl. Geophys.*, 116, 615-626, 1978.

Cardwell, R. K., D. S. Chinn, G. F. Moore, and D. L. Turcotte, Frictional heating on a fault of finite thickness, *Geophys. J. Roy. Astron. Soc.*, 52, 525-530, 1978.

Carslaw, H.C., and J.C. Jaeger, **Conduction of Heat in Solids**, 386pp., Oxford University Press, New York, 1959.

Chapman, R.E., Mechanical versus thermal cause of abnormal high pore pressure in shales, *Am. Assoc. Pet. Geol. Bull.*, 64, 2179-2183, 1980.

Cooper, H.H., Jr., The equation of groundwater flow in fixed and deforming coordinates, *J. Geophys. Res.*, 71, 4785-4790, 1966.

Daines, S., Aquathermal pressuring and geopressure evaluation, *Am. Assoc. Pet. Geol. Bull.*, 66, 931-939, 1982.

Das, S., and K. Aki, Fault plane with barriers: A versatile earthquake model, *J. Geophys. Res.*, 5658-5670, 1977.

Das, S., and C.H. Scholz, Theory of time-dependent rupture in the earth, *J. Geophys. Res.*, 6039-6051, 1981.

Delaney, P.T., Rapid intrusion of magma into wet rock: Groundwater flow due to pore pressure increases, *J. Geophys.*

Res., 87, 7739-7756, 1982.

Dickey, P.A., Abnormal formation pressure: discussion, *Am. Assoc. Pet. Geol. Bull.*, 60,1124-1128, 1975.

Dietrich, J.H., Earthquake mechanisms and modeling, *Ann. Rev. Earth Planet. Sci.*, 2, 275-302, 1974.

Dietrich, J.H., Modeling of rock friction: 1. Experimental results and constitutive equations, *J. Geophys. Res.*, 84, 2161-2168, 1979a.

Dietrich, J.H., Modeling of rock friction: 2. Simulation of preseismic slip, *J. Geophys. Res.*, 84, 2161-2168, 1979b.

Domenico, P.A. and M.D. Mifflin, Water from low-permeability sediments and and land subsidence, *Water Resour. Res.*, 1, 563-576, 1965.

Domenico, P.A., and V.V. Palciauskas, Thermal expansion of fluids and fracture initiation in compacting sediments, I, *Bull. Geol. Soc. Am.*, 90, 953-979, 1979a.

Domenico, P.A., and V.V. Palciauskas, Thermal expansion of fluids and fracture initiation in compacting sediments, II, *Bull. Geol. Soc. Am.*, 90, 953-979, 1979b.

Faust, C.R., and J.W. Mercer, Geothermal reservoir simulation 1. Mathematical models for liquid- and vapor dominated hydrothermal systems, *J. Geophys. Res.*, 15, 23-30, 1979.

Fleitout, L. and C. Froidevaux, Thermal and mechanical evolution of shear zones, *J. Struct. Geol.*, 2, 159-164, 1980.

Flinn, D., Transcurrent faults and associated cataclasis in Shetland, *J. Geol. Soc. London,* 133, 231-248, 1977.

Flinn, D., The Walls Boundary Fault, Shetland, British Isles, Analysis of Actual faults in Bedrock, *U.S. Geol. Surv. Open File Rep.*, 79-1239, 181-200, 1979.

Gambolati, G., Second-order theory of flow in 3D deforming media, *Water Resour. Res.*, 10(6), 1217-1228, 1974.

Garg, S.K., and J.W. Pritchett, On pressure-work, viscous dissipation, and the energy balance equation for geothermal reservoirs, *Adv. Water Resources*, 1, 41-47, 1977.

Habib, Production of gaseous pore press during rock slides, *J. Rock Mech.*, 7, 193-197, 1975.

Handin, J., R.V. Hager Jr., M. Friedman, and J.N. Feather, Experimental deformation of sedimentary rocks under confining pressure: pore pressure tests, *Bull. Am. Assoc. Petrol. Geol.*,

47, 717-755, 1963.

Holcomb, D.J., A quantitative model of dilatancy in dry rock and its application to Westerly granite, *J. Geophys. Res.*, 83(B10), 4941-4950, 1978.

Holcomb, D.J., Memory, relaxation, and microfracturing in dilatant rock, *J. Geophys. Res.*, 86(B7), 6235-6248, 1981.

Hubbert, M.K. and W.W. King, Role of fluid pressure in mechanics of overthrust faulting. I. Mechanics of fluid-filled porous solids and its application to overthrust faulting, *Bull. Geol. Soc. Am.*, 70, 115-166, 1959.

Huyakorn, P.S., and G.F. Pender, A pressure-enthalpy finite element model for simulating hydrothermal reservoirs, Second International Symposium on Computer Methods for Partial Differential Equations, Lehigh Univ., Bethlehem, Pa., June 22-24, 1977.

Israel, M., and A. Nur, A complete solution of a one-dimensional propagating fault with nonuniform stress and strength, *J. Geophys. Res.*, 84(B5), 2223-2234, 1979.

Jaegar, J.C., Moving sources of heat and temperature at sliding contacts, *J. Proc. R. Soc. N.S.W.*, 76, 203-224, 1942.

Jaeger, K.C., and N.G.W. Cook, **Fundamentals of Rock Mechanics.**, Methuen and Co., Ltd., London, 513p., 1979.

Johnson, A.I., R.P. Moston, and D.A. Morris, Physical and hydrologic properties of water-bearing deposits in subsiding areas in central California, *U.S. Geol. Surv. Prof. Paper 497A,* 1968.

Jorgensen, D.G., Relationships between basic soils-engineering equations and basic ground-water flow equations, *U.S. Geol. Survey Water-Supply Paper*, 2064, 46pp., 1981.

Kanamori, H., and G.S. Stewart, Seismological aspects of the Guatemala earthquake of February, 4, 1976, *J. Geophys. Res.*, 83, 3427-3434, 1978.

Keenan, J.H., F.G. Keyes, P.G. Hill, and J.G. Moore, **Steam Tables**, 162pp., John Wiley, New York, 1978.

Kestin, J., Thermal conductivity of water and steam, *Mech. Eng.*, 100(8), 1255-1258, 1978.

Knopoff, L., J.O. Mouton, and R. Burridge, The dynamics of a one-dimensional fault in the presence of friction, *Geophys. J. R. Astr. Soc.*, 35, 168-184, 1973.

Lachenbruch, A.H., Frictional heating, fluid pressure, and the

resistance to fault motion, *J. Geophys. Res.*, 85(B11), 6097-6112, 1980.

Lachenbruch, A.H., and J.H. Sass, Heat flow and energetics of the San Andreas Fault zone, *J. Geophys. Res.*, 85, 6185-6207, 1980.

Landau, L.D., and E.M. Lifshitz, **Fluid Mechanics**, Pergamon Press, New York, 1959.

Li, V.C., and J.R. Rice, Preseismic rupture progression and great earthquake instabilities at plate boundaries, *J. Geophys. Res.*, 88, 4231-4246, 1983.

Lindh, A.G., and D.M. Boore, Control of rupture by fault geometry during the 1966 Parkfield earthquake, *Bull. Seis. Soc. Am.*, 71, 95-116, 1981.

Lockett, J.M. and N.S. Ksuznir, Ductile shear zones: some aspects of constant slip velocity and constant shear stress models, *Geophys. J. R. Astr. Soc.*, 69, 477-494, 1982.

Lockner, D.A., and P.G. Okubo, Measurements of frictional heating in granite, *J. Geophys. Res.*, 88(B5), 4313-4320, 1983.

Logan, J.M., Brittle phenomena, *Rev. Geophys. Space Phys.*, 17, 1121-1132, 1979.

McGarr, A., Analysis of peak ground motion in terms of a model of inhomogeneous faulting, *J. Geophys. Res.*, 3901-3912, 1981.

McKenzie, D. P. and J. N. Brune, Melting of fault planes during large earthquakes, *Geophys. J. R. Astr. Soc.*, 29, 65-78, 1972.

Madariaga, R., On the relation between seismic moment and stress drop in the presence of stress and strength hetrogeneity, *J. Geophys. Res.*, 84, 2243-2250, 1979.

Mahrer, K.D., and A. Nur, Strike slip faulting in a downward varying crust, *J. Geophys. Res.*, 84, 2296-2302, 1979.

Mase, C.W. and L. Smith, Pore-fluid pressures and frictional heating on a fault surface, *Pure and Appl. Geophys.*, 122, 583-607, 1985.

Mavko, G.M., Mechanics of motion on major faults, *Ann. Rev. Earth Planet. Sci.*, 9, 81-111, 1981.

Melosh, H.J., Plate motion and thermal instability in the astenosphere, *Tectonophysics*, 35, 363-390, 1976.

Melosh, H.J., Acoustic fluidization: A new geologic process?, *J. Geophys. Res.*, 84, 7513-7520, 1979.

Mikumo, T., and T. Miyatake, Dynamical rupture process on a three-dimensional fault with non-uniform friction and near-field seismic waves, *Geophys. J. R. Astr. Soc.*, 54, 417-438, 1978.

Morrow, C.A., L.Q. Shi, and J.D. Byerlee, Permeability and strength of San Andreas fault gouge under high pressure, *Gephys. Res. Let.*, 8, 325-328, 1981.

Morrow, C.A., L.Q. Shi, and J.D. Byerlee, Strain hardening and strength of clay-rich fault gouges, *J. Geophys. Res.*, 87, 6771-6780, 1982.

Morrow, C.A., L.Q. Shi, and J.D. Byerlee, Permeability of fault gouge under confining pressure and shear stress, *J. Geophys. Res.*, 89, 3193-3200, 1984.

Murrell, S.A.F., D.L. Turcotte, and K.E. Torrance, Studies of finite amplitude non-Newtonian convection with application to convection in the earth's mantle, *J. Geophys. Res.*, 81, 1939-1946, 1976.

Myer, C.A., R.B. McClintoch, G.J. Silvestri, and R.C. Spencer, **ASME Steam Tables - Thermodynamic and Transport Properties of Steam**, ASME, New York, 1967.

Nowacki, W., **Dynamic Problems of Thermoelasticity**, Noordhoff, Leyden, The Netherlands, 1975.

Nowinski, J.L., **Theory of Thermoelasticity with applications**, Sijthoff & Noordhoff, Leyden, The Netherlands, 1978.

Nur, A., Dilatancy, pore fluids, and premonitory variations of t_s/t_p travel times, *Bull. Seis. Soc. Am.*, 62, 1217-1222, 1972.

Nur, A., Nonuniform friction as a physical basis for earthquake mechanics, *Pure and Appl. Geophys.*, 116, 964-988, 1978.

Nur, A. and J.R. Booker, Aftershocks caused by pore fluid flow, *Science*, 146, 1003-1010, 1972.

Nur, A., and J. D. Byerlee, An exact effective stress law for elastic deformation of rock with fluids, *J. Geophys. Res.*, 76, 6414-6419,1971.

Okubo, P.G., and J.H. Dietrich, Effects of physical fault properties on frictional instabilities produced on simulated faults, *J. Geophys. Res.*, 89, 5817-5827, 1984.

O'Neil, K., and G.F. Pinder, A derivation of the equations for transport of liquid and heat in three dimensions in a fractured medium, *Adv. Water Resources*, 4, 150-164, 1981.

Palciauskas, V.V., and P.A. Domenico, Characterization of thermally loaded repository rocks, *Water Resour. Res.*, 18, 281-290, 1982.

Papageorgiou, A.S., and K. Aki, A specific barrier model for the quantitative description on inhomogeneous faulting and prediction of strong ground motion. Part I. Description of the model, *Bull. Seis. Soc. Am.*, 73, 693-723, 1983a.

Papageorgiou, A.S., and K. Aki, A specific barrier model for the quantitative description on inhomogeneous faulting and prediction of strong ground motion. Part I. Applications of the model, *Bull. Seis. Soc. Am.*, 73, 953-987, 1983b.

Platten, J.K., and J.C. Legros, **Convection in Liquids**, Springer-Verlag, New York, 1984.

Plumley, W.J., Abnormally high fluid pressure: survey of some basic principles, *Am. Assoc. Pet. Geol. Bull.*, 64, 414-430, 1980.

Raleigh, C.B., Frictional heating, dehydration and earthquake stress drops, in *Proceedings of Conference II Experimental Studies of Rock Friction with Application to Earthquake Prediction*, pp 291-304, U.S. Geological Survey, Menlo Park, CA, 1977.

Raleigh, B., and J. Everden, Case for low deviatoric stress in the lithosphere, in *The Mechanical Behavior of Crustal Rocks, Geophys. Monogr. Ser.*, vol. 24, edited by N.L. Carter, M. Friedman, J.M. Logan, and D.W. Stearns, pp. 173-186, AGU, Washington, D.C., 1981.

Reid, H.F., The mechanisms of the earthquake, in *The California Earthquake of April 18, 1906*, Rep. State Earthquake Investigation Comm., Carneige Inst., Washington, D.C., 1910.

Reid, H.F., The elastic rebound theory of earthquakes, *Univ. Calif. Publ. Geol.*, 6 413-444, 1911.

Rice, J.R., Constitutive relations for fault slip and earthquake instabilities, *Pure and Appl. Geophys.*, 121, 443-475, 1983.

Rice, J.R. and M.P. Cleary, Some basic stress diffusion solutions for fluid-saturated elastic porous media with compressible constituents, *Rev. Geophys. Space Phys.*, 14, 227-241, 1976.

Rice, J.R. and J.W. Rudnicki, Earthquake precursory effects due to pore fluid stabilization of a weakening fault zone, *J. Geophys. Res.*, 84(B5), 2177-2193, 1979.

Rice, J.R., and A.L. Ruina, Stability of steady frictional

slipping, *J. Appl. Mech.*, 50, 343-349, 1983.

Rice, J.R. and D.A. Simons, The stabilization of spreading shear faults by coupled deformation-diffusion effects in fluid-infiltrated porous media, *J. Geophys. Res.*, 81, 5322-5334, 1976.

Rice, J.R., and S.T. Tse, Dynamic motion of a single degree of freedom system following a rate and state dependent friction law, *J. Geophys. Res.*, 91,521-530,1986.

Richards, P.G., Dynamic motions near an earthquake fault: a three dimensional solution, *Bull. Seis. Soc. Am.*, 66, 1-32, 1976.

Rieke, H.H., and G.V. Chilingarian, *Compaction of argillaceous sediments*, 424 pp., Elsevier, New York, 1974.

Rudnicki, J.W., The inception of faulting in a rock mass with a weakened zone, *J. Geophys. Res.*, 82, 844-854, 1977.

Rudnicki, J.W., The stabilization of slip on a narrow weakening fault zone by coupled deformation-pore fluid diffusion, *Bull. Seis. Soc. Am.*, 69, 1011-1026, 1979.

Rudnicki, J.W., Fracture mechanics applied to the earth crust's, in **Ann. Rev. Earth Planet. Sci.**, Vol. 8 (Ed. F.A. Donath), Annual Reviews Inc., Palo Alto, CA, 489-525, 1980.

Rudnicki, J.W., and H. Kanamori, Effects of fault interaction on moment, stress drop, and strain energy release, *J. Geophys. Res.*, 86, 1785-1793, 1981.

Ruina, A.L., Slip instabilities and state friction laws, *J. Geophys. Res.*, 88, 10359-10370, 1983.

Ruina, A.L., Constitutive relations for frictional slip, in *Mechanics of Geomaterials*, edited by Z.P. Brant, John Wiley, New York, 1984.

Rundle, J.B., H. Kanamori, and K.C. McNally, An inhomogeneous fault model for gaps, asperities, barriers and seismicity migration, *J. Geophys. Res.*, 89, 10219-10231, 1984.

Sass, J.H., A.H. Lachenbruch, and R.J. Munroe, Thermal conductivity of rocks from measurements on fragments and its application to heat-flow determinations, *J. Geophys. Res.*, 76, 3391-3401, 1971.

Savage, S.B., Gravity flow of cohesionless granular materials in chutes and channels, *J. Fluid. Mech.*, 92, 53-96, 1979.

Scholz, C.H., Shear heating and the state of stress on faults, *J. Geophys. Res.*, 85(B11), 6174-6184, 1980.

Scholz, C.H., L.R. Sykes, and Y.P. Aggarwal, Earthquake prediction - a physical basis, *Science*, 181, 803-810, 1973.

Sharp, J.M., Jr., Permeability controls on aquathermal pressuring, *Am. Assoc. Pet. Geol. Bull.*, 67, 2057-2061, 1983.

Sibson, R.H., Interactions between temperature and fluid pressure during earthquake faulting - A mechanism for partial or total stress relief, *Nature*, 243, 66-68, 1973.

Sibson, R.H., Kinetic shear resistance, fluid pressures, and radiation efficiency during seismic faulting, *Pure and Appl. Geophys.*, 115, 387-400, 1977.

Sibson, R.H., Power dissipation and stress levels on faults in the upper crust, *J. Geophys. Res.*, 85, 6239-6247, 1980.

Sieh, K.E., Prehistoric large earthquakes produced by slip on the San Andreas fault at Pallet Creek, California, *J. Geophys. Res.*, 83, 3907-3939, 1978.

Simpson, D.W., Seismicity changes associated with reservoir loading, *Eng. Geol.*, 10, 123-150, 1976.

Slattery, J.C., **Momentum, Energy, and Mass Transfer in Continua**, McGraw-Hill, New York, 1972.

Smith, J.E., Shale compaction, *Soc. Pet. Eng. J.*, 13, 12-22, 1973.

Snow, D., Fracture deformation and changes of permeability and storage upon changes in fluid pressure, **Colo. Sch. Mines Q.**, 63, 201-244, 1969.

Sorey, M.L., Numerical modeling of liquid geothermal systems, *U.S. Geol. Surv. Prof. Pap., 1044-D*, 1978. Stallman, R.W., Notes on the use of temperature data for computing velocity, paper presented at 6th Assembly on Hydraulics, Soc. Hydrotech. France, Nancy, June 28-30, 1960.

Stallman, R.W., Computation of groundwater velocity from temperature data, *U.S. Geol. Surv. Water Supply Pap. 1544-H*, H36-H40, 1963.

Straus, J.M., and G. Schubert, Thermal convection of water in a porous medium: effects of temperature- and pressure-dependent thermodynamic and transport properties, *J. Geophys. Res.*, 82(2), 325-333, 1977.

Stuart, W.D., Strain-softening instability model for the San Fernando earthquake, *Science*, 203, 907-910, 1979.

Stuart, W.D., R.J. Archuleta, and A.G. Lindh, Forecast model for moderate earthquakes near Parkfield, California, *J.*

Geophys. Res., 592-604, 1985.

Stuart, W.D., and G.M. Mavko, Earthquake instability on a strike-slip fault, *J. Geophys. Res.*, 84, 2153-2160, 1979.

Sukanek, P.C. and R.L. Laurence, An experimental investigation of viscous heating in some simple shear flows, *Am. I. Chem. Eng. J.*, 20, 474-484, 1974.

Teufel, L.W., and J.M. Logan, Effect of displacement rate on the real area of contact and temperatures generated during frictional sliding of Tennessee sandstone, *Pure and Appl. Geophys.*, 116, 840-865, 1979.

Touloukian, Y.S., W.R. Judd, and R.F. Roy, *Physical Properties of Rocks and Minerals*, vol. II-2, McGraw-Hill, New York, 1981.

Turcotte, D.L. and E.R. Oxbaugh, A fluid theory for the deep structure of dip-slip fault zones, *Phys. Earth Planet. Interiors*, 1, 381-387, 1968.

Verruijt, A., Elastic storage of aquifers, in **Flow Through Porous Media**, edited by R.J.M DeWeist, Academic Press, New York, 1969.

Voight, B., and C. Faust, Frictional heat and strength loss in some rapid landslides, *Geotechnique*, 32(1), 43-54, 1982.

Walash, J.B., Mechanics of strike-slip faulting with friction, *J. Geophys. Res.*, 73, 761-776, 1968.

Walder, J. and A. Nur, Porosity reduction and crustal pore pressure, *J. Geophys. Res.*, 89, 11539-11548, 1984.

Watson, J.T.R., R.S. Basu, and J.V. Sengers, An improved representative equation for the dynamic viscosity of water substance, *J. Phys. Chem. Ref. Data*, 9(3), 1255-1279, 1980.

Weeks, J.D., and T.E. Tullis, Frictional sliding on dolomite: A variation in constitutive behavior, *J. Geophys. Res.*, 90, 7821-7826, 1985.

Weertman, J. and J.R. Weertman, High temperature creep of rock and mantle viscosity, *Annu. Rev. Earth Planet. Sci.*, 3, 293-315, 1975.

White, F.M., **Viscous Fluid Flow**, McGraw-Hill, New York, 1974.

Wilson, C.R., Jr., *The mechanical properties of the shear zone of the Lewis overthrust, Glacier National Park, Montana*, Ph.D. Dissertion, Texas A&M University, Texas, 1970.

Woodside, W. and J.H. Messmer, Thermal conductivity of porous media, *J. Appl. Phys.*, 32, 1688, 1961. Yuen, D.A., L.

Fleitout, G. Schubert, and C. Froideaux, Shear deformation zones along major transform faults and subducting slabs, *Geophys. J. R. Astr. Soc.*, 54, 93-119, 1978.

Yuen, D.A. and G. Schubert, On the stability of frictionally heated shear flows in the asthenosphere, *Geophys. J. R. Astr. Soc.*, 57, 189-207, 1979.

PUBLICATIONS

Abstracts of Oral Presentations

Mase, C.W. and L. Smith, *The effects of frictional heating on the thermal, hydrologic, and mechanical response of a fault zone during an earthquake*, EOS (Transactions, American Geophysical Union), 67, 242, 1986.

Mase, C.W. and L. Smith, *Transient temperature and fluid pressure effects within a fault zone during slip*, EOS (Transactions, American Geophysical Union), 65, 1114, 1984.

Mase, C.W. and L. Smith, *The role of shear-strain heating and pore-fluid pressures in the dynamics of fault zone processes*, EOS (Transactions, American Geophysical Union), 64, 851, 1983.

Mase, C.W., J.H. Sass, and A.H. Lachenbruch, *Preliminary heat-flow investigations of the California Cascades*, EOS (Transactions, American Geophysical Union), 61, 1150, 1980.

Sass, J.H., and C.W. Mase, *The downhole heat-flow probe as a geophysical exploration tool*, Soc. Explor. Geophysicists Annual Meeting, Houston, Texas, October 1980, Program Abstracts, p. 112, 1980.

Mase, C.W., and D.S. Chapman, *Geophysical study of the Monroe Utah, geothermal system*, Rocky Mountain Section of GSA Annual meeting Provo, Utah, April 1978.

Chapman, D.S., K.T. Kilty, and C.W. Mase, *Characteristics of fault-controlled geothermal systems*, EOS (Transactions, American Geophysical Union), 59, p. 1201, 1978.

Published Papers and Reports

Mase, C.W. and L. Smith, *The effects of frictional heating on the thermal, hydrologic, and mechanical response of a fault*, (submitted to *J. Geophys. Res.*).

Smith, L., C.W. Mase, and F.W. Schartz, *A stochastic model for transport in networks of planar fractures*, Intl. Assoc. Hydraul. Res., Sym. on the Stochastic Approach to Subsurface Flow, Paris, June 1985.

Mase, C.W., and L. Smith, *Pore-fluid pressures and frictional heating on a fault surface*, Pure and Appl. Geophy., 122, 583-607, 1985.

Smith, L., C.W. Mase, F.W. Schartz, and D. Chorley, *A numerical model for transport in networks of planar fractures*, Proceedings Conference on Hydrogeology of Rocks of Low Permeability, Intl. Assoc. of Hydrologists, 17th Intl. Conference, 666-675, 1985.

Mase, C.W., J.H. Sass, A.H. Lachenbruch, and R.J. Munroe, *Preliminary heat-flow investigations of the California Cascades*, U.S. Geol. Survey Open File Rept.

82-150, 240p., 1982.

Brook, C.A., and C.W. Mase, *The hydrothermal system at the East Brawley KGRA, Imperial Valley, California*, Geothermal Resources Council Transactions, 5, 157-163, 1981.

Mase, C.W., J.H. Sass, C.A. Brook, and R.J. Monroe, *Shallow hydrothermal regime of the East Brawley and Glamis KGRA's, Salton Trough, California*, U.S. Geol. Survey Open File Rept. 81-834, 57p., 1981.

Chapman, D.S., M.D. Clement, and C.W. Mase, *Thermal regime of the Escalante Desert, Utah, with an analysis of the Newcastle geothermal system*, J. Geophys. Res., 86(B12), 11735-11746, 1981.

Mase, C.W., and J.H. Sass, *Heat flow from the western arm of the Black Rock Desert, Nevada*, U.S. Geol. Survey Open File Rept. 80-1238, 38p., 1980.

Mase, C.W., J.H. Sass, and A.H. Lachenbruch, *Near-surface hydrothermal regime of the Lassen KGRA, California*, U.S. Geol. Survey Open File Rept. 80-1230, 31p., 1980.

Sass, J.H., A.H. Lachenbruch, and C.W. Mase, *Analysis of thermal data from drill holes UE25a-3 3 and UE25a-1, Calico Hills and Yucca Mountain, Nevada Test Site*, U.S. Geol. Survey Open File Rept. 80-826, 25p., 1980.

Mase, C.W., S.P. Galanis, and R.J. Monroe, *Near-surface heat flow in Saline Valley, California*, U.S. Geol Survey Open File Rept. 79-1136, 52p., 1979.

Kilty, K.T., D.S. Chapman, and C.W. Mase, *Forced convective heat transfer in the Monroe hot springs geothermal system*, J. Volcanology and Geothermal Res., 6, 257-277, 1979.

Mase, C.W., D.S. Chapman, and S.H. Ward, *Geophysical study of the Monroe-Red Hill geothermal system*, U.S. Dept. of Energy, Rept. No. EY-76-S-07-1601, Univ. of Utah, 89p., 1979.

Kilty, K.T., D.S. Chapman, and C.W. Mase, *Aspects of forced convective heat transfer in geothermal systems*, U.S. Dept. of Energy, Rept. EG-78-C-07-1701, Univ. of Utah, 62p., 1978.

Chapman, D.S., K.T. Kilty, and C.W. Mase, *Temperature and their dependence on groundwater flow in shallow geothermal systems*, Geothermal Resource Council Transactions, 2, 134-137, 1978.

McEuen, R.B., C.W. Mase, and W.E. Loomis, *Geothermal tectonics of the Imperial Valley as deduced from earthquake occurence*, Geothermal Resource Council Transactions, 1, 211-215, 1977.